

Ordered Peptide-based Assemblies as Functional Materials

**by
Gagandeep Kaur**



**Department of Chemistry
Indian Institute of Technology, Kanpur
January, 2017**

Ordered Peptide-based Assemblies as Functional Materials

A Thesis Submitted

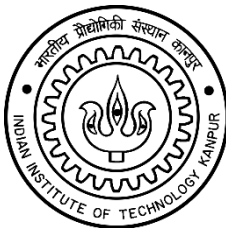
In Partial Fulfillment of the Requirements

For the Degree of

DOCTOR OF PHILOSOPHY

By

Gagandeep Kaur



to the

Department of chemistry
Indian Institute of Technology, Kanpur
Kanpur-208016, India
January, 2017

STATEMENT

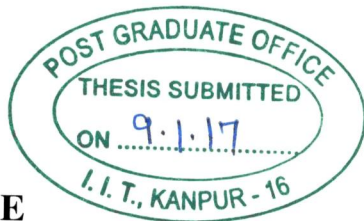
I hereby declare that the matter manifested in this thesis
“Ordered Peptide-based Assemblies as Functional Materials”
is the result of research carried out by me in the Department of
Chemistry, Indian Institute of Technology, Kanpur, India under the
supervision of Professor Dr. Sandeep Verma.

In keeping with general practice of reporting scientific
observations, due acknowledgements have been made whatever the
work described is based on the findings of other investigators.

IIT-Kanpur

January, 2017



Gagandeep Kaur



CERTIFICATE

It is to certify that the work reported on the thesis entitled,
“Ordered Peptide-based Assemblies as Functional Materials”
by Gagandeep Kaur has been carried out under my guidance and
this work has not been submitted elsewhere for a degree.

IIT-Kanpur
January, 2017


Prof. Sandeep Verma
(Thesis Supervisor)
Department of Chemistry
Indian Institute of Technology
Kanpur, India

**Department of Chemistry
Indian Institute of Technology, Kanpur**

Certificate of Course Work

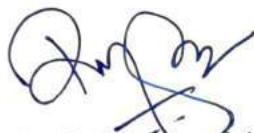
This is to certify that **Gagandeep Kaur** has satisfactorily completed all the courses required for the Ph.D. degree. The courses include:

CHM 602	Advanced Organic Chemistry II
CHM 609	Principles of Organic Chemistry
CHM 612	Frontiers of Organic Chemistry
CHM 631	Applications of Modern Instrumental methods
CHM 646	Bio-Inorganic Chemistry
CHM 651	Crystal and Molecular Structure Determination
CHM 799	Research
CHM 800	General Seminar
CHM 801	Graduate Seminar

Gagandeep Kaur was admitted to the candidacy of the Ph.D. degree in April 2012 after she successfully completed the written and oral qualifying examinations.



Prof. S. Verma
Head,
Department of Chemistry,
IIT Kanpur



Dr. R. Ramapannicker
Convener, DPGC
Department of Chemistry,
IIT Kanpur

Sandeep Verma

Professor & Head

Department of Chemistry

I.I.T. Kanpur-208016 (India)

SYNOPSIS

Ordered Peptide-based Assemblies as Functional Materials

by
Gagandeep Kaur
(10207067)
C/o Prof. Sandeep Verma
Department of Chemistry
Indian Institute of Technology, Kanpur
Kanpur, India

This thesis covers synthesis and characterization of peptide-based self-assembled supramolecular architectures and their implications for various applications such as catalysis, bio-imaging, cancer cell detection, and potential energy storage scaffolds.

Chapter 1 introduces self-assembly properties of short peptides and folic acid. It also covers applications of self-assembled peptide structures in nanotechnology, material science and biological sciences.

Chapter 2 discusses general experimental procedures, instruments and techniques used throughout this thesis.

Chapter 3 highlights molecular level arrangements in self-assembling ultrathin layer of a C_3 symmetric construct formed by the conjugation of phenylalanine to benzene tricarboxylic acid. This molecule self-assembled as long uniform nanofibers with diameter of ~ 70 -90 nm. Self-assembled ultrathin monolayer of this molecule was studied at low concentration ($10\ \mu\text{M}$) through atomic force microscopy (AFM), which revealed the formation of two different kinds of assemblies: namely, one- and two-dimensional nano-islands. C_3 symmetric molecules are generally known to form two-dimensional islands, but the formation of one-dimensional islands is unusual. Working models for one- and two-dimensional islands were proposed by using DREIDING force field method.

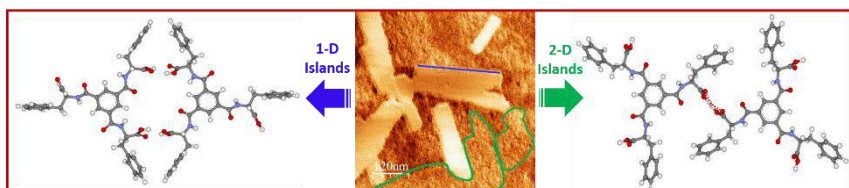


Figure 1: AFM image of ultrathin layer of C_3 symmetric molecule on HOPG surface showing formation of two types of self-assembled structures: one dimensional nano-islands (marked with blue line) and two dimensional nano-islands (marked with green line). The respective molecular level arrangement of dimer molecules was proposed through DREIDING force field method as shown in the image.

Peptides and proteins offer interesting starting points for triggering self-assembly process, owing to the chemical diversity of side-chains, ease of chemical modifications and the possibility of exploiting several non-covalent and metal-assisted interactions, to stabilize higher order ensembles. Consequently, a variety of nanoscale morphologies such as fibers, vesicles, nanotubes are observed for modified amino acids and short peptides and these biocompatible soft materials have been used for diverse biological, medical and material applications. **Chapter 4** uncovers the effect of metal ion coordination on self-assembled supramolecular architectures of Phe-Phe based synthetic peptide conjugate, containing a pyridyl connector. This construct was synthesized by covalent conjugation of Phe-Phe with dipicolinic acid, which afforded a planar ‘*crescent-like*’ conformation. The spherical structures so formed in solution interacted with metal ions to afford coalescence in these structures. Copper ion coordination, with the metal-binding peptide conjugate, was confirmed by single crystal analysis. Notably, this coalescence could be reversed in the case of Au-mediated soft structures with thiol interference. Based on these observations, a model depicting possible interactions leading to soft structure formation and metal-aided coalescence is presented. Such constructs provide a facile entry into metallopeptide materials.

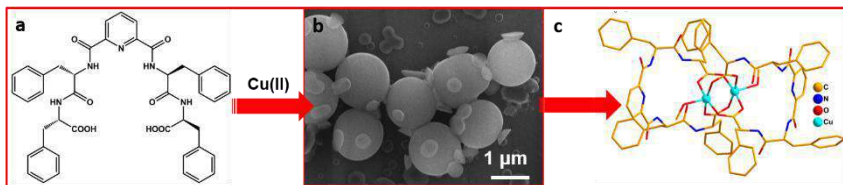


Figure 2: (a) Molecular structure of peptide designed by covalent conjugation of Phe-Phe with dipicolinic acid resulted in formation of spherical self-assembled structures which result in (b) coalescence in presence of coinage metal ion due to metal ion coordination interactions, confirmed by single crystal analysis in case of copper ions (c).

Folic acid (FA) is a low-molecular-weight micronutrient, which plays a critical role in the prevention of birth defects and cancers. It is also essential for biochemical pathways responsible for DNA synthesis and maintenance and for the generation of new red blood cells. Cellular trafficking of FA and folate is based on its high-affinity binding to cognate folate receptor, a protein commonly expressed in several human cancers. Thus, folate conjugates of drugs, plasmids, biosensors, contrast, and radio diagnostic imaging agents have been used for assisted delivery in folate receptor-positive cancer cells, via endocytosis pathways. **Chapter 5A** describes synthesis and self-assembly of diphenylalanine folic acid peptide as a bio-imaging agent. Cancer cell uptake of fully characterized FA–diphenylalanine conjugate and its detailed mechanistic studies were tracked with the help of inherent fluorescence of the conjugate. Uptake in HeLa and H460

cells was ascribed to macropinocytosis-mediated pathway, based on rottlerin interference. In the case of MCF7 cell line, chlorpromazine and nocodazole inhibited internalization of the peptide, which suggested a probable role of clathrin-mediated endocytosis in the uptake process in this cell line.

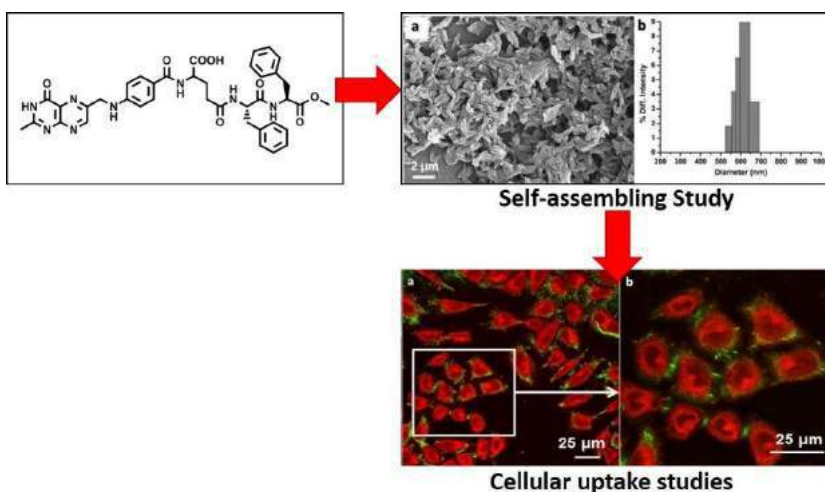


Figure 3: Self-assembled structure of diphenylalanine folic acid peptide. Cellular uptake studies were tracked by the inherent green fluorescence ($\lambda_{em} = 488$ nm) of the conjugate in confocal microscopy where cancer cells were stained with deep red plasma membrane dye ($\lambda_{em} = 633$ nm).

Electrospun polymer nanofibers are valuable for a number of applications ranging from catalysis to drug delivery. At times, the lack of biocompatibility and hydrophobicity presents hindrance to their use in tissue engineering, cell culture and proliferation. Aromatic amino acids are veritable precursors for biocompatible

nanofibers, which could also be chemically modified with suitable addressable recognition tags to invoke specific binding events. **Chapter 5B** explores self-assembly of dityrosine folic acid conjugate in the electrospun mat for selective cell adhesion.

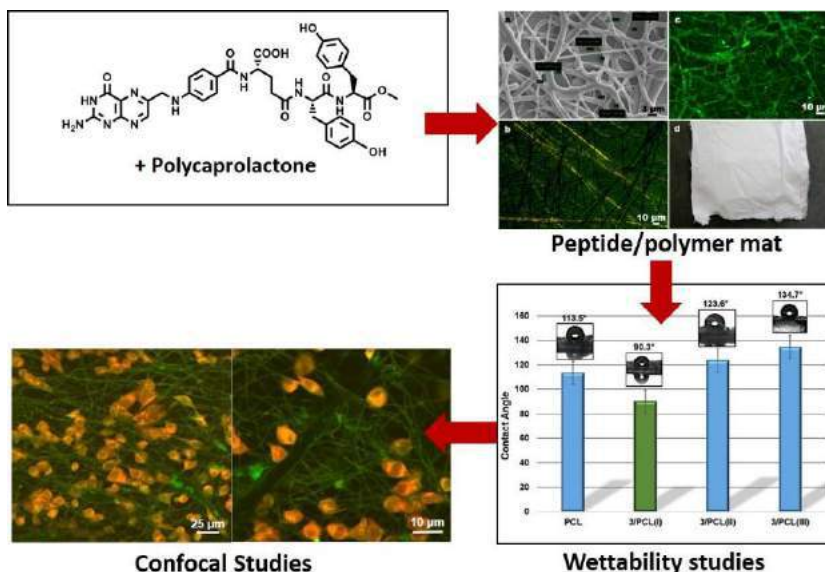


Figure 4: Dityrosine folic acid-peptide conjugate/ polycaprolactone (PCL) mat synthesized through electrospinning process and characterized through various microscopic methods. Hydrophilic nature of the new hybrid material was studied through contact angle measurement. Cell adhesion studies were done by tracking the inherent green fluorescence ($\lambda_{\text{em}} = 488 \text{ nm}$) of the conjugate in confocal microscopy, where cancer cells were stained with deep red plasma membrane dye ($\lambda_{\text{em}} = 633 \text{ nm}$).

This study presented an attractive strategy for constructing electrospun fibrous nanomats from dityrosine folic acid conjugate and polycaprolactone (PCL) to afford a new hybrid material, displaying excellent biocompatibility and cell adhesion. The appropriate choice of peptide-to-polymer ratio gave mats with sufficient hydrophilic character and allowed favorable interaction of folate receptor presenting cells (HeLa cells) with nanomats, while the ones lacking folate receptor (HEK 293 cells) did not exhibit binding. Such a selectivity could be possibly invoked for separation and also for custom synthesis of nanomats for healthcare applications.

Energy storage or supercapacitor materials are the green and clean alternatives for handling the energy crisis in coming future. Supercapacitor materials have been used in renewable energy harvesting appliances such as the wind, thermal and solar panels. But, the existing supercapacitor materials are very costly with limited cycle life and becoming environmental hazards itself. The porous nitrogen-doped carbon materials are gaining attention due to simple preparation methods, low cost and the conductivity of material due to the electronegativity difference between carbon and nitrogen. Vitamins and amino acid containing nitrogen in their skeleton are attractive precursors for the nitrogen-doped carbon materials due to environmentally compatible, economically cheap

and easy availability. **Chapter 5C** deals with co-assembly of melamine with folic acid-tyrosyl phenylalanine peptide and its use in electrochemical capacitive storage. This co-assembly of folic acid tyrosyl phenylalanine peptide with melamine resulted in interesting architectures with morphology similar to graphene sheets.

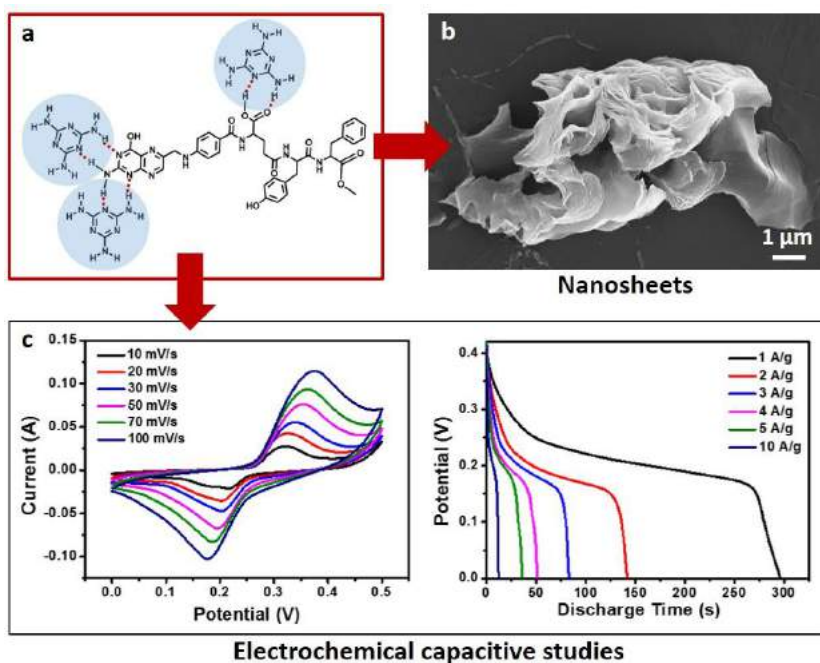


Figure 5: Peptide-based graphene-like morphological structures (b) were obtained when co-self-assembly of melamine with folic acid-tyrosyl phenylalanine peptide was studied. These structures were carbonized at 900 $^{\circ}\text{C}$ to form a black shiny material and tested for electrochemical capacitive performance (c).

Folic acid tyrosyl phenylalanine peptide/melamine sheets were studied for electrochemical capacitive performance by carbonizing the material at 900 °C, followed by determining their electrochemical capacitive performance for application in energy storage field.

ACKNOWLEDGEMENTS

Completing the Ph.D. and writing this thesis was an amazing journey that would not have been possible without the support and encouragement of many outstanding people.

First and foremost, my greatest appreciation and gratitude goes to my advisor Prof. Sandeep Verma for his trust and support. The joy and enthusiasm he has for his research were contagious and motivational for me, even during tough times in the Ph.D. pursuit. I hope that I could be as lively, enthusiastic, and energetic as him and to someday be able to command an audience as well as he can. I really admire his ability to balance research interests and personal pursuits. He was and remains my best role model for a scientist, mentor and teacher. To work with him has been a real pleasure to me, with heaps of fun and excitement. During the most difficult times during Ph.D. and when writing this thesis, he gave me the moral support and the freedom I needed to move on. He guided me academically and emotionally through the rough road to finish this thesis. I believe that the kind of training I have received under his guidance will help me throughout my future life.

I would like to extend my heartfelt gratitude to Dr. Richa Verma for being a source of love and energy ever since we met.

I am extremely thankful to Prof. Ehud Gazit, Dr. Rahul Banerjee, Prof. S. Ganesh, Prof. S. Sivakumar and Dr. Sandip Patil for their fruitful collaborations.

I sincerely thank Prof. Y. D. Vankar, Prof. P. K. Bharadwaj, Prof. M. L. N. Rao, Dr. S. P. Rath and Dr. R. Ramapanicker for teaching me courses during my first year of the Ph.D. program. I would like to thank Prof. J. K. Bera, Prof. V. Chandrasekhar, Dr. A. K. Patra and Dr. N. Verma for allowing me to use their lab facilities.

I thank Prof. Ashutosh Sharma, Dr. Prabhat Dwivedi and the staff of Thematic Unit of Excellence, IIT Kanpur for access to their facilities and timely cooperation. I also thank Advanced Imaging, IIT Kanpur for TEM and AFM facilities.

I am thankful to Dr. N. Banerji and Mr. S. Krishnasamy (Department of Physics, IIT Kanpur) for the FIB-SEM studies.

I sincerely thank my seniors Dr. A. K. Mishra, Dr. J. Kumar, Dr. S. Mondal, Dr. K. Vijaya Krishna, Dr. A. K. Barman, Dr. V. Venkatesh, Dr. R. Kumar, Dr. N. Nagapradeep and Dr. S. Khanna for teaching me lab techniques. I appreciate and thank my fellow labmates Dr. N. K. Mishra, Dr. B. Mohapatra. Anisha, Pratibha, Astha, Ilesha, Hilal, Kamal, Eram, Bhagwat, Apurva, Swati, Narendra, Saurabh, Dr. R. Gaur and Dr. M. Pandey for their timely help, discussions and fun we had together.

I am very thankful to members of X-ray facility, glass blowing section and liquid nitrogen plant, IIT Kanpur for their timely help. I am thankful to NMR, Mass and IR operators for data collections. I also thank Mr. P. Sharma for providing chemicals for research activities. I sincerely thank all chemistry office staff members, especially Sudha Madaam and Geeta Madam for their prompt action and timely help.

I acknowledge UGC, India for financial support and IIT Kanpur for infrastructure.

I owe sincere gratitude to Mrs. Kulwant Singh and her family, Dr. R .S. Anand and Mrs. Anand for helping me in difficult times.

My dearest thanks to great people who became friends over the last several years. Growing up with you guys was fun!

Finally, I would like to thank my family for their infinite love, encouragement and support throughout everything. Dear Mom and Dad, you guys are the best! A special thanks to Tejewant, Inderpal and Manmeet!

Gagandeep Kaur

“You are what you believe yourself to be.”

.....Paulo Coelho

CONTENTS

Chapter 1

Peptide Self-assembly and Applications

1.1. Bio-inspired self-assembly	2
1.2. Peptide self-assembly	2
1.2.1. Driving forces for peptide self-assembly	4
1.2.2. Rules to design self-assembling peptide	6
1.2.3. Self-assembled nanostructures	8
1.3. Folic acid self-assembly.....	14
1.4. Implication of peptide self-assembly	17
1.4.1. Cell culture scaffolds for tissue engineering	18
1.4.2. Skin care and cosmetic	18
1.4.3. Nanofabrication and bio-mineralization templates	18
1.4.4. Drug Delivery.....	19
1.4.5. Bio-imaging.....	20
1.5. References.....	21

Chapter 2

General Experimental Procedures and Technical Details

2.1. Introduction.....	30
------------------------	----

2.2. Chemicals and reagents	30
2.3. Purification of solvents and reagents	33
2.4. Instrumentation	34
2.5. Ion exchange chromatography	37
2.6. Sample Preparation	38
2.7. X-ray structure analysis	39
2.8. References.....	39

Chapter 3

One- and Two Dimensional Nano-island Growth in C₃ Symmetric Molecule

3.1. Introduction.....	42
3.2. Synthesis and Characterization	44
3.3. Microscopy Studies.....	46
3.4. Results and Discussion	47
3.4.1. Solution phase self-assembly	47
3.4.2. AFM study and DREIDING force field analysis	49
3.5. Conclusions.....	56
3.6. References.....	56

Chapter 4

Ultrastructure of metallopeptide-based soft spherical morphologies

4.1. Introduction.....	60
4.2. Synthesis and Characterization.....	62
4.3. Microscopy Studies.....	66
4.4. Results and Discussion	69
4.4.1. Molecular design of peptide conjugate (4).....	69
4.4.2. Solution phase self-assembly of 4.....	74
4.4.3. Interaction of 4 with copper (II) ions	76
4.4.4. Interaction of 4 with silver (I) ions.....	78
4.4.5. Interaction of 4 with gold (III) ions.....	79
4.4.6. Dynamic light scattering analysis.....	82
4.4.7. Thiol displacement studies	83
4.4.8. UV-Vis studies	85
4.4.9. Catalytic studies	89
4.5. Conclusions.....	91
4.6. References.....	92

Chapter 5A

Soft Structure formation and Cancer Cells Transport Mechanism of a Folic Acid-dipeptide Conjugate

5A.1. Introduction.....	98
5A.2. Synthesis and Characterization	101
5A.3. Microscopy Studies.....	103
5A.4. Cell assay	104
5A.5. Results and Discussion	107

5A.5.1. Cellular uptake	112
5A.5.2. Elucidation of uptake mechanism	114
5A.6. Conclusions.....	119
5A.7. References.....	120

Chapter 5B

Dityrosine-Folic acid Conjugate in Electrospun Nanofibres for Selective Cell Adhesion

5B.1. Introduction.....	124
5B.2. Experimental Section	127
5B.2.1. Materials	127
5B.2.2. Peptide conjugate synthesis	128
5B.2.3. Cell assays	130
5B.2.4. Microscopy Studies	133
5B.2.5. Electrospinning Method	134
5B.2.6. Contact angle Measurement	134
5B.3. Results and discussion.....	135
5B.3.1 Solution phase self-assembly of 3	135
5B.3.2 Preparation of 3 /PCL mat	136
5B.3.3 Cytotoxicity of 3	140
5B.3.4. Cell adhesion properties of 3 /PCL.....	141
5B.4. Conclusions	146
5B.5. References	147

Chapter 5C

Folic acid Peptide scaffolds for electrochemical capacitive energy storage

5C.1. Introduction.....	152
5C.2. Experimental section.....	154
5C.2.1. Material	154
5C.2.2. Peptide conjugate Synthesis	154
5C.2.3. Microscopy Studies	157
5C.3. Results and discussion	159
5C.3.1. Solution phase self-assembly	159
5C.3.2. Melamine co-incubation.....	160
5C.3.3. Carbonization of Melamine doped 3	164
5C.3.4. Electrochemical Capacitive performance.....	168
5C.4. Conclusions.....	170
5C.5. References.....	171

Appendix I

A1.1. Crystal data for Chapter 4.....	176
A1.2. Spectral Data for Chapter 3.....	177
A1.3. Spectral Data for Chapter 4.....	182
A1.4. Spectral Data for Chapter 5A.....	194
A1.5. Spectral Data for Chapter 5B.....	200
A1.6. Spectral Data for Chapter 5C.....	208

Curriculum Vitaé.....	213
Reprints of publications	217

AMINO ACID ABBREVIATION AND PROPERTIES

Amino Acids	Three letter code	Single letter code	Side-chain polarity	Absorbance ¹ λ_{\max} (nm)
Alanine	Ala	A	Nonpolar	
Arginine	Arg	R	Basic polar	
Asparagine	Asn	N	Polar	
Aspartic acid	Asp	D	Acidic polar	
Cysteine	Cys	C	Nonpolar	250
Glutamic Acid	Glu	E	Acidic Polar	
Glutamine	Gln	Q	Polar	
Glycine	Gly	G	Nonpolar	
Histidine*	His	H	Basic Polar	211
Isoleucine*	Ile	I	Nonpolar	
Leucine*	Leu	L	Nonpolar	
Lysine*	Lys	K	Basic polar	
Methionine*	Met	M	Nonpolar	
Phenylalanine*	Phe	F	Nonpolar	257,206,188
Proline	Pro	P	Nonpolar	
Serine	Ser	S	Polar	
Threonine*	Thr	T	Polar	
Tryptophan*	Trp	W	Nonpolar	280,219
Tyrosine	Tyr	Y	Polar	274,222,193
Valine*	Val	V	Nonpolar	

References:

Freifelder, D. M.; *Physical Biochemistry: Applications to Biochemistry and Molecular Biology* 2nd Edition, W. H. Freeman, **1983**.

*Essential amino acids.

ABBREVIATIONS

AFM	Atomic force microscopy
CD	Circular Dichroism
CLSM	Confocal Laser scanning microscopy
DCC	N,N'-Dicyclohexylcarbodiimide
DCM	1,2-dichloromethane
DMC	Dimethyl carbonate
DMF	N,N-dimethylformamide
DMSO	Dimethyl sulfoxide
DMSO- <i>d</i> ₆	Deuterated DMSO
DNA	Deoxyribonucleic acid
EDC	N-Ethylene (3-Dimethylaminopropyl)-N'-ethylcarbodiimide
EDX	Energy-dispersive X-ray spectroscopy
FA	Folic Acid
FESEM	Field emission scanning electron microscopy
FM	Fluorescence Microscopy
FTIR	Fourier transform Infrared
HOBt	1-Hydroxy benzotriazole
HOPG	Highly oriented pyrolytic graphite
HPLC	High-performance liquid chromatography
HRMS	High resolution mass spectrum

M.P.	Melting point
MOF	Metal organic framework
MPF	Metal Peptide framework
MTT	3-(4,5-dimethylthiazol-2-yl)-2,5-diphenyltertazolium bromide
NHS	N-hydroxysuccinimide
NMR	Nuclear magnetic resonance
OM	Optical Microscopy
STM	Scanning tunneling microscopy
ppm	Parts per million
PXRD	Powder X-ray diffraction
RNA	Ribonucleic acid
TEM	Transmission electron microscopy
TEA	Trimethylamine
TFA	Trifluoroacetic acid
THF	Tetrahydrofuran
TGA	Thermogravimetric analysis
TMS	Tetrametylsilane
UV-Vis	Ultraviolet-visible

Chapter 1

Peptide self-assembly to Applications

1.1. Bio-inspired Self-assembly

Self-assembly^{1a} is a highly ubiquitous process in nature, such as protein folding, DNA double helix, viral capsid, cell membranes, bacterial flagella, microtubules, ribosomes etc., stabilized by various non-covalent interactions.¹ It plays a vital role in physiological functions. Biologically-inspired self-assembling materials (proteins, peptides, lipids, vitamins and carbohydrates) have gained quite an attention with respect to the applications in fields of molecular biology, material sciences and nanotechnology.¹ⁱ

1.2. Peptide Self-assembly

Peptides (short peptides, peptide amphiphile and surfactant-like peptides) has been very popular bio-inspired material because of many attractive advantages like biocompatibility, low immunogenicity, degradability, easy availability and cost effectiveness. Peptide self-assembly has been utilized in the area of biological, photonic, food sciences, cosmetics, biomedicine, nanotechnology and many other fields, due to tunability and functional versatility for bottom-up fabrication.² Peptide self-assembly is a spontaneous thermodynamic process which results in highly ordered

supramolecular architecture with functionality. Many non-covalent interactions like van der Waal's forces, π - π stacking, electrostatic forces, hydrogen bonding and hydrophobic interactions play an essential role in the stability of self-assembled structures.³ Peptide self-assembly is affected by many kinetic parameters such as temperature, pH, electrolyte concentration, solvents etc. Therefore, a competitive pathway between kinetic and thermodynamic parameter decides the shape of self-assembled nanostructures (Figure 1.1).⁴

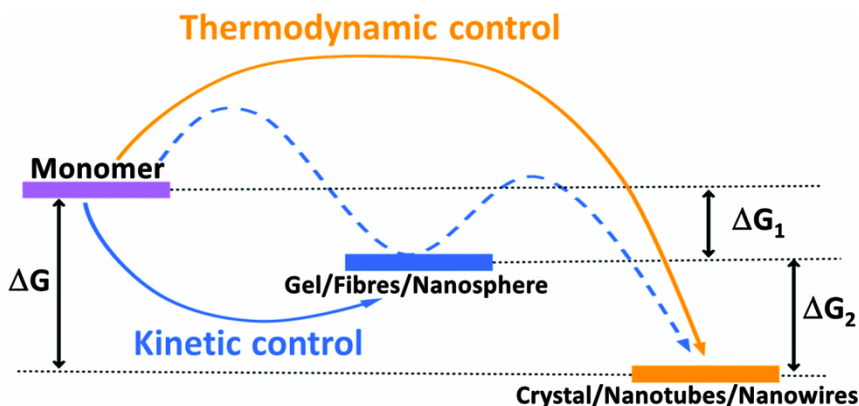


Figure 1.1: Schematic representation of thermodynamically and kinetically controlled peptide self-assembly pathways. (Adapted from reference 4)

As shown in Figure 1, crystal, nanotubes and nanowires are the outcome of thermodynamic control considering their minimum free energy states whereas kinetic control results into the gel,

fibers, ribbons, nanosphere as trapped metastable state. The relative energy of each structure (like nanosphere, nanotube or nanowire) varies with the different peptide.

1.2.1. Driving forces for peptide self-assembly:

Self-assembly is a delicate balance between three forces: attractive driving forces which bring molecule together, repulsive opposition forces which balance driving forces and a directional force.^{3a} The basic driving forces for self-assembly process are non-covalent interactions.

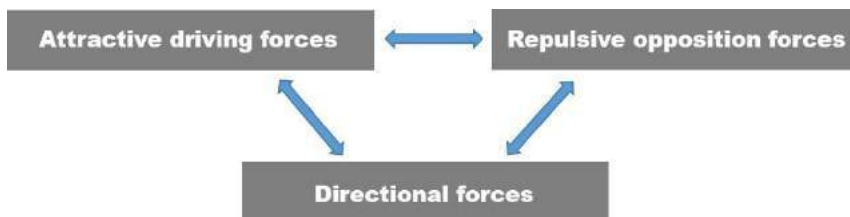


Figure 1.2: Forces responsible for self-assembly.

In order to understand and control self assembled structures in peptides, it is very important to know about these noncovalent interactions responsible for peptide self-ssembly, described below:

Hydrogen-bonding: Amino and carboxylic group of amide/peptide bonds in proteins and peptides contribute to the formation of hydrogen bonding which play a crucial role in 2D and

3D structures formation and stabilization.⁵ α -helix and β -sheet formation are balanced by hydrogen bonding which are strong and directional. The H-bonding strength in peptide self-assembled structures is generally 10-40 kJ/mol per bond at 298K.^{5e}

Hydrophobic interactions and π - π stacking: In aromatic peptides, hydrophobic interactions along with π - π stacking play a central role in molecular self-assembly, e.g. formation of nanotubes in the case of diphenylalanine dipeptide, when dissolved in polar solvents.⁶ The unfavorable enthalpy contribution of the solvent is compensated by a large amount of entropy, resulting in stable structural output.^{6c} Apparently, hydrophobic interactions do not occur due to the attraction between hydrophobic regions, but due to the thermodynamic stability of system.

Electrostatic interaction: The electrostatic interactions are attractive or repulsive forces which originate from interactions between charged species like N-terminal, C-terminal carboxylate end or oppositely charged residues in the side chains of peptides and proteins.^{3a, 5c, 7}

Van der Waal's interactions: These are weak attractive or repulsive forces between dipoles (permanent or induced dipole) at the atomic or molecular level with a bond strength of 5 kJ/mol.^{5e} However, these forces play a significant role in maintaining the tertiary structures in proteins and peptides.

Coordination interactions: Coordination with metal ions can dramatically change the self-assembled structures and properties peptides and proteins.^{8a, b} Coordination interactions are a powerful tool to construct significantly varied self-assembled architectures in peptides with artificial or natural ligands for metal ion binding.⁸

1.2.2. Rules to design self-assembling peptide:

The 20 amino acids encoded by codon present on DNA or RNA provide a marvelous set of ingredient for all protein based structure formation and cellular machinery, which are basis of life at the molecular level. In general, naturally occurring known protein sequences are the basis for designing self-assembling peptides. For example, neurodegenerative diseases such as Alzheimer's disease (AD), Huntingtin's disease (HD), Parkinson's disease (PD) and prion diseases have been discovered to contain misfolded protein aggregates with a β -sheet conformation.^{9a} The misfolded proteins or amyloids are an inspiration for many short self-assembling peptide designs. A well known, short, aromatic, self-assembling peptide, FF is inspired from amyloid beta (A β) protein itself. Examination of naturally occurring proteins, α -helices, β -sheets and coils help in the thorough and careful selection of amino acids being used to design self-assembling peptides.

In order to expand the area of self-assembling peptide apart from nature, an in-deep study about nature of amino acids is required.⁹ The amino acids are divided into 4 types- hydrophobic, hydrophilic, charged, or “other” based on properties of the R group.

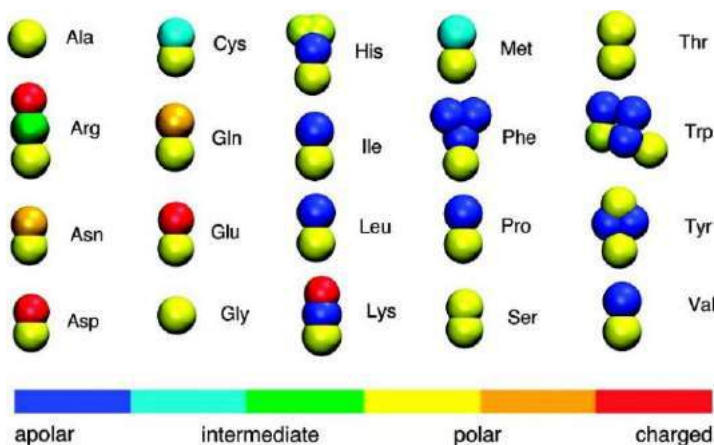


Figure 1.3: Representation of 20 amino acids in the MARTINI force field. Different colors represent different type of particle. (Reprinted with permission from reference 9e)

A computational protocol to design self-assembling protected tripeptides was developed Prof. Floudas and coworkers from 128 peptides library by using Ac-IVD mutations as the template.^{9f} Prof. Ulijn and co-workers demonstrated design rules for the creation of supramolecular architectures under aqueous, neutral pH conditions by studying 8,000 tripeptides using CG MARTINI force field.^{9d} The placement of selected amino acids in

a particular position in tripeptide promote self-assembly (Figure 1.4). Aromatic amino acids (F, Y and W) are very convenient for position 2 and 3 in tripeptide. Acid side chain containing amino acid (E and D) are favorable in position 3 as C-terminal. Positively charged amino acids, basic side chain containing amino acid and hydroxyl containing amino acids (K, R, S and T) are favourable in position 1 as N-terminal. Proline favours position 1 as N-terminal due to unique conformation. The average AP_H scores are used to know the self-assembling ability of tripeptide. A high AP_H score denotes high tendency to self-assemble into hydrogels.

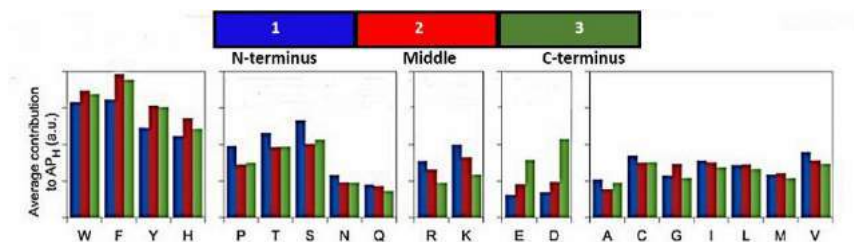


Figure 1.4: Average AP_H scores for tripeptides with the 20 amino acids. (Adapted from reference 9d)

1.2.3. Self-assembled nanostructures: As stated before, there are total 20 natural L-amino acids which serve as the basic units for all peptides and proteins present in humans. The possible combinations achieved by using 20 amino acids into peptide material makes it a very versatile field. Depending upon the arrangement of amino acids, peptides can have different properties

and self-assembled into different structures like nanotubes, nanofibers, nanorods, nanoribbons, nanosheets, nanowires, nanospheres, etc. The most frequent self-assembled structures obtained in peptides are discussed below:

Nanotubes: Nanometer-scaled tube-like structures with a definite inner hole are called Nanotubes.

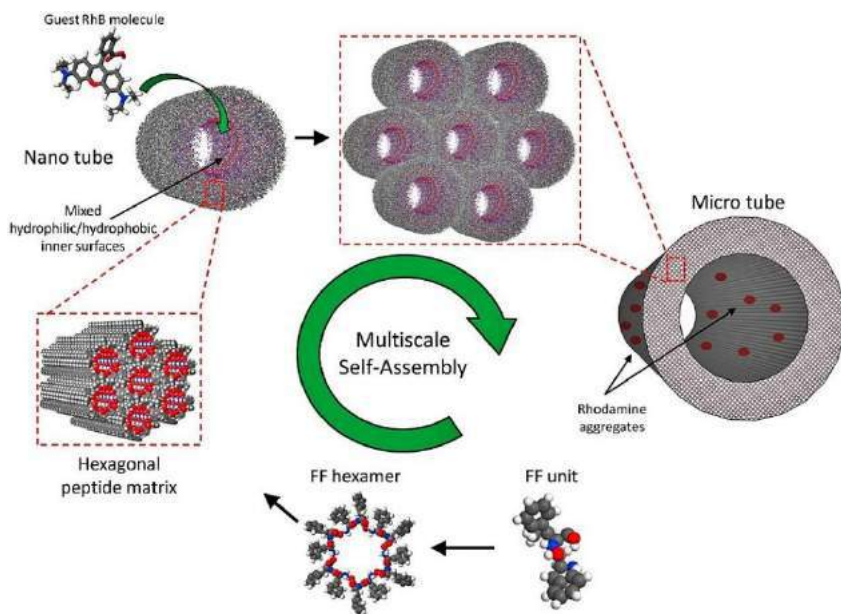


Figure 1.5: Schematic representation of the FF-microtubes formation and rhodamine B (RhB) loading. (Reprinted with permission from reference 10b)

A known example of nanotube forming peptide is diphenylalanine (FF), pioneered by Prof. Gazit and coworkers^{6a}

and obtained from Alzheimer's β -amyloid polypeptide. FF forms long tubular nanotubes with persistent length ($\sim 100 \mu\text{m}$) through π - π stacking interactions and hydrogen bonding interactions.^{10a} Basically, six FF units come together to form cyclic hexamers which stack to produce narrow channels resulting in the formation of self-assembled sheets which finally coil to produce nanotubes (Figure 1.5).^{10b}

Nanofibres and gels: Nanofibres are fibrous structures, diameter in nanometers. Amyloid polypeptides generally self-assemble to form nano-fibrils.^{11a} As shown in Figure 1.6, peptide monomers can self-assemble to form nanofibrils and gels.¹¹

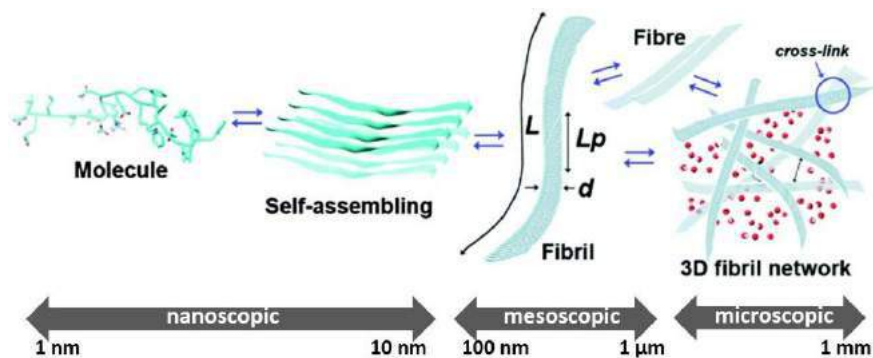


Figure 1.6: Nanofibrils formation from peptide monomer. (Adapted from reference 11a)

9-fluorenylmethoxycarbonyl protected diphenylalanine (Fmoc-FF) self-assemble to form nanofibrils in water which results

into a hydrogel formation. The self-assembly occurs probably due to H-bonding, hydrophobic interactions and π - π stacking.¹¹ Fmoc-FF formed a stiff and strong hydrogel which can stay stable at the broad range of temperature and pH. Prof. Ulijn and coworkers proposed a molecular model of Fmoc-FF hydrogel formation, revealing an antiparallel β -sheet alignment in the peptide. The formation of a cylindrical structure occurs due to interlocking of adjacent sheets through lateral π - π interactions (Figure 1.7).^{11j}

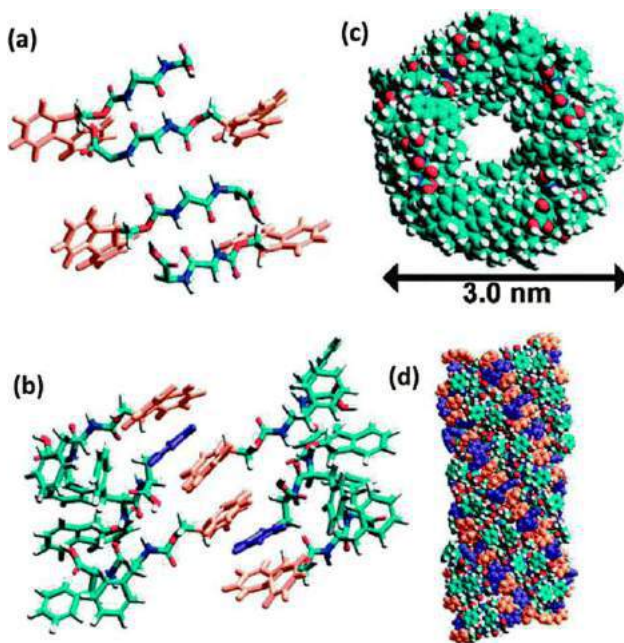


Figure 1.7: A model structure describing the antiparallel β -sheet arrangement of Fmoc-FF monomers in the hydrogel. (Reprinted with permission from reference 11j)

Recently, Prof. Bianco and co-workers have demonstrated the capacity of amino acid tyrosine alone to self-assemble into nanoribbons and fern-like structures.¹²

Nanosphere: Nanometer-scaled sphere-like hollow or solid core structures are called nanospheres. Various peptides are known to self-assemble into nanospheres or vesicles.¹³ An example is the diphenylglycine peptide, a simpler analogue which forms nanovesicles in aqueous solution, probably due to closure of self-assembled β -sheets along two axes (Figure 1.8).^{13a}

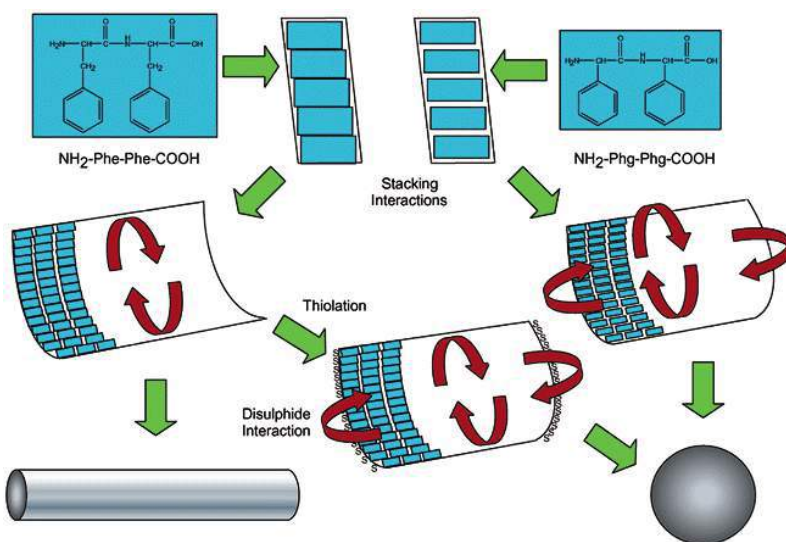


Figure 1.8: Schematic presentation of nanosphere formation in diphenylglycine peptide and comparison with diphenylalanine peptide nanotube formation. (Reprinted with permission from reference 13a)

As stated earlier in the beginning of this chapter, many kinetic factors can affect the outcome of self-assembled structures in the peptide. Levin, Mason *et al.* reported Boc-FF self-assembled into nanospheres which transform into nanotubes over time via Ostwald ripening (the change of structures to the most stable form with time) (Figure 1.9).^{14a}

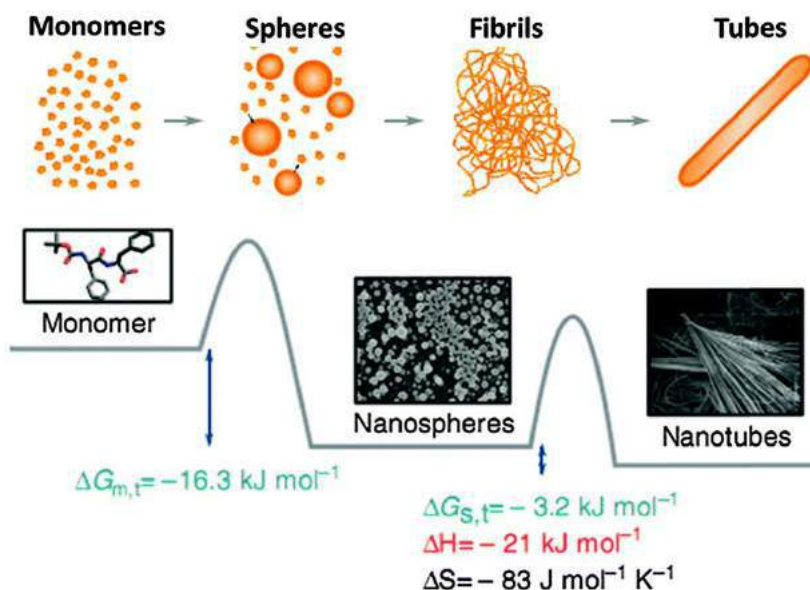


Figure 1.9: Schematic presentation of transition of nanospheres to fibers in Boc-FF. Free energy changes during the phase transition. (Reprinted with permission from reference 14a)

Recently, Prof. Kim and co-workers showed that self-assembly of covalent tyrosine-crosslinking of short peptide initiated by UV rays yielded different nanostructures at pH 10 in water or methanol solutions (Figure 1.10).^{14b}

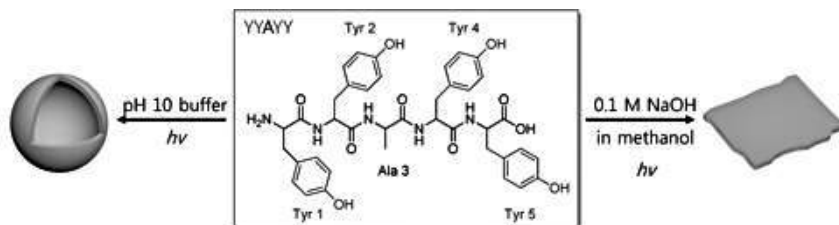


Figure 1.10: Diagrammatic representation of self-assembled nanostructures of tyrosine-based building blocks. (Reprinted with permission from reference 14b)

There are many reports in literature where peptides (short peptide, peptide amphiphiles and surfactant-like peptides) showed self-assembled supramolecular structures other than the ones being discussed above, for example, nanosheets, nanowires, nanorods, twisted nanofibers, nanotapes, nanocrystals, nano-necklaces etc.¹⁵ A detailed discussion about these is not in range for this chapter.

1.3. Folic acid self-assembly

Folic acid is an essential vitamin, required for synthesis of DNA, RNA, amino acids (methionine and serine), for cell division, red blood cell formation and preventing neural tube defects.¹⁶ Folic acid has been enormously studied in cancer-related research

because of the exceptional affinity to bind with folate receptors which are overly expressed in cancer cells.¹⁷

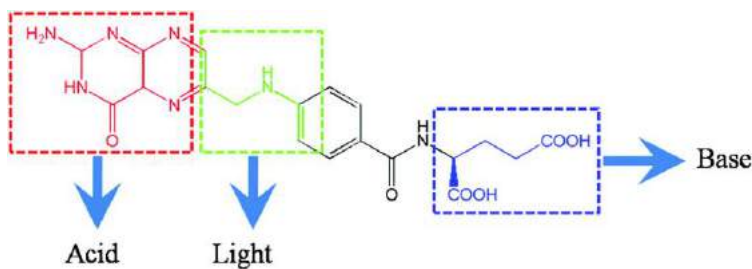


Figure 1.11: Molecular formula of folic acid and its sensitive groups which can be affected by three stimuli. (Adapted from reference 19a)

Folic acid exhibits green auto-fluorescence ($\lambda_{em} = 488$ nm)¹⁸ and is sensitive to heat, light, acid and bases (Figure 1.11).^{19a} The pterin ring in folic acid exists in two types of H-bonded structures: (a) Linear aggregation or ribbon-like style (H-type aggregation); (b) cyclic aggregation or disk-like style (J-type aggregation).¹⁹

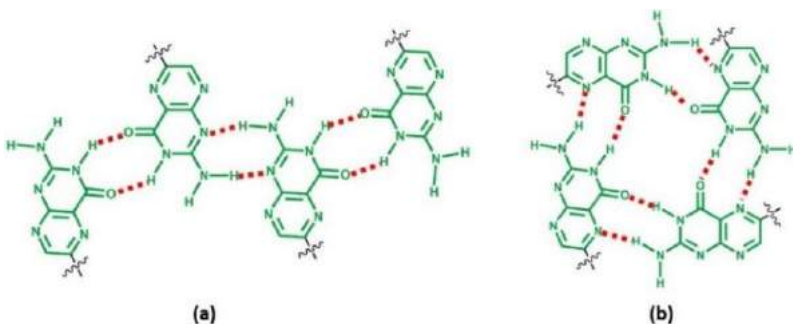


Figure 1.12: The pterin ring in folic acid self-assembled into (a) Linear aggregation style, (b) cyclic aggregation style. (Adapted from reference 19a)

G-quartet formation and liquid crystal (cholesteric and hexagonal mesophases) formation of folic acid and its salts in the presence of alkali metals has been well documented in literature.^{19e-19m} It formed various self-assembled architectures including vesicles, fibers/vesicles, fibers/nanoparticles, nanoparticles with increasing concentration in aqueous DMSO (Figure 1.13).^{19a}

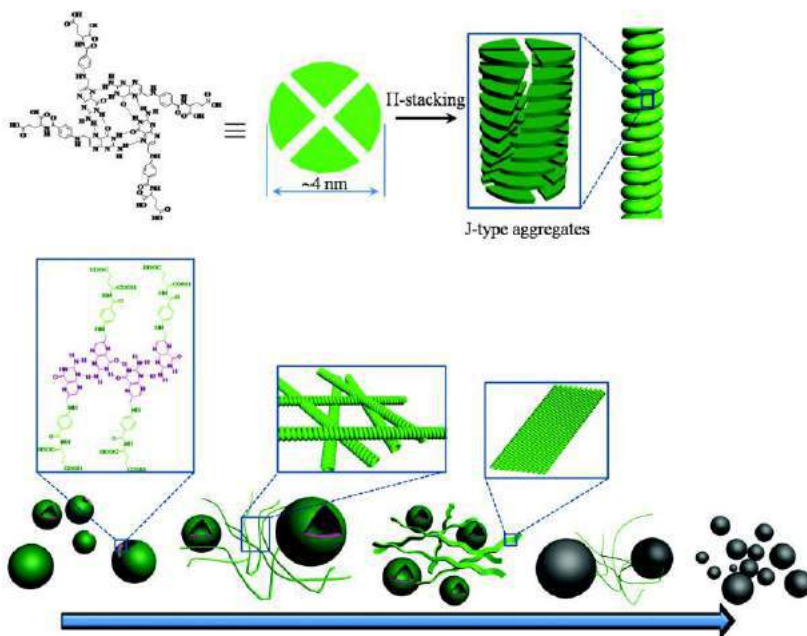


Figure 1.13: Schematic representation showing supramolecular architectures formation in case of folic acid with the increase of concentration. (Reprinted with permission from reference 19a)

1.4. Implication of peptide self-assembly and future outlook

The supramolecular architectures obtained from self-assembly of peptides or peptide amphiphiles have been reported to show various applications including bioimaging, biosensors, drug delivery agents, biomineralization, tissue engineering, nanomedicines and nanotechnology.

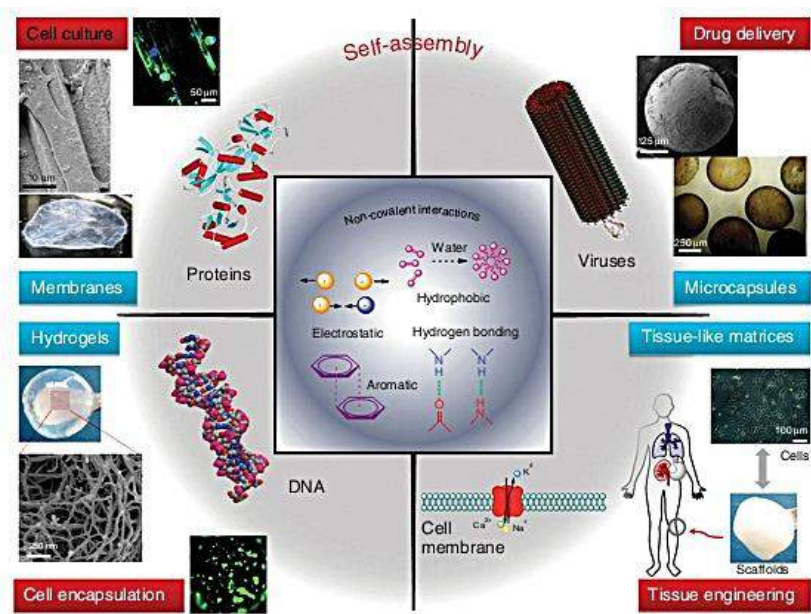


Figure 1.14: Peptide-based biomaterials for various applications in regenerative medicine. (Reprinted with permission from reference 20c)

1.4.1. Scaffolds for cell culture and tissue engineering:

Nanofibres and gel formation in peptide self-assembly is an attractive feature which makes it suitable for tissue engineering and regenerative medicine.²⁰ Zhou and coworkers developed a Fmoc-FF and Fmoc-RGD based bioactive hydrogel capable of mimicking extracellular matrix (ECM). The hydrogel displayed a suitable 3D cell culture model for the adhesion, spreading, and proliferation of dermal fibroblasts.^{20b} Several other examples of peptide for cell culture and tissue engineering usage are present in literature.^{20c,20d}

1.4.2. Skin care and cosmetic: Certain peptides and peptide amphiphiles can act as a surfactant along with fundamental biological functions including anti-microbial, anti-aging activities etc. Hence, they are of great potential in cosmetic industries.²¹ Peptide sequences are known to stimulate the growth of fibroblast cells, collagen formation.^{21f}

1.4.3. Nanofabrication and biomineralisation templates: A process with which ordered structured materials are produced biologically is called biomineralization. Self-assembling peptides can act as templates for nanofabrication and biomineralisation.²² Nanofibres have been reported to use as the template for growing CdS nanocrystals.^{22b} Self-assembling peptides have been utilized

for mineralization of hydroxyapatite for bone tissue engineering.²² FF nanotubes have been used as template to cast silver nanowires.^{6a}

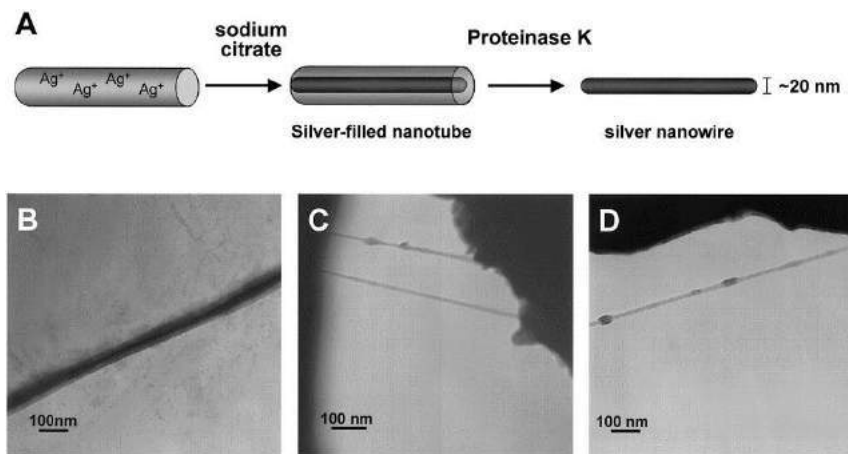


Figure 1.15: (A) Schematic presentation of casting of silver nanowires with FF nanotubes (B-D) TEM images showing formation of silver nanowires. (Reprinted with permission from reference 6a)

1.4.4. Drug Delivery: In medicinal and pharmaceutical fields, it is a challenging task to deliver the biologically active molecules or drugs in a controlled way to the desired target. Self-assembling peptides are smart materials which have been explored for the target-specific delivery of biologically important molecules (dyes, drugs, enzymes, antibodies etc.).²³ Webber and coworkers demonstrated the encapsulation of doxorubicin (anticancer drug) in peptide nanofibres and its release through enzymatic dissolution of peptides.^{23f}

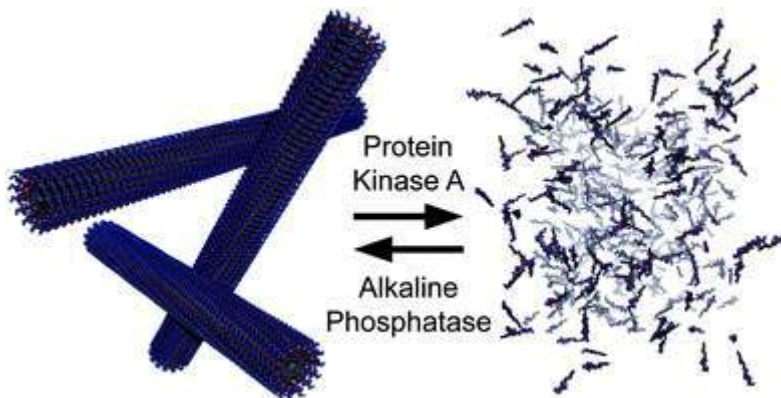


Figure 1.16: Schematic presentation of doxorubicin release from peptide nanofibres upon enzymatic reaction. (Reprinted with permission from reference 23f)

1.4.5. Bio-imaging: Self-assembling peptide has also been explored for cell imaging.²⁴ Optical properties of tryptophan have been used in cancer cell imaging by Zhang and co-workers. Zn(II) tryptophan-phenylalanine dipeptide nanoparticles (DNPs) have been used for bioimaging and sensing due to its intrinsic fluorescence signals ranging in the visible range of the spectrum.^{24a} The enhancement of fluorescence was due to metal coordination and π - π stacking. These visible fluorescent emitting DNPs were functionalized with aptamer and doxorubicin for targeting cancer cells and to monitor the drug release. Lu and coworkers reported a fluorescent peptide ZD2-Cy5, specific for glycoprotein, Extra domain-B fibronectin (EDB-FN) for bio-imaging and targeting

prostate cancer. ZD2 had the capability to bind EDB-FN produced by nude mouse prostate tumor xenographs and PC3 cells.^{24b}

Nano-electronics, nanoreactors, bone regenerating smart materials, biosensors are few more applications of self-assembling peptides. Beside such progress in the field, there are many unanswered questions for the better use of such material in various fields. The better understanding of structural design and self-assembly can help in improvement and exploit new applications in future.

In this thesis, various self-assembling peptides based on phenylalanine and tyrosine amino acids are synthesized in coming chapters. Natural (folic acid) and synthetic linkers (trimesic acid and dipicolinic acid) has been used to synthesize peptides for applications like catalysis, bio-imaging, capacitor studies etc.

1.5. References:

1. (a) Whitesides, G. M.; Grzybowski, B. *Science* **2002**, 295, 2418–2421. (b) Whitesides, G. M.; Mathias, J. P.; Seto, C. T. *Science* **1991**, 254, 1312–1319. (c) Kushner, D. J. *Bacteriol. Rev.* **1969**, 33, 302–345. (d) Mendes, A. C.; Baran, E. T.; Reis, R. L.; Azevedo, H. S.; *Wiley Interdiscip. Rev. Nanomed. Nanobiotechnol.* **2013**, 5, 582–612. (e) Philp, D.; Stoddart, J. F. *Angew. Chem. Int. Ed. Engl.* **1996**, 35, 1154–1196. (f) Winfree, E.; Liu, F.; Wenzler, L. A.; Seeman, N. C. *Nature* **1998**, 394, 539–544. (g) Neidle, S. *Oxford handbook of Nucleic acid Structure*. Oxford, U. K., Oxford Univ.

- Press; **1999**. (h) Korolkov, V. V.; Allen, S.; Roberts, C. J. *Faraday Discuss.* **2013**, *166*, 257–267. (i) Whitesides, G. M.; Mathias, J. P.; Set, C. T. *Science* **1991**, *254*, 1312–1319.
2. (a) De Santis, E.; Ryadnov, M. G. *Chem. Soc. Rev.*, **2015**, *44*, 8288–8300. (b) Zhao, X.; Pan, F.; Xu, H.; Yaseen, M.; Shan, H.; Hauser, C. A.; Zhang, S.; Lu, J. R., *Chem. Soc. Rev.* **2010**, *39*, 3480–3498. (c) Gazit, E. *Nat. nanotechnol.* **2016**, *11*, 309–310. (d) Ulijn, R. V.; Woolfson, D. N. *Chem. Soc. Rev.* **2010**, *39*, 3349–3350. (e) Gazit, E. *Chem. Soc. Rev.* **2007**, *36*, 1263–1269. (f) Bong, D. T.; Clark, T. D.; Granja, J. R.; Ghadiri, M. R. *Angew. Chem. Int. Ed.*, **2001**, *40*, 988–1011. (g) Zelzer, M.; Ulijn, R. V. *Chem. Soc. Rev.* **2010**, *39*, 3351–3357. (h) Zhaoab, X.; Zhang, S. *Chem. Soc. Rev.* **2006**, *35*, 1105–1110. (i) Kholkin, A.; Amdursky, N.; Bdikin, I.; Gazit, E.; Rosenman, G. *ACS Nano* **2010**, *4*, 610–614. (j) Matson, J. B.; Zha, R. H.; Stupp, S. I. *Curr. Opin. Solid State Mater. Sci.* **2011**, *15*, 225–235. (k) Salgado, E. N.; Radford, R. J.; Tezcan, F. A. *Acc. Chem. Res.* **2010**, *43*, 661–672.
3. (a) Lee, Y. S. Self-assembly and nanotechnology: A force balance approach, A John & Wiley Sons, Inc., Publication, **2008**. (b) Mahadevi A. S.; Sastry, G. N. *Chem. Rev.* **2016**, *116*, 2775–2825. (c) Adler-Abramovich, L., Vaks, L.; Carny, O.; Trudler, D.; Magno, A.; Caflisch, A.; Frenkel, D., Gazit, E. *Nat. Chem. Biol.* **2012**, *8*, 701–706. (d) Zhang, S. G. *Nat. Biotechnol.* **2003**, *21*, 1171–1178.
4. Wang, J.; Liu, K.; Xing, R.; Yan, X. *Chem. Soc. Rev.* **2016**, DOI: 10.1039/C6CS00176A.
5. (a) Mohamed, M. G.; Tu, J. H.; Huang, S. H.; Chiang, Y. W.; Kuo, S. W. *RSC Adv.* **2016**, *6*, 51456–51469. (b) Yang, P. P.; Zhao, X. X.; Xu, A. P.; Wang, L.; Wang, H. *J. Mater. Chem. B*, **2016**, *4*, 2662–2668. (c) Mondal, S.; Gazit, E. *ChemNanoMat* **2016**, *2*, 323–332. (d) Paramonov, S. E.; Jun,

- H. W.; Hartgerink, J. D. *J. Am. Chem. Soc.* **2006**, *128*, 7291–7298. (e) Israelachvili, J. N. *Intermolecular and Surface Forces*, Academic Press, San Diego, 3rd edn, **2011**, 151–167. (f) Chen, Y. *Cooperative Hydrogen-bonding in Models of Self-assembled Peptide Nanomaterials*, City University of New York, **2007**. (g) Lehn, J. M. *Science* **2002**, *295*, 2400–2403. (h) Shimizu, T.; Masuda, M.; Minamikawa, H. *Chem. Rev.* **2005**, *105*, 1401–1443.
6. (a) Reches, M.; Gazit, E. *Science* **2003**, *300*, 625–627. (b) Andersen, K. B.; Castillo-Leon, J.; Hedström, M.; Svendsen, W. E., *Nanoscale*, **2011**, *3*, 994–998. (c) Toksoz, S.; Acar, H.; Guler, M. O. *Soft Matter* **2010**, *6*, 5839–5849.
7. Castillo, J.; Sasso, L.; Svendsen, Self-Assembled Peptide Nanostructures: Advances and Applications in Nanobiotechnology, W. E. Taylor and Francis group, **2012**.
8. (a) Albrecht, M.; Stortz, P. *Chem. Soc. Rev.* **2005**, *34*, 496–506. (b) Zhang, S. *Nat. Biotechnol.* **2003**, *21*, 1171–1178. (c) Zou, R.; Wang, Q.; Wu, J.; Wu, J.; Schmuck, C.; Tian, H. *Chem. Soc. Rev.* **2015**, *44*, 5200–5219. (d) Przybyla, D. E.; Rubert, P.; Gleaton, C. M. J.; Nandwana, V.; Chmielewski, J. *J. Am. Chem. Soc.* **2013**, *135*, 3418–3422. (e) Jiang, H.; Kasten, B. B.; Liu, H.; Qi, S.; Liu, Y.; Tian, M.; Barnes, C. L.; Zhang, H.; Cheng, Z.; Benny, P. D. *Bioconjugate Chem.* **2012**, *23*, 2300–2312. (f) Lata, S.; Reichel, A.; Brock, R.; Tampé, R.; Pichler, J. *J. Am. Chem. Soc.* **2005**, *127*, 10205–10215.
9. (a) Ross, C. A.; Poirier, M. A. *Nat. Med.* **2004**, *10*, S10–S17. (b) Ulijn, R. V.; Smith, A. M. *Chem. Soc. Rev.* **2008**, *37*, 664–675. (c) Fleming, S.; Ulijn, R. V. *Chem. Soc. Rev.* **2014**, *43*, 8150–8177. (d) Frederix, P. W.; Scott, G. G.; Abul-Haija, Y. M.; Kalafatovic, D.; Pappas, C. G.; Javid, N.; Hunt, N. T.; Ulijn, R. V.; Tuttle, T. *Nat. chem.* **2015**, *7*, 30–37. (e)

- Monticelli, L.; Kandasamy, S. K.; Periole, X.; Larson, R. G.; Tieleman, D. P.; Marrink, S. J. *J. Chem. Theory Comput.* **2008**, *4*, 819–834. (f) Smadbeck, J.; Chan, K. H.; Khoury, G. A.; Xue, B.; Robinson, R. C.; Hauser, C. A.; Floudas, C. A. *PLOS Comput. Biol.* **2014**, *10*, e1003718.
10. (a) Reches, M.; Gazit, E. *Nano Lett.* **2004**, *4*, 581–585. (b) Silva, F. R.; Araujo, D. R.; Silva, E.; Ando, R. A.; Alves, W. *Langmuir* **2013**, *29*, 10205–10212.
11. (a) Schleegeer, M.; Deckert-Gaudig, T.; Deckert, V.; Velikov, K. P.; Koenderink, G.; Bonn, M. *Polymer* **2013**, *54*, 2473–2488. (b) Deng, M.; Yu, D.; Hou, Y.; Wang, Y. *J. Phys. Chem. B* **2009**, *113*, 8539–8544. (c) Hettiarachchi, C. A.; Melton, L. D.; Gerrard, J. A.; Loveday, S. M. *Biomacromolecules* **2012**, *13*, 2868–2880. (d) Tsurkan, M. V.; Ogawa, M. Y. *Biomacromolecules* **2007**, *8*, 3908–3913. (e) Zhang, S. G.; Gelain, F.; Zhao, X. J. *Semin. Cancer Biol.* **2005**, *15*, 413–420. (f) Mahler, A.; Reches, M.; Rechter, M.; Cohen, S.; Gazit, E. *Adv. Mater.* **2006**, *18*, 1365–1370. (g) Jayawarna, V.; Ali, M.; Jowitt, T. A.; Miller, A. E.; Saiani, A.; Gough, J. E.; Ulijn, R. V. *Adv. Mater.* **2006**, *18*, 611–614. (h) Raeburn, J.; Pont, G.; Chen, L.; Cesbron, Y.; Lévy, R.; Adams, D. J. *Soft Matter* **2012**, *8*, 1168–1174. (i) Dudukovic, N. A.; Zukoski, C. F. *Langmuir* **2014**, *30*, 4493–4500. (j) Smith, A. M.; Williams, R. J.; Tang, C.; Coppo, P.; Collins, R. F.; Turner, M. L.; Saiani, A.; Ulijn, R. V.; *Adv. Mater.* **2008**, *20*, 37–41. (k) Tao, K.; Levin, A.; Adler-Abramovich, L.; Gazit, E. *Chem. Soc. Rev.* **2016**, *45*, 3935–3953.
12. Ménard-Moyon, C.; Venkatesh, V.; Krishna, K. V., Bonachera, F.; Verma, S.; Bianco, A. *Chem. Eur. J.* **2015**, *21*, 11681–11686.
13. (a) Reches, M.; Gazit, E. *Nano letters* **2004**, *4*, 581–585. (b) Ghosh, S.; Reches, M.; Gazit, E.; Verma, S. *Angew. Chem.* **2007**, *119*, 2048–2050. (c) Wang, J. X.; Cai, T. T.; Li, J. L.; Zhuo, R. X.; Zhang, X. Z. *RSC Adv.* **2014**,

- 4, 14993–14996. (d) Matsuura, K.; Murasato, K.; Kimizuka, N. *J. Am. Chem. Soc.* **2005**, *127*, 10148–10149. (e) Mondal, S.; Swaroop, S.; Gurunath, R.; Verma, S. *Tetrahedron Lett.* **2010**, *51*, 6111–6115.
14. (a) Levin, A.; Mason, T. O.; Adler-Abramovich, L.; Buell, A. K.; Meisl, G.; Galvagnion, C.; Bram, Y.; Stratford, S. A.; Dobson, C. M.; Knowles, T. P. J.; Gazit, E. *Nat. Commun.* **2014**, *5*, 5219. (b) Min, K. I.; Yun, G.; Jang, Y.; Kim, K. R.; Ko, Y. H.; Jang, H. S.; Lee, Y. S.; Kim, K.; Kim, D. P. *Angew. Chem.* **2016**, *128*, 7039–7042.
15. (a) Marchesan, S.; Waddington, L.; Easton, C.D.; Winkler, D.A.; Goodall, L.; Forsythe, J.; Hartley, P.G. *Nanoscale* **2012**, *4*, 6752–6760. (b) Marchesan, S.; Easton, C. D.; Styan, K. E.; Waddington, L. J.; Kushkaki, F.; Goodall, L.; McLean, K. M.; Forsythe, J. S.; Hartley, P. G. *Nanoscale* **2014**, *6*, 5172–5180. (c) Ryu, J.; Park, C. B. *Adv. Mater.* **2008**, *20*, 3754–3758. (d) Marchesan, S.; Styan, K.; Easton, C. D.; Waddington, L.; Vargiu, A. V. *J. Mater. Chem. B* **2015**, *3*, 8123–8132. (e) Yuran, S.; Razvag, Y.; Rechtes, M. *ACS Nano* **2012**, *6*, 9559–9566.
16. (a) Lucock, M. *Mol. Gen. metab.* **2000**, *71*, 121–138. (b) Stokstad, E. L. R.; Koch, J. *Physiol. Rev.* **1967**, *47*, 82–116. (c) Blakley, R. L.; Benkovic, S. J. *Folates and Pterins*, Wiley, New York, **1984**. (d) J. D. Finkelstein, *J. Nutr. Biochem.* **1990**, *1*, 228–237. (e) E. Morrison, Y. H. Edwards, S. A. Lynch, *J. Med. Genet.* **1997**, *34*, 958–960.
17. (a) Chen, C.; Ke, J.; Zhou, X. E.; Yi, W.; Brunzelle, J. S.; Li, J.; Yong, E. L.; Xu, H. E.; Melcher, K. *Nature* **2013**, *500*, 486–489. (b) Low, P. S.; Henne, W. A.; Doorneweerd, D. D. *Acc. Chem. Res.* **2007**, *41*, 120–129. (c) Lu, Y.; Low, P. S. *Adv. Drug Deliv. Rev.* **2012**, *64*, 342–352. (d) Liu, W.; Nie, L.; Li, F.; Aguilar, Z. P.; Xu, H.; Xiong Y.; Fu, F.; Xu, H. *Biomater. Sci.* **2016**, *4*, 159–166. (e) Cal, P. M.; Frade, R. F.; Chudasama, V.; Cordeiro, C.; Caddick, S.; Gois, P. M. *Chem. Comm.* **2014**, *50*, 5261–5263.

- (f) Castillo, J. J.; Svendsen, W. E.; Rozlosnik, N.; Escobar, P.; Martínez, F.; Castillo-León, J. *Analyst* **2013**, *138*, 1026–1031. (g) Leamon, C. P.; Low, P. S. *Drug Discov. Today* **2001**, *6*, 44–51.
18. Tyagi, A.; Penzkofer, A. *Chem. Phys.* **2010**, *367*, 83–92.
19. (a) Xing, P.; Chu, X.; Ma, M.; Li, S.; Hao, A. *Phys. Chem. Phys.* **2014**, *16*, 8346–8359. (b) Würthner, F.; Kaiser, T. E.; Saha-Möller, C. R. *Angew. Chem., Int. Ed.* **2011**, *50*, 3376–3410. (c) Kanie, K.; Yasuda, T.; Ujiie, S.; Kato, T. *Chem. Comm.* **2000**, *19*, 1899–1900. (d) Goodby, J. W.; Collings, P. J.; Kato, T.; Tschierske, C.; Gleeson, H.; Raynes, P. *Handbook of Liquid Crystals 2nd Edition*, Wiley-VCH Verlag GmbH & Co. KGaA, **2014**, *5*, 513. (e) Kato, T.; Matsuoka, T.; Nishii, M.; Kamikawa, Y.; Kanie, K.; Nishimura, T.; Yashima, E.; Ujiie, S. *Angew. Chem., Int. Ed.*, **2004**, *43*, 1969–1972. (f) Davis, J. T. *Angew. Chem., Int. Ed.*, **2004**, *43*, 668–698 (g) Davis, J. T.; Spada, G. P. *Chem. Soc. Rev.* **2007**, *36*, 296–313. (h) Chakraborty, P.; Roy, B.; Bairiand, P.; Nandi, A. K. *J. Mater. Chem.* **2012**, *22*, 20291–20298. (i) Sakai, N.; Kamikawa, Y.; Nishii, M.; Matsuoka, T.; Kato T.; Matile, S. *J. Am. Chem. Soc.* **2006**, *128*, 2218–2219. (j) Kato, T. *Science* **2002**, *295*, 2414–2418. (k) Kato, T.; Matsuoka, T.; Nishii, M.; Kamikawa, Y.; Kanie, K.; Nishimura, T.; Yashima, E.; Ujiie, S. *Angew. Chem., Int. Ed.* **2004**, *43*, 1969–1972. (l) Bonazzi, S.; DeMoraes, M. M.; Gottarelli, G.; Mariani, P.; Spada, G. P. *Angew. Chem., Int. Ed.* **1993**, *32*, 248–250. (m) Motkar, G.; Lonare, M.; Patil, O.; Mohanty, S. *AIChE J.* **2013**, *59*, 1360–1368.
20. (a) Ghanaati, S.; Webber, M. J.; Unger, R. E.; Orth, C.; Hulvat, J. F.; Kiehna, S. E.; Barbeck, M.; Rasic, A.; Stupp, S. I.; Kirkpatrick, C. J. *Biomaterials* **2009**, *30*, 6202–6212. (b) Zhou, M.; Smith, A. M.; Das, A. K.; Hodson, N. W.; Collins, R. F.; Ulijn, R. V.; Gough, J. E. *Biomaterials* **2009**, *30*, 2523–2530. (c) Mendes, A. C.; Baran, E. T.; Reis, R. L.; Azevedo, H. S. *Wiley*

- Interdiscip. Rev. Nanomed. Nanobiotechnol.* **2013**, *5*, 582–612. (d) Collier, J. H.; Rudra, J. S.; Gasiorowski, J. Z.; Jung, J. P. *Chem. Soc. Rev.* **2010**, *39*, 3413–3424. (e) Mata, A.; Hsu, L.; Capito, R.; Aparicio, C.; Henriksone, K.; Stupp, S. I. *Soft Matter* **2009**, *5*, 1228–1236. (f) Harrington, D. A.; Cheng, E. Y.; Guler, M. O.; Lee, L. K.; Donovan, J. L.; Claussen, R. C.; Stupp, S. I. *J. Biomed. Mater. Res., Part A* **2006**, *78a*, 157–167.
21. (a) Kanlayavattanakul, M.; Lourith, N. *Int. J. Cosmet. Sci.* **2010**, *32*, 1–8. (b) Sun, L.; Lu, Z.; Bie, X.; Lu, F.; Yang, S. *World J. Microbiol. Biotechnol.* **2006**, *22*, 1259–1266. (c) Guglielmo, M.; Montanari, D. *U.S. Patent Application* **2002**, 10/481, 185. (d) Kanlayavattanakul, M.; Lourith, N. *Int. J. Cosmet. Sci.* **2010**, *32*, 1–8. (e) Robinson, L. R.; Fitzgerald, N. C.; Doughty, D. G.; Dawes, N. C.; Berge, C. A.; Bissett, D. L. *Int. J. Cosmet. Sci.* **2005**, *27*, 155–166. (f) Chirita, R.-I.; Chaimbault, P.; Archambault, J.-C.; Robert, I.; Elfakir, C. *Anal. Chim. Acta*, **2009**, *641*, 95–100.
22. (a) Dickerson, M. B.; Sandhage, K. H.; Naik, R. R. *Chem. Rev.* **2008**, *108*, 4935–4978. (b) Bose, P. P.; Banerjee, A. *J. Nanopart. Res.* **2010**, *12*, 713–718. (c) Hartgerink, J. D.; Beniash, E.; Stupp, S. I. *Science* **2001**, *294*, 1684–1688. (d) Zhao, X. B.; Pan, F.; Xu, H. Yaseen, M. Shan, H. H.; Hauser, C. A. E; Zhang, S. G.; Lu, J. R. *Chem. Soc. Rev.* **2010**, *39*, 3480–3498. (e) Sone, E. D.; Stupp, S. I. *J. Am. Chem. Soc.* **2004**, *126*, 12756–12757.
23. (a) Panda, J. J.; Chauhan, V. S. *Poly. Chem.* **2014**, *5*, 4418–4436. (b) Webber, M. J.; Appel, E. A.; Meijer, E. W.; Langer, R. *Nat. Mater.* **2016**, *15*, 13–26. (c) Koutsopoulos, S.; Zhang, S. G. *J. Control. Release* **2012**, *160*, 451–458. (d) Behanna, H. A.; Donners, J. J.; Gordon, A. C.; Stupp, S. I. *J. Am. Chem. Soc.* **2005**, *127*, 1193–1200. (e) Cheetham, A. G.; Zhang, P. C.; Lin, Y. A.; Lock, L. L.; Cui, H. G. *J. Am. Chem. Soc.* **2013**, *135*, 2907–2910. (f) Webber, M. J.; Newcomb, C. J.; Bitton, R.; Stupp, S. I. *Soft Matter*

- 2011**, 7, 9665–9672. (g) Aronsson, C.; Selegård, R.; Aili, D. *Macromolecules*, **2016**, 49, 6997–7003.
24. (a) Fan, Z.; Sun, L.; Huang, Y.; Wang, Y.; Zhang, M. *Nat. Nanotechnol.* **2016**, 11, 388–394. (b) Han, Z.; Zhou, Z.; Shi, X.; Wang, J.; Wu, X.; Sun, D.; Chen, Y.; Zhu, H.; Magi-Galluzzi, C.; Lu, Z. R. *Bioconjug. Chem.* **2015**, 26, 830–838. (c) Feyzizarnagh, H.; Yoon, D. Y.; Goltz, M.; Kim, D. S. *Wiley Interdiscip. Rev. Nanomed. Nanobiotechnol.* **2016**, 8, 730–743.

Chapter 2

General Experimental Procedures and Technique Details

2.1. Introduction

The essence of research is to seek the answers to problems. Regardless of the results, the experiments should be carried out with utmost care by minimizing probable mistakes. In a chemistry lab, it is very important to follow the proper guidelines and procedures for various reactions.

This chapter covers the purification of solvents and details of reagents required for synthesis of various peptides. All the chemicals were purchased from commercial sources and used as supplied unless otherwise stated. This chapter also includes the instruments, sample preparation procedures for the UV-Visible spectrophotometer, fluorescence spectrophotometer and microscopy.

2.2. Chemicals and Reagents

Amino acids and vitamins: L-phenylalanine, L-tyrosine, L-tryptophan, L-glycine, L-arginine, L-lysine, L-aspartic acid, L-cysteine were obtained from Spectrochem Pvt. Ltd., Mumbai, India. Folic acid (Vitamin B₉) and ascorbic acid were purchased from S. D. Fine-Chem Ltd., Mumbai, India.

Protecting agents for amino acids: Thionyl chloride, F-moc chloride, benzyloxy carbonyl chloride, trityl chloride were procured from Spectrochem Pvt. Ltd., Mumbai, India. Boc

anhydride (di-tert-butyl dicarbonate) was obtained from Avra synthesis Pvt. Ltd., Hyderabad, India.

Coupling agents for amino acids: N, N'-dicyclohexylcarbodiimide (DCC), 1-Ethyl-3-(3-dimethylaminopropyl) carbodiimide (EDC.HCl), N-hydroxybenzotriazole (HoBt), N-hydroxysuccinimide (NHS) were obtained from S. D. Fine-Chem Ltd., Mumbai, India.

Resins: Dowex 1-X8 (Strong anion exchange resin) was obtained from HiMedia Laboratories Pvt. Ltd. and Amberlite IR-120 (Strong cation exchange resin) were purchased from S. D. Fine-Chem Ltd., Mumbai, India.

Metal salts: Copper chloride, Copper sulphate, Zinc acetate, Zinc chloride, Zinc dust, Cobalt chloride, silver nitrate, Chloroauric acid, cadmium acetate, selenium powder, potassium carbonate, sodium carbonate, potassium carbonate, potassium chloride were obtained from (Rankem) Avantor Performance Materials India Ltd., Haryana, India. Ferric Chloride and Ferrous sulphate were purchased from S. D. Fine-Chem Ltd., Mumbai, India.

Anhydrous sodium sulphate, sodium chloride, sodium hydrogen carbonate were obtained from Titan Biotech Ltd., Rajasthan, India.

Acids: Glacial acetic acid was purchased from Merck Ltd., Mumbai, India. HCL was obtained from (Rankem) Avantor

Performance Materials India Ltd., Haryana, India. Nitric acid and sulphuric acid were obtained from Fisher Scientific India Pvt. Ltd., India. Trifluoroacetic acid (TFA) was obtained from Avra synthesis Pvt. Ltd., Hyderabad, India.

Other chemicals: 2,6-dipicolinic acid, trimesic acid, Ethylenediaminetetraacetic acid (EDTA), Silica gel for column chromatography were purchased from Merck Pvt. Ltd., Mumbai, India. Triethylamine was Avra synthesis Pvt. Ltd., Hyderabad, India.

Solvents: Dichloromethane (DCM), methanol (MeOH), ethyl acetate, N,N-dimethylformamide (DMF), ethanol (EtOH), tetrahydrofuran (THF), pyridine were obtained from Merck Ltd., Mumbai, India. Chloroform, petroleum ether, acetone, 1,4-dioxan, diethyl ether were obtained from RFCL Ltd., New Delhi, India. Dimethyl sulphoxide (DMSO), n-pentane, n-hexane were obtained from S.D. Fine-Chem Ltd. Mumbai, India. HPLC grade methanol, water, tetrahydrofuran, dichloromethane, isopropanol were purchased from RFCL Ltd., New Delhi, India.

Material for Cell assay: 3-(4, 5-Dimethylthiazol-2-yl)-2, 5-diphenyltetrazolium bromide (MTT), trypsin-EDTA, Dulbecco's modified eagle's medium (DMEM), penicillin-streptomycin antibiotic, bisBenzimide H 33258 and gelatin (from cold water fish

skin) were purchased from Sigma-Aldrich (Bangalore, India) and used without further purification. Dimethyl sulphoxide (DMSO) was obtained from Merck (Bangalore, India). Fetal bovine serum and CellMask™ Deep Red Plasma Membrane stain was purchased from Gibco® Life Technologies (Bangalore, India).

2.3. Purification of solvents and reagents¹

Dichloromethane (DCM): Calcium hydride^{1d} was used to store the laboratory grade DCM for 12 h and distilled. The solvent was stored in brown bottles over activated 4 Å molecular sieves for 1-2 days. The solvent was handled under nitrogen with the aid of T-joint piece.

Methanol (MeOH): The commercial grade MeOH was refluxed over freshly activated calcium oxide for 6 h and distilled. Distilled MeOH was dried over activated magnesium turnings and distilled under the nitrogen atmosphere. The resulting dry MeOH was stored in brown bottles over activated 4 Å molecular sieves for 1-2 days. The solvent was handled under the nitrogen atmosphere.

N, N-dimethylformamide (DMF): Azeotropic distillation with benzene followed by treatment with activated alumina to remove all traces of water present in DMF. The solvent was distilled under reduced pressure and stored over activated 4 Å molecular sieves

for 1-2 days. The solvent was handled under the nitrogen atmosphere.

Dimethyl sulfoxide (DMSO): Freshly activated alumina was used to store the analytical grade DMSO for 12 h. After filtration, the solvent was distilled over calcium hydride under reduced pressure and stored over 4 Å molecular sieves for 1-2 days. The solvent was handled under the nitrogen atmosphere.

Triethylamine (TEA): Potassium hydroxide pellets were used to store the commercial grade TEA for 24 h. followed by reflux for 3h. TEA was distilled and stored in amber coloured bottles over potassium hydroxide pellets.

N-hydroxysuccinimide (NHS): Ethyl acetate was used as the solvent for recrystallization of commercially available NHS.

1-hydroxy benzotriazole (HOBt): 50% aqueous ethanol was used as the solvent for recrystallization of commercially available HOBt.

2.4. Instrumentation:

High-Resolution mass spectroscopy (HRMS): High-resolution mass spectra were recorded on Waters Q-ToF Premier Micromass HAB 213 mass spectrometer (Waters Ltd., Manchester, U.K.) using capillary voltage 2.6-3.2 kV. The samples dissolved in

suitable solvents were introduced into the HRMS source through a syringe pump at the rate of 3 $\mu\text{L}/\text{min}$.

Nuclear magnetic resonance spectroscopy (NMR): ^1H and ^{13}C NMR were recorded either on JEOL-JNM LAMBDA 400 (JEOL Ltd., Tokyo, Japan) model operating at 400 and 100 MHz, respectively or on JEOL ECX-500 model (JEOL Ltd., Tokyo, Japan) operating at 500 MHz and 125 MHz respectively. The chemical shifts were referenced with respect to tetramethylsilane.

Fourier Transfer infrared spectroscopy (FTIR): FTIR spectra were recorded on a Bruker FT-IR Vector 22 model (Bruker, Massachusetts, USA) from 400-4000 cm^{-1} .

High-performance liquid chromatography (HPLC): HPLC was recorded with 1200 infinity series system from Agilent Technology.

Melting Point: Melting points of the synthesized compounds were measured with the help of DBK-programmable melting point apparatus (Model DBK 5067/1; DBK instruments, Mumbai, India).

UV-Vis Spectrophotometer: Absorption spectra were recorded on CARY 100 Bio UV-Vis spectrophotometer with 10 mm quartz cell at 25 ± 0.1 $^{\circ}\text{C}$.

Fluorescence Spectrophotometer: Fluorescence spectra were recorded on Varian Luminescence Cary eclipsed spectrophotometer with 10 mm quartz cell at 25 ± 0.1 $^{\circ}\text{C}$.

Optical microscopy (OM): OM images were acquired on Leica DM2500M microscope, equipped with a fluorescence laser and DFC420 camera.

Fluorescence Microscopy (FM): Dye stained samples were examined under a fluorescent microscope (Leica DM2500M), provisioned with a rhodamine filter (absorption 540 nm/emission 625 nm).

Scanning electron microscopy (SEM): SEM images were acquired on FEI Quanta 200 microscope, equipped with a tungsten filament gun, operating at WD 3 mm and 10 kV.

Focused Ion Beam-Scanning Electron Microscopy (FIB-SEM): FIB-SEM images were acquired on FEI make Nova 600 Nanolab workstation equipped with a field emission Ga ion source, operating at 14 KV.

Transmission electron microscopy (TEM): Samples were viewed using a JEOL 1200EX electron microscope operating at 80 kV.

Atomic force microscopy (AFM): AFM Samples were imaged with an atomic force microscope (Molecular Imaging, USA) operating under the Acoustic AC mode (AAC), with the aid of a cantilever (NSC 12(c) from MikroMasch). The force constant was 0.6 N/m, while the resonant frequency was 150 kHz. The images were taken at room temperature, with the scan speed of 1.5-2.2

lines/sec. The data acquisition was done using PicoView 1.4® software, while the data analysis was done using PicoView.

Confocal laser scanning microscopy: Cell assays samples were observed under confocal laser scanning microscope (CLSM, Leica sp5, Germany).

Electrospinning: Electrospun fibrous mats were synthesized on a Super ES-2 model electrospinning unit (E-Spin Nanotech Pvt. Ltd., SIBDI Innovation and Incubation Centre, IIT Kanpur).

2.5. Ion exchange chromatography

Anion exchange resin (Dowex 1-X8): The commercially available Dowex 1-X8 was washed with 2N NaOH (100 mL) and the excess of NaOH was removed by washing with triple distilled water, monitored by pH paper till it becomes neutral. Then, this resin was used for the exchange of anions with OH⁻.

Cation exchange resin (Amberlite IR-120): The commercially available amberlite IR-120 was washed with 2N HCl (100 mL) and the excess of HCl was removed by washing with triple distilled water, monitored by pH paper till it becomes neutral. Then, this resin was used for the exchange of cations with H⁺.

2.6. Sample Preparation

UV-Vis Studies and Fluorescence Studies: The solutions were prepared in HPLC methanol for the UV-Vis and fluorescence studies.

Microscopy sample preparations: 10 μ L aliquots of the samples were deposited on a suitable surface (glass surface, silicon wafer, copper grids or HOPG (highly ordered pyrolytic graphite) surface) and allowed to dry at room temperature. Subsequently, the samples were dried *in vacuo* for 30 min prior to imaging.

10 μ L aliquots of the sample were placed on a 400-mesh carbon coated copper grid for TEM samples. After 1 min any excess fluids were removed. Due to the present of metal samples were imaged without any further staining.

SEM samples were imaged with and without (for EDX) gold coating.

For confocal laser scanning microscopy, Cells (10^4 cells/well) were seeded on a sterilized glass cover slip (13 mm, 0.2% gelatin-coated) for 10 h. To study cellular uptake of peptides by confocal laser scanning microscopy, a solution of peptides were added to the cell culture media which was incubated at 37 °C with 5% CO₂ humidified incubator. After incubation cells were washed thrice with PBS buffer and fixed with 4% formaldehyde solution for 20 min. After washing, cells were stained with deep red plasma

membrane dye and washed again with PBS buffer. Coverslips were then mounted on slides coated with buffered mounting medium to prevent fading and drying.

2.7. X-ray structure analysis

Single Crystal of the peptide was coated with light hydrocarbon oil and mounted in the 100 K dinitrogen stream of a Bruker SMART APEX CCD diffractometer equipped with CRYO Industries low-temperature apparatus and intensity data was collected using graphite-monochromated Mo K α radiation. The data integration and reduction were processed with the SAINT software.¹ An absorption correction was applied.² Structure was solved by the direct method using SHELXS-97 and refined on F^2 by a full-matrix least-squares technique using the SHELXL-97 program package.³ Non-hydrogen atoms were refined anisotropically. In the refinement, hydrogens were treated as riding atoms using the SHELXL default parameters.

2.8. References

1. (a) Leonard, J.; Lygo, B.; Procter, G. *Advanced Practical Organic Chemistry*, 3rd edition, CRC Press, **2013** (b) Armarego, W. L. F.; Chai, C. *Purification of Laboratory Chemicals*, 7th Edition, Butterworth-Heinemann, **2012** (c) Furniss, B. S.; Hannaford, A. J.; Smith, P. W. G.;

Tatchel, R. R. *Vogel's Text book of Practical Organic Chemistry*, 5th edition, ELBS and Longman: London, **1989**.

(d) Williams, D. B. G.; Lawton, M. J. *Org. Chem.* **2010**, 75, 8351–8354.

2. SAINT+, 6.02 ed.; Bruker AXS, Madison, WI, **1999**.
3. Sheldrick, G. M. SADABS 2.0; University of Gottingen: Gottingen, Germany, **2000**.
4. Sheldrick, G. M.; University of Goettingen, Germany, **1997**.

Chapter 3

One- and Two Dimensional Nano-island Growth in C₃ Symmetric Molecule

3.1. Introduction

Understanding the driving force for the formation of self-assembled structures is an essential step for designing bio-inspired materials for various applications.¹ The design of molecule plays an important role, as the functional groups present in molecule dictate the outcome of self-assembled structures. The detailed understanding of the molecular arrangement in self-assembled monolayers is an essential step in the fabrication of molecular devices.² It is valuable to explore the structural details of organic molecules on various surfaces for refining their part and capability in the applications. The arrangement of monolayer of organic molecules on various solid surfaces depends mainly on the molecular size and molecular symmetry of the organic moieties, as well as on the lattice arrangement of the solid surface used.³ Different types of structures are reported depending on the nature of the interaction.⁴

C₃ symmetric molecules play an important role in nature⁵, for example, triskelion-shaped clathrin molecules, which help in endocytosis, facilitate the formation of nano-cage like supramolecular architectures.⁶ Benzene tricarboxylic acid (BTA), a C₃ symmetric molecule, has been widely used in synthetic fiber, plasticizer, antiseptic, cross-linking agents to prepare extended assemblies, dendrimers and reverse osmosis membrane materials.⁷

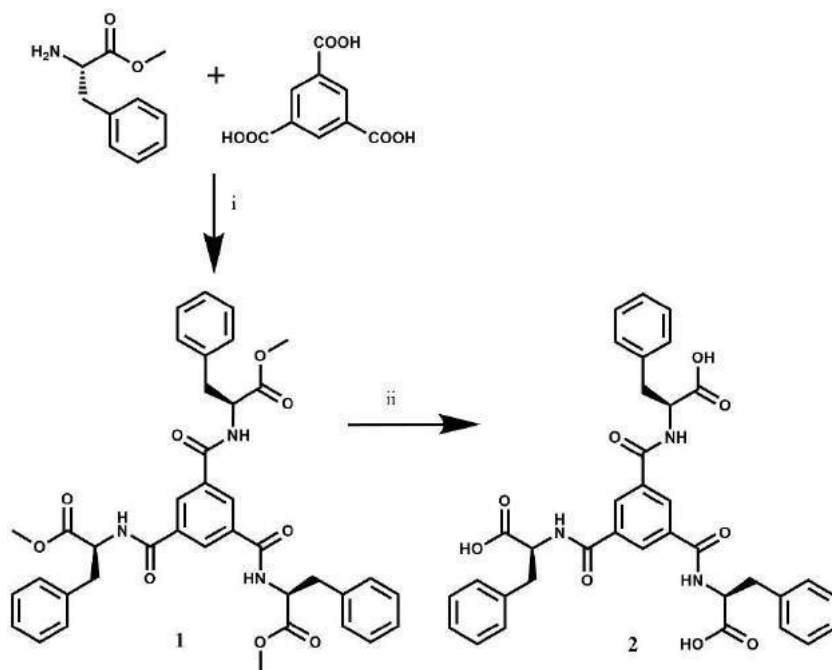
It is a planar molecule with flexible carboxylic acid groups, capable of forming hydrogen bonding and π - π stacking interactions. Two-dimensional (2-D) assemblies of BTA molecule and its derivatives have been extensively studied through many techniques such as circular dichroism (CD), UV-Vis, STM and various theoretical methods.^{8,9}

The conjugation of carboxylic acid groups of BTA with amino acid side chains offer biocompatibility, biodegradability and possibility of producing enantiopure chiral structures with enantioselective synthesis or detection capability.¹⁰ Moreover, amino acid side chains can play an important role in formation of self-assembled structures because of their capability to form hydrogen bonding, π - π stacking interactions (in aromatic amino acid chains) and metal ion interactions. Crystal structures of a few BTA amino acid derivatives has also been reported in literature.¹¹ Atomic force microscopy (AFM) is a particularly useful tool to investigate the detailed structural arrangements of organic molecule monolayers on various solid surfaces up to very high (atomic or submolecular) resolutions. In this study, we have synthesized L-phenylalanine derivative of BTA moiety and studied the assemblies formed in ultrathin layer of BTA L-phenylalanine derivative on the basal plane of Highly Oriented

Pyrolytic Graphite (HOPG) at ambient condition through atomic force microscopy.

3.2. Synthesis and Characterization

The peptide was synthesized through solution phase synthesis as shown below:



Scheme 1: Synthetic scheme for peptide 2: (i) HOBt, DCC, 0 °C, TEA, N₂ atm. (ii) 6 N NaOH, MeOH, 6 h.

Trimesic acid tris L-phenylalanine methyl ester conjugate (1):

Trimesic acid (0.50 g, 2.37 mmol), and HOBt (1.09 g, 7.13 mmol)

were dissolved in dry DMF (15 mL) under nitrogen atmosphere and the reaction mixture was cooled to 0 °C in an ice bath. A solution of DCC in DCM (1.47 g, 7.13 mmol) was then added dropwise to the reaction mixture. The reaction mixture was stirred at 0 °C for 1 h, after which, L-phenylalanine methyl ester hydrochloride (1.63 g, 7.58 mmol) was added to it followed by triethylamine (2.313 mL, 16.5 mmol). The reaction mixture was monitored and stirred for 24 h at room temperature under nitrogen atmosphere. The reaction mixture was concentrated *in vacuo*, redissolved in ethyl acetate and filtered to remove DCU. The organic layer was then washed with 1N HCl (3×30 mL), 10% NaHCO₃ (3×30 mL) and brine (30 mL). The organic layer was dried over anhydrous sodium sulfate and concentrated *in vacuo*. The crude compound was purified by silica gel column chromatography by using DCM and methanol (98:2) solvent system to isolate pure **1** (0.365 g, 72% yield). m.p. 199–203 °C, R_f [4% methanol in DCM] = 0.5; ¹H NMR (500 MHz, d₆-DMSO, TMS, δ ppm): 3.06-3.16 (m, 6H), 3.61 (s, 9H), 4.64-4.69 (m, 3H) 7.15-7.26 (m, 15H), 8.33 (s, 3H), 9.11-9.14 (m, 3H); ¹³C NMR (125 MHz; d₆-DMSO, δ ppm): 37.8, 52.5, 54.9, 127.0, 128.8, 129.5, 134.7, 166.1, 172.5; HRMS (M+H)⁺ for C₃₉H₄₀N₃O₉: 694.2765 (Calcd.), 694.2767 (Anal.).

Trimesic acid tris-l-phenylalanine conjugate (2): 1 (0.1 g, 0.144 mmol) was dissolved in methanol to form a clear solution. To this 6N NaOH (0.03 g, 0.865 mmol) was added and stirred for 6 h at room temperature. The solution obtained was passed over activated cation exchange resin. The filtrate was evaporated under reduced pressure to obtain pure **2** (0.07 g, 72.9% yield). ¹H NMR (400 MHz, d₆-DMSO, TMS, δ ppm): 2.97-3.22 (m, 6H), 4.40-4.48 (m, 3H), 7.04-7.19 (m, 15H), 8.13-8.15 (m, 3H), 8.30-8.31 (m, 3H); ¹³C NMR (100 MHz; d₆-DMSO, δ ppm): 36.8, 54.8, 126.9, 128.7, 129.5, 134.9, 138.5, 166.1, 173.4; HRMS (M-H)⁺ for C₃₆H₃₄N₃O₉: 652.2295 (calcd.), 652.2297 (Anal.).

3.3. Microscopy Studies:

Optical Microscopy: OM images were acquired on Leica DM2500M microscope, equipped with a bright and dark field imaging.

Field Emission Scanning Electron Microscopy (FE-SEM):

10 μL aliquots of the samples were deposited on a silicon wafer and allowed to dry at room temperature. Subsequently, the samples were dried in vacuo for 30 min prior to imaging. The samples were imaged with and without (for EDX) gold coating. SEM images were acquired on FEI Quanta 200 microscope, equipped with a tungsten filament gun, operating at WD 4 mm and 10 kV.

Atomic force microscopy (AFM):

Freshly prepared HOPG surface (ZYG grade from μ -masch) was used as a substrate for the preparation of ultrathin films. 3-4 μL of 10^{-6} M solution was drop casted on graphite by positioning the surface at an angle of $\sim 30^\circ$ to make sure the smooth flow of the solution. After air drying, AFM studies were carried out at an ambient condition where temperature (23–25 $^\circ\text{C}$) and relative humidity ($\sim 50\%$) were maintained using air conditioning. All measurements were performed on Agilent Technologies 5500 scanning probe microscope in intermittent contact mode. Aluminum coated silicon cantilevers (Budget sensors) were used as AFM probes. During scanning, cantilevers had resonance frequency around 270 kHz and force constant was around 35 N/m. Images were processed using WSxM software from Nanotec.¹²

3.4. Results and Discussions:

3.4.1. Solution phase self-assembly: We designed and synthesized benzene tricarboxylic acid (BTA) based C_3 symmetric molecule by chemically conjugating it with L-phenylalanine amino acid. BTA is a planar molecule and has the ability to crystallize from water in hydrogen-bonded networks with wide unidimensional empty channels.¹³

Molecule **1** with protected caboxylic ends, was studied for the self-assembled behavior in methanol at 1 mM concentration on silicon (100) surface and discovered to form two different kinds of supramolecular architectures- long nanofibers and small nanorods simultaneously. The probable interactions for the formations of these self-assembled structures could be π - π interactions due to aromatic rings and hydrogen bonding interactions of amide/ester bonds. A simple change of ester moieties to acid group in molecule **2** resulted in formation of uniform long nanofibers with diameter \sim 70-90 nm (Figure 3.1).

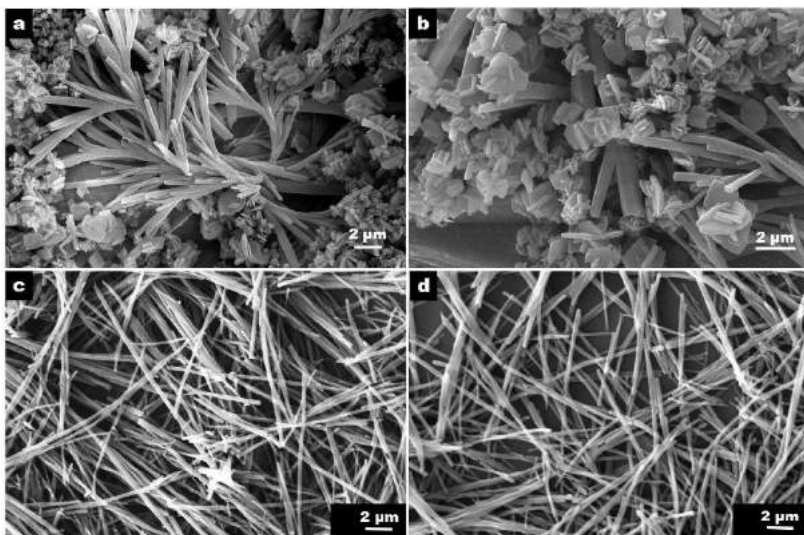


Figure 3.1. (a,b) SEM images of **1** (1mM, MeOH, Si wafer) (c,d) SEM Images of **2** (1mM, MeOH, Si wafer).

Further, upon diluting **2** sample resulting in the formation of small spherical structures along with nanofibers (Figure 3.2).

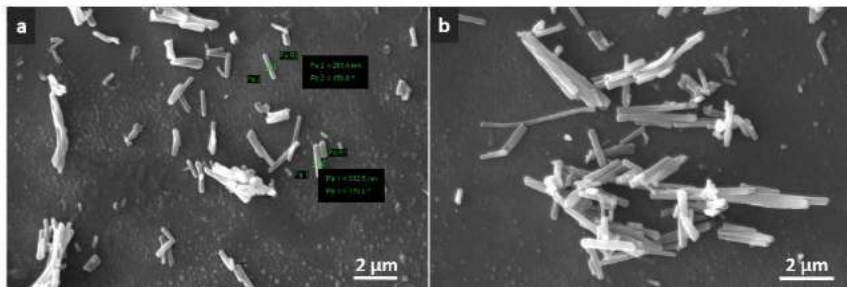


Figure 3.2. (a,b) SEM images of **2** (10 μM, MeOH, Si wafer).

3.4.2. Atomic force microscopy and DREIDING force field analysis: The self-assembled structures of **2** were further analyzed through atomic force microscopy to understand molecular level arrangements. The ultrathin film of **2** was studied for molecular assembling behaviors on HOPG (0001) surface.

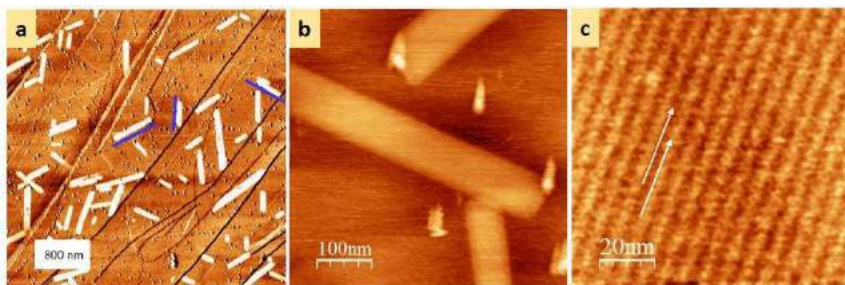


Figure 3.3. (a-c) AFM images of **2** (10 μM, MeOH, HOPG surface).

AFM images revealed the presence on two kinds of molecular self-assembled structures on HOPG surface similar to Si wafer (Figure 3.3). These structures were classified into one-dimensional (long edged long molecular aggregation) and two-dimensional (spherical aggregation) islands depending on the nature of aggregation.

One-dimensional (1-D) islands appeared bright in phase diagram due to the positive phase shift. 1-D islands were assigned as crystalline regions, with apparent height 0.6 ± 0.1 nm which agreed with the typical height of a monolayer. A statistical analysis was performed to understand the relative orientation of those islands with respect to HOPG. Analysis over several frames showed that the location of major peaks was around 2° , 63° and $122 \pm 5^\circ$ (Figure. 3.4).

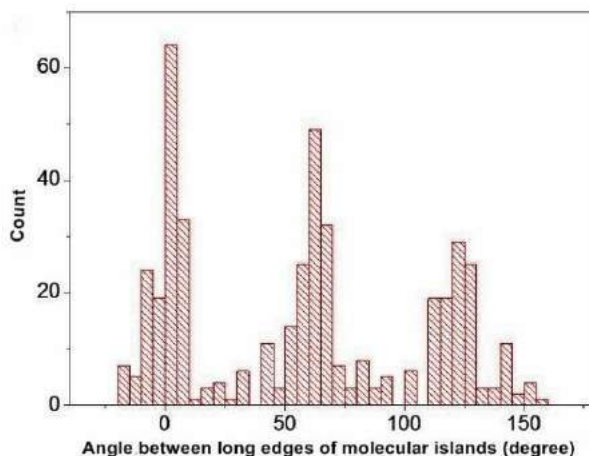


Figure 3.4. A statistical analysis of relative orientation of One-dimensional islands with respect to HOPG.

It implied that 1-D islands were following three graphite lattice directions. The electron rich system of **2** molecule might be interacting with graphite lattice symmetry through π - π interactions. High-resolution images revealed the molecular level ordering of 1-D islands which consisted of bright and dark strips (Figure 3.3 b,c). The interval between two neighboring molecular chains was ~ 6.2 nm. Height variation between the adjacent rows of different contrast was found out to be ~ 0.1 nm. This variation was not consistent with the typical apparent height of a monolayer, confirming that the dark strips were formed due to self-assembly of molecule. The width of both kinds of strips was calculated to be in between 2.9-3.2 nm which was double the size of a single **2** molecule. As tip apex has its limitation to resolve the features smaller than 3 nm, we assume that each strip corresponds to two molecular rows. Further, DREIDING force field method was used to understand the molecular level picture. A dimer was optimized as a building unit with $-\text{COOH}$ groups facing each other with the possibility to form eight hydrogen bonds (Figure 3.5 a). A lattice was grown with the optimized dimer structure (Figure 3.5 b) with unit cell vectors A (horizontal line) and B (vertical line) marked with green lines. Along the A vector, dimers interacted through

four hydrogen bonds but along B, there was a high possibility of π - π stacking between the phenyl groups of dimers.

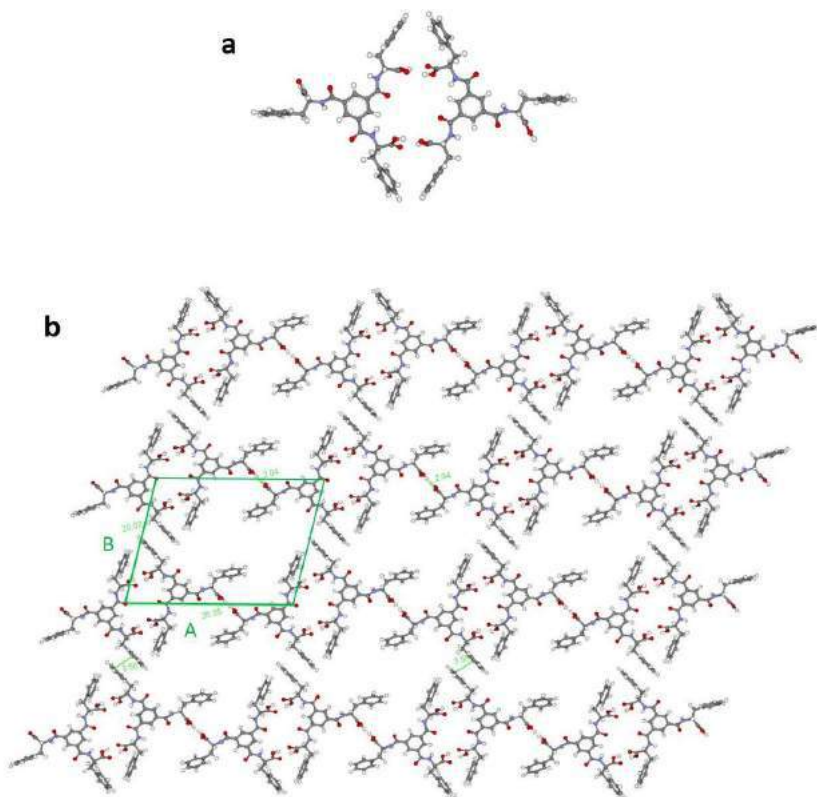


Figure 3.5. a) Optimized dimer geometry of **2** molecules using a force field. b) The possible self-assembled pattern for the observed 1D-island.

In the DREIDING force field method, typical $\text{-C=O}\cdots\text{H-O-}$ bond energy is considered approximately 9 Kcal mol^{-1} and for π - π stacking interactions, bond energy is variable around $2\text{-}3 \text{ Kcal}$

mol^{-1} .¹⁴ The interaction energy along A was calculated to be approximately 30 Kcal mol^{-1} ($-\text{C}=\text{O} \cdots \text{H}-\text{O}-$ interactions) and along B it was approximately 3 Kcal mol^{-1} ($\pi-\pi$ interaction). It revealed that the growth of islands along the direction of vector A was 10 times more favorable than that of vector B. These outcomes perfectly summarized the shape of 1-D islands.

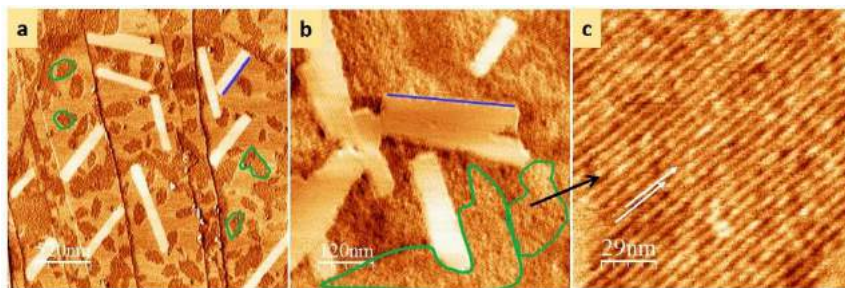


Figure 3.6. (a-c) AFM images of **2** (10 μM , MeOH, HOPG surface).

Along with 1-D islands, several dark spherical self-assembled structures (highlighted with green lines, Figure 3.6) were observed designated as two-dimensional (2-D) islands (considering the aspect ratio of these islands). A high-resolution image of these regions showed periodic patterns similar to 1-D islands. These images depicted molecular level ordering within those regions due to the presence of dark and light strips. Statistical analysis showed that direction of these molecular strips within

molecular layers was also following graphite lattice direction like 1D-islands. The apparent height difference between successive rows (marked by white arrows in Figure 3.6 c) was approximately 0.15 nm which was higher in comparison with the thickness of 1-D islands. The interval between neighboring molecular chain was 5.6 nm which was few angstrom lesser than 1-D islands, revealing that 2-D islands were compactly packed as compared to 1-D islands. Although both kinds of islands followed the symmetry of surface, adsorption geometry of molecule due to intermolecular interaction could be different. Different adsorption geometry of **2** on HOPG could lead to enhancement in intermolecular interactions namely -C=O·····H-O- (B.E. ~ 9 Kcalmol⁻¹), -C=O·····H-N- (B.E. ~ 8 Kcalmol⁻¹) and π - π stacking (B.E. ~ 3 Kcalmol⁻¹) leading to 2-D growth. This understanding was supported by proposing a model of 2-D assemblies based on an optimized geometry of a dimer using DREIDING force field method (Figure 3.7a). A lattice was grown with this optimized dimer structure (Figure 3.7b) with unit cell vectors A (horizontal line) and B (vertical line) marked with blue lines. It was observed that molecules were interacting with each other equally through hydrogen bonding along both A and B vectors. It was clear from the molecular picture that the assembly adopted three-fold symmetry on the HOPG surface (angle between two vectors $\sim 120^\circ$). Packing density for 2-D growth was found to

be 0.38 molecules/nm² whereas the packing density for the 1-D region was relatively less *i.e.* 0.32 molecules/nm² and thus supported the experimental observation difference in packing.

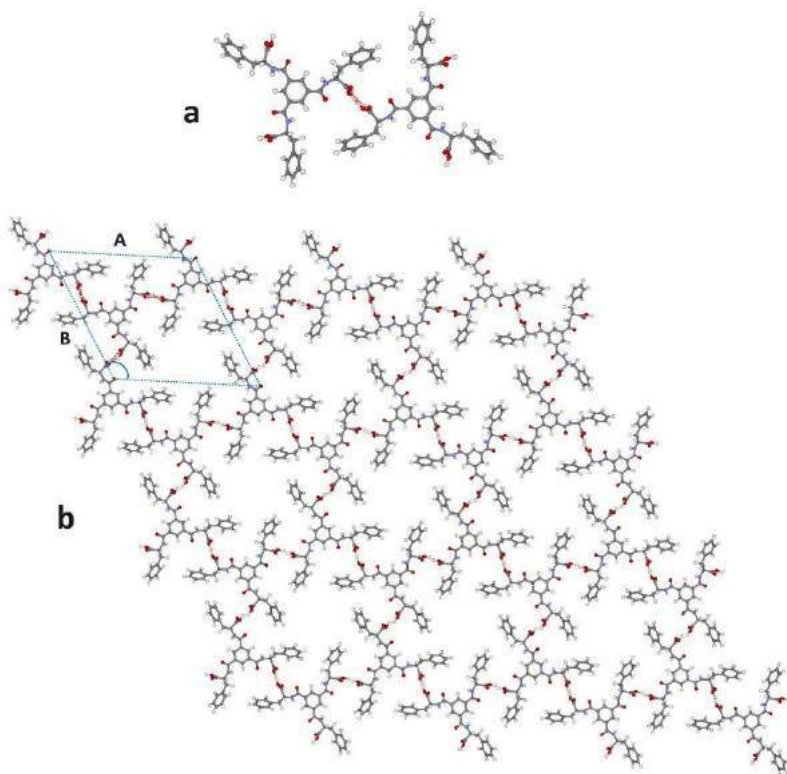


Figure 3.7. a) Optimized dimer geometry of **2** molecules using a force field. b) The possible self-assembled pattern for the observed 2D regions.

3.4. Conclusions:

C₃ symmetric molecule **2** was designed, synthesized and studied for self-assembling behavior. This molecule self-assembled as long uniform nanofibers with diameter of ~70-90 nm. Self-assembled ultrathin monolayer of this molecule was studied at low concentration (10 μ M) through atomic force microscopy (AFM), which revealed the formation of two different kinds of assemblies: namely, one- and two-dimensional nano-islands. C₃ symmetric molecules are generally known to form two-dimensional islands, but the formation of one-dimensional islands is unusual in this case. Working models for one- and two-dimensional islands were proposed by using DREIDING force field method.

3.5. References:

1. (a) Heitzer, H. M.; Marks, T. J.; Ratner, M. A. *J. Am. Chem. Soc.*, **2013**, *135*, 9753–9759. (b) Amigoni, S.; Taffinde Givenchy, E.; Dufay, M.; Guittard, F. *Langmuir* **2009**, *25*, 11073–11077. (c) Minari, T.; Lui, C.; Kano, M.; Tskukagoshi, K. *Adv. Mater.* **2012**, *24*, 299–306. (d) Halik, M.; Hirsch, A. *Adv. Mater.* **2011**, *23*, 2689–2695. (e) Zhang, S. *Nat. Biotechnol.* 2003, *21*, 1171–1178
2. Uosaki, K.; Yamada, R. *J. Am. Chem. Soc.* **1999**, *121*, 4090–4091.
3. Griessl, S.; Lackinger, M.; Edelwirth, M.; Hietschold, M. *Single Mol.* **2002**, *3*, 25–31.
4. (a) Silly, F. *J. Phys. Chem. C* **2012**, *116*, 10029–10032. (b) Gopakumar,

- T. G.; Matino, F.; Schwager, B.; Bannwarth, A.; Tuczek, F.; Kroger, J.; Berndt, R. *J. Phys. Chem. C* **2010**, *114*, 18247–18251. (c) Ha, N. T. N.; Gopakumar, T. G.; Hietschold, M. *Surf. Sci.* **2013**, *607*, 68–73. (d) Hauptmann, N.; Scheil, K.; Gopakumar, T. G.; Otte, F. L.; Schütt, C.; Herges, R.; Berndt, R. *J. Am. Chem. Soc.* **2013**, *135*, 8814–8817.
5. (a) van Gestel, J.; Palmans, A. R. A.; Titulaer, B.; Vekemans, J. A. J. M.; Meijer, E. W. *J. Am. Chem. Soc.* **2005**, *127*, 5490–5494. (b) Kim, S.-G.; Kim, K.-H.; Kim, Y. K.; Shin, S. K.; Ahn, K. H. *J. Am. Chem. Soc.* **2003**, *125*, 13819–13824.
6. (a) Fotin, A.; Cheng, Y.; Sliz, P.; Grigorieff, N.; Harrison, S. C.; Kirchhausen, T.; Walz, T. *Nature* **2004**, *432*, 573–579. (b) Ferguson, M. L.; Prasad, K.; Sackett, D. L.; Boukari, H.; Lafer, E. M.; Nossal, R. *Biochemistry* **2006**, *45*, 5916–5922.
7. Sikkenga, D. L.; Pandya, A. K.; Zaenger, I. C.; Abrams, K. J.; Bartos, T. M. U.S. Patent 6562997, **2003**.
8. Yan, H.-J.; Lu, J.; Wan, L.-J.; Bai, C.-L. *J. Phys. Chem. B*, **2004**, *108*, 11251–11255.
9. (a) P. J. M. Stals, J. F. Haveman, R. Martin- Rapun, C. F. C. Fitie, A. R. A. Palmans, E. W. Meijer, *J. Mater. Chem.*, **2009**, *19*, 124–130. (b) Iancu, V.; Braun, K. F.; Schouteden, K.; Van Haesendonck, C. *Langmuir* **2013**, *29*, 11593–11599. (c) Cantekin, S.; de Greef, T. F. A.; Palmans, A. R. A. *Chem. Soc. Rev.*, **2012**, *41*, 6125–6137.
10. (a) Bose, P. P.; Drew, M. G. B.; Das, A. K.; Banerjee, A. *Chem. Commun.*, **2006**, 3196–3198. (b) Chen, Z.; Liu, X.; Zhang, C.; Zhang, Z.; Liang, F. *Dalton Trans.*, **2011**, *40*, 1911–1918.
11. (a) Karmakar, A.; Oliver, C. L.; Platero-Prats, A. E.; Laurila, E.; Öhrström, L. *CrystEngComm*. **2014**, *16*, 8243–8251. (b) Srinivasulu, G.; Sridhar, B.; Kumar, K. R.; Sreedhar, B.; Ramesh, V.; Srinivas, R.; Kunwar, A. C.; J.

- Mol. Struct.* **2011**, 1006, 180–184. (c) Eissmann, D. S. F.; Weber, E. *Struct. Chem. Commun.* **2010**, 3–4.
12. Horcas, I.; Fernández, R.; Gómez-Rodríguez, J. M.; Colchero, J. Gómez-Herrero J.; Baro, A. M. *Rev. Sci. Instrum.* **2007**, 78, 013705.
13. Duchamp, D. J.; Marsh, R. E. *Acta Cryst.* **1969**, B25, 5–19. (b) F.H. Herbstein, *Molecular Inclusion and Molecular Recognition—Clathrates I*, Springer Berlin Heidelberg publishing group, **2005**, 107–139.
14. Jurečka, P.; Šponer, J.; Černý, J.; Hobza, P. *Phys. Chem. Chem. Phys.* **2006**, 8, 1985–1993.
- .

Chapter 4

Ultrastructure of Metallopeptide-based Soft Spherical Morphologies

(Work published in *RSC Adv.* **2014**, *4*, 64457)

4.1 Introduction

Self-assembling peptides offer a versatile platform for the formation of ordered nanoscale systems, with varied applications in catalysis, delivery, and tissue engineering, to name only a few.¹ Control over physicochemical properties of constituent amino acids, possibility of predictable design on the basis of secondary structural signatures, and high compatibility interaction with biological systems, are hallmarks of peptide-based nanoscale materials. Consequently, it is quite advantageous to employ short self-assembling peptides, to obtain diverse hierarchical structures with desired functions. Recent advances on these lines concerns interaction of metal ions with self-assembling peptides to afford bio-inspired metal-peptide frameworks (MPF),² which may offer combined investigated properties of metal-organic framework (MOF) with biocompatibility.

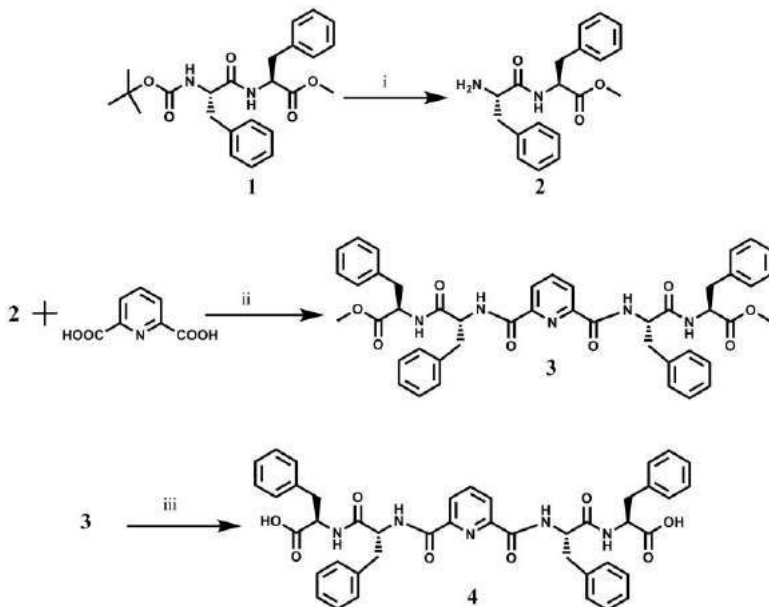
Three different approaches could be envisaged for constructing MPFs: (i) introducing amino acids side chains capable of metal binding³ (ii) use of exogenous ligands supporting MOF architecture⁴ (iii) use of covalently linked chiral/achiral connectors. The latter approach appears to be a followed avenue for designing novel, abiotic oligomers for supramolecular studies. For example, Lehn, Huc and other groups have reported family of oligoamides based on achiral connectivity of 2,6-pyridinedicarboxylic acid,

where the resultant oligomers not only have the ability to self-organize into single helices, but also support formation of double helices.⁵ Notably, short oligomers with 2,6-pyridinedicarboxylic acid and related connectors afford planar ‘crescent-like’ conformation, while longer oligomers exhibit more pronounced propensity to form helices.⁶ In particular, pyridine diacid oligomers offer hydrogen bonding at the inner rim of helices resulting in ~4.5 monomer per turn of the ensuing helix.

Diphenylalanine (FF) dipeptide motif exhibits spontaneous self-assembly to generate peptide nanotubes in solution. FF nanotubes offer interesting applications as scaffolds for the synthesis of metal nanowires, possess improved mechanical properties, semi-conductivity and serve as drug delivery agents.⁷ Side chain aromaticity in phenylalanine is implicated for self-assembly and for control over structural features in the solid state.⁸ In current study, given our continued interest in hierarchical self-assembled peptides systems and our ongoing efforts to prepare covalently linked conjugates of FF dipeptide,^{5b, 9} we decided to synthesize a symmetric FF conjugate using pyridinedicarboxylic acid as a achiral linker. The ability of this new peptide conjugate to self-assemble and its binding to various metals including copper, silver and gold leading to formation of metallopeptide soft structures is described.

4.2. Synthesis and Characterization:

Peptide **4** was synthesized through solution phase synthesis:



Scheme 1: Synthetic scheme of peptide conjugate **4**: (i) 75% TFA-DCM, 4 h, N₂ atm. (ii) HOBt, DCC, 0 °C, TEA, N₂ atm. (iii) THF, 1N NaOH, 6 h, N₂ atm.

N-(tert-butyloxycarbonyl)-L-phenylalanine-L-phenylalanine methyl ester (1): N-(Boc)-L-phenylalanine (5 g, 18.8 mmol), and HOBt (2.55 g, 18.8 mmol) were dissolved in dry DMF (25 mL) under nitrogen atmosphere and the reaction mixture was cooled to 0 °C in an ice bath. A solution of DCC in DCM (4.66 g, 22.6 mmol) was then added drop wise to the reaction mixture. The reaction

mixture was stirred at 0 °C for 1 h, after which, L- phenylalanine methyl ester hydrochloride (4.05 g, 22.6 mmol) was added to it followed by triethylamine (13.1 mL, 94.2 mmol). The reaction mixture was monitored and stirred for 24 h at room temperature under nitrogen atmosphere. Reaction mixture was concentrated in vacuo, redissolved in ethyl acetate and filtered to remove DCU. The organic layer was then washed with 1N HCl (3×30 mL), 10% NaHCO₃ (3×30 mL) and brine (30 mL). The organic layer was dried over anhydrous sodium sulfate and concentrated in vacuo. The crude compound was purified by silica gel column chromatography by using hexane and ethyl acetate (80:20) solvent system to isolate pure **1** (6.17 g, 76.76% yield). m.p. 102–105 °C, R_f [30% ethylacetate in hexane] = 0.5, ¹H NMR (500 MHz, CDCl₃, TMS, δ ppm): 1.38 (s, 9H); 2.99-3.08 (m, 4H); 3.65 (s, 3H); 4.32 (m, 1H); 4.77-4.93 (m, 1H); 6.96-6.97 (m, 2H); 7.17-7.29 (m, 10H, overlapped aromatic signal and CDCl₃ peak); ¹³C NMR (125 MHz; CDCl₃, δ ppm): 28.3, 38.0, 38.3, 52.3, 53.3, 55.7, 77.3, 80.4, 127.2, 128.6, 128.7, 129.3, 129.4, 170.8, 171.4; HRMS (M+H)⁺ for C₂₄H₃₀N₂O₅: 427.2233 (Calcd.), 427.2236 (Anal.).

L-phenylalanine-L-phenylalanine methyl ester (2): **1** (5g, 9.5 mmol) was dissolved in 75% TFA-DCM and stirred for 1 h under nitrogen atmosphere. After completion of the reaction, the solvent was evaporated in vacuo and was subsequently washed with

diethylether resulting in a white solid. The white solid then dissolved in methanol and passed through activated anion exchange resin and evaporated under reduced pressure to obtain pure **2** (3.27g, 85.4% yield). R_f [50% ethylacetate in hexane] = 0.5; ^1H NMR (500 MHz, DMSO- d_6 , TMS, δ ppm): 2.89-3.09 (m, 4H), 3.57 (s, 3H); 4.02 (m, 1H); 4.51-4.55 (m, 1H); 7.18-7.30 (m, 10H), 8.16 (s, 3H); ^{13}C NMR (125 MHz; DMSO- d_6 , δ ppm): 39.8, 40.0, 40.1, 40.3, 52.2, 54.1, 54.3, 128.4, 128.7, 129.5, 162.8, 172.1; HRMS ($M+H$) $^+$ for $\text{C}_{19}\text{H}_{22}\text{N}_2\text{O}_3$: 327.1709 (Calcd.), 327.1700 (Anal.).

Pyridyl-bis-L-phenylalanine-L-phenylalanine methyl ester (3): 2, 6-pyridinedicarboxylic acid (0.25 g, 1.49 mmol) was dissolved in DMF and cooled to 0 °C in ice bath under nitrogen atmosphere. To this solution, HOBt (0.404 mg, 2.99 mmol) and a solution of DCC (0.617 g, 2.99 mmol) in DCM was added and stirred for 1h under nitrogen atmosphere at 0 °C. Subsequently **2** (1.07 g, 3.29 mmol) was added into the reaction mixture followed by triethylamine (0.76 mL, 9.48 mmol). The reaction mixture was monitored and stirred for 24 h at room temperature under nitrogen atmosphere. Reaction mixture was concentrated in vacuo, redissolved in ethyl acetate and filtered to remove DCU. The organic layer was then washed with 1N HCl (3×30 mL), 10% NaHCO_3 (3×30 mL) and brine (30 mL). The organic layer was

dried over anhydrous sodium sulfate and concentrated in vacuo. Crude compound was then purified through silica gel column chromatography by using methanol-DCM (4:96) resulting in pure **3**. (0.45 g, 38.5% yield). m.p.= 142-144 °C, R_f [5% methanol in DCM] = 0.5; ^1H NMR (500 MHz, DMSO- d_6 , TMS, δ ppm) = 2.46-3.18 (m, 8H), 3.54 (s, 6H), 4.48-4.53 (m, 2H), 4.70-4.77 (m, 2H), 7.08-7.29 (m, 20H) 8.07 (m, 2H), 8.59-8.60 (m, 1H), 8.92-8.93 (2s, 4H); ^{13}C NMR (125 MHz; DMSO- d_6 , δ ppm): 37.1, 37.8, 39.5, 40.0, 40.4, 40.5, 52.3, 54.3, 54.7, 125.2, 126.8, 127.0, 128.7, 137.5, 139.9, 149.0, 163.5, 170.3, 172.1; HRMS ($\text{M}+\text{Cl}$) $^-$ for $\text{C}_{45}\text{H}_{45}\text{N}_5\text{O}_8$: 818.2957 (Calcd.), 818.2957 (Anal.).

Pyridyl-bis-L-phenylalanine-L-phenylalanine conjugate (4): 3 (0.1 g, 0.127 mmol) was dissolved in tetrahydrofuran to form a clear solution. To this 1N NaOH (0.03 g, 0.765mmol) was added and stirred for 6 h at room temperature. The solution obtained was passed over activated cation exchange resin. The filtrate was evaporated under reduced pressure to obtain pure **4**. (0.07 g, 72.9% yield); m.p. 120-122 °C; ^1H NMR (500 MHz, DMSO- d_6 , TMS, δ ppm): 2.46-3.34 (m, 8H.), 4.46-4.73 (m, 2H), 4.74-4.83 (m, 2H), 7.06-7.34 (m, 20H), 8.12-8.13 (m, 1H), 8.41-8.46, (m, 2H), 8.85-8.95 (m, 4H), 9.23-9.31 (m, 2H); ^{13}C NMR (125 MHz; DMSO- d_6 , δ ppm): 37.1, 37.4, 39.5, 40.0, 40.2, 40.3, 54.3, 55.5, 125.3, 126.7, 126.9, 128.6, 129.6, 139.0, 148.9, 157.1, 163.9, 171.8, 173.4; FTIR

(KBr, cm⁻¹): 1220, 1528, 1655 (C=O ,amide I, II and III), 1736 (C=O, acid), 2931 (CH-aliph.), 3029 (CH-Ar), 3310 (NH, str); HRMS (M-H)⁻ for C₄₃H₄₁N₅O₈: 754.2877 (Calcd.), 754.2877 (Anal.)

4.3. Microscopy Studies:

Field Emission Scanning Electron Microscopy (FE-SEM): 10 μ L aliquots of the samples (1mM in 50% methanol-water) were deposited on a silicon wafer and allowed to dry at room temperature. Subsequently, the samples were dried in vacuo for 30 min prior to imaging. The samples were imaged with and without (for EDX) gold coating. SEM images were acquired on FEI Quanta 200 microscope, equipped with a tungsten filament gun, operating at WD 3 mm and 10 kV.

Atomic force microscopy (AFM): 10 μ L aliquots of samples (1 mM in 50% methanol-water) was placed on a silicon wafer at room temperature and allowed to dry by slow evaporation. Subsequently, the samples were dried in vacuo for 30 min prior to imaging. AFM Samples were imaged with an atomic force microscope (Molecular Imaging, USA) operating under the Acoustic AC mode (AAC), with the aid of a cantilever (NSC 12(c) from MikroMasch). The force constant was 0.6 N/m, while the resonant frequency was 150 kHz. The images were taken at room temperature, with the scan

speed of 1.5-2.2 lines/sec. The data acquisition was done using PicoView 1.8® software, while the data analysis was done using PicoView.

Focused Ion Beam- Scanning Electron Microscopy (FIB-SEM): 10 μ L aliquots of the samples (1mM in 50% methanol-water) were deposited on a silicon wafer and allowed to dry at room temperature. Subsequently, the samples were dried in vacuo for 30 min prior to imaging. FIB-SEM images were acquired on FEI make Nova 600 Nanolab workstation equipped with a field emission Ga ion source, operating at 15 KV.

The milling process of peptide-based soft material depended upon beam current, accelerating voltage and mill depth to minimize surface artifacts.

Accelerating Voltage: The interaction volume of gallium (Ga^+) ions is smaller at the lower voltage which may cause less damaging to the soft structure compare to the higher voltage. Therefore, the FIB system which usually worked at 30 kV, operated at an accelerating voltage of 20 kV in the initial milling stage. We used a lower accelerating voltage up to 15 kV for ion beam and electron beam.

Beam Currents: Usually the high beam current for peptide-based soft structure were not applicable because the fragile specimens may not be stable under high beam current. Due to this reason, we

used a set of current in the range of 1 pA- 2.1 nA to determine least possible beam current which was less damaging in nature. Initially, 2.1 nA current for 1 min was used for the irradiation and effect of this irradiation caused more damage to the soft specimen, another beam current of 81 pA also caused damage to the soft specimen under 1-2 mins time duration. Therefore, a current of 37 pA for 1 min apply to mill the soft-specimen which gave a fine cutting and less damage to the specimen. Since, the milling time is inversely proportional to beam current strength, therefore, we did not use this beam current for the longer time which may cause sputtering and melting of the soft-specimen (melting due to the heat generated by ion irradiation). The optimal beam current of 10 pA for milling the specimen typically for 5 mins was used for the present sample.

Transmission electron microscopy (TEM): 10 μ L aliquots of the sample (1 mM in 50% methanol-water) were placed on a 400-mesh carbon coated copper grid. After 1 min any excess fluids were removed. Due to the present of metal samples were imaged without any further staining. Samples were viewed using a JEOL 1200EX electron microscope operating at 80 kV.

Dynamic Light Scattering (DLS): Particle size distribution of **4**, **4**+Cu(II), **4**+Ag(I) and **4**+Au(III) complexes were measured using dynamic light scattering analyzer at a wavelength 657 nm, with

Delsa Nano C Particle analyzer (Beckman Coulter). Samples were measured at 25 °C.

4.4. Results and Discussion:

4.4.1. Molecular design of peptide conjugate, 4: We designed and synthesized **4**, which is a hybrid of two diphenylalanine moieties conjugated using 2,6-pyridinedicarboxylic acid as the linker (Scheme 1). We envisioned the following advantages for the proposed conjugate: [i] possibility to engender a structure containing the ability of 'crescent-like' conformation in an aggregating dipeptide (Figure 4.1a); [ii] introduction of metal ion coordination sites to further interrogate peptide self-assembly process.

2,6-pyridyl disubstituted linkers have been utilized to engender a crescent conformation or a curvature in many foldameric systems.¹⁰ In addition, pyridyl ring also offers additional advantage of metal ion interaction, which may further lead to useful coordination features and varied geometries. A simple energy minimization of **4**, MM+ molecular mechanics force field with steepest descent algorithm in the vacuum, showed that it indeed presents a curved, crescent-like conformation (Figure 4.1 b). It can be surmised that such curved conformation, upon

solution-phase self-assembly eventual culminate into spherical structures.

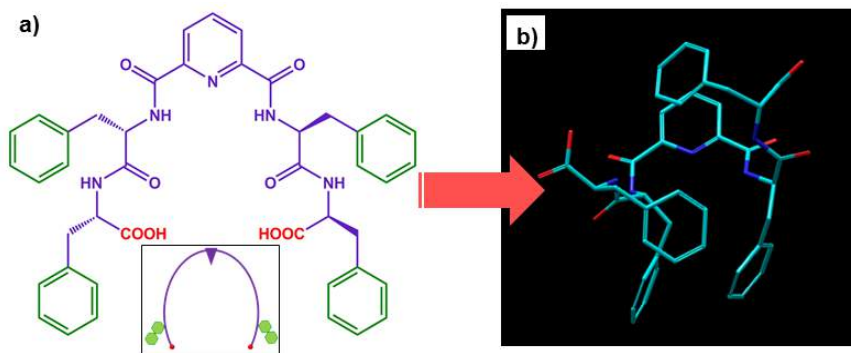


Figure 4.1: (a) **4**. (b) MM+ optimized structure of **4**.

The presence of pyridyl group as a linker gave us an impetus to focus our attention on metal ion coordination. As envisaged, we surmised that such interaction may offer an entry metal-mediated peptide soft matter, perhaps with tunable size and cavities. To start, we decided to assess metal ion interaction by growing appropriate crystal to ascertain the possible site of metal binding. **4** was interacted with Cu(II) ions and studied through single-crystal diffraction analysis (Figure 4.2). A methanolic solution of **4** was treated with CuSO₄·5H₂O and the respective crystals were grown by slow evaporation. Crystal analysis revealed M₂L₂ coordination, *via* carboxylate groups, to afford a Cu(II)-

supported paddle-wheel structure.¹¹ These dimeric units were further stabilized by hydrogen bonding (Table 4.1) between --N--H and --C=O of adjacent dimeric units in the range of 2.11-2.12 Å (Figure 4.3 a) as well as $\text{C--H}\cdots\pi$ interactions (2.47 Å)¹² (Figure 4.3 b) to form a lattice structure (Figure 4.2 b). Notably, Cu(II) ions, in this case, did not interact with pyridyl nitrogens.

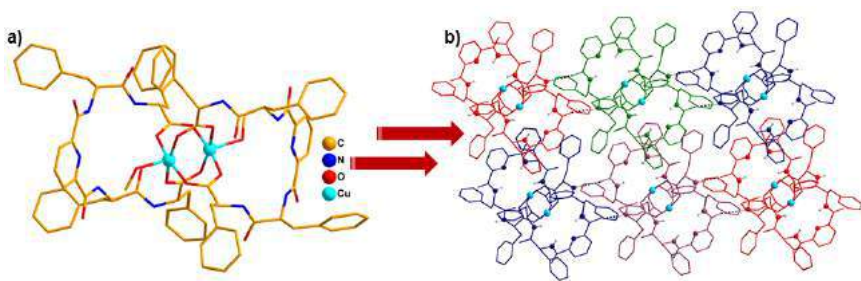


Figure 4.2: Crystal structure of Cu_2L_2 metalloprotein ($\text{L} = 4$): (a) dinuclear paddle wheel-type of structure (b) lattice structure showing peripheral interactions.

Formation of M_2L_2 -type of discrete dinuclear copper cluster evinces interest not only due to interesting coordination geometry, but also due to the fact that coordination-driven self-assembled structures offer facile entry to the construction of novel metallocupramolecular ensembles such as two-dimensional polygons and three-dimensional spherical cages, prisms, and polyhedral.¹³ It is envisaged that these designed superstructures, which combine multiple weak interactions including π – π stacking,

CH- π interactions, hydrogen bonds and metal-coordination, could extend application in domains ranging from optoelectronic materials to drug delivery to storage and catalysis.

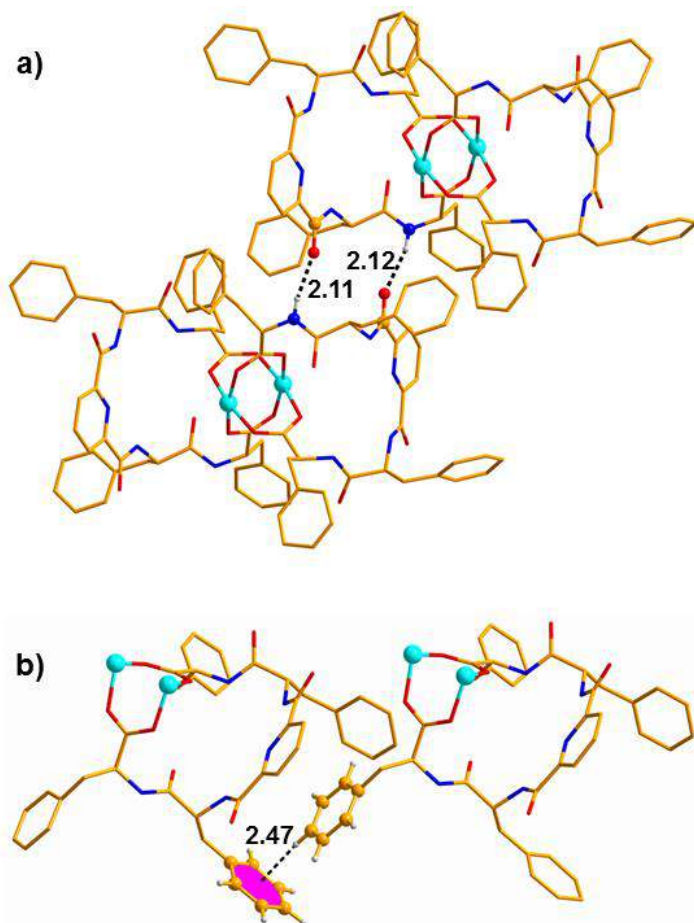


Figure 4.3: (a) H-bonding (Å) (b) CH- π interactions (Å) in 4+Cu(II) complex.

D—H...A [#]	D...A	H...A	D—H...A
4+Cu(II)			
N(2)—H(2')...O(25)	3.0652	2.26	157
N(2)—H(2')...N(1)	2.7046	2.33	107
N(3)—H(3')...O(1) ^{iv}	2.9319	2.12	156
N(4)—H(4')...O(25)	2.9659	2.17	153
N(4)—H(4')...N(1)	2.6849	2.32	106
N(5)—H(5')...O(25)	2.9582	2.14	158
N(5)—H(5')...O(25)	2.8091	2.47	104
N(7)—H(7')...O(23)	3.1644	2.38	152
N(7)—H(7')...N(6)	2.7078	2.33	107
N(8)—H(8')...O(23)	2.8942	2.04	174
N(9)—H(9')...O(23)	3.0987	2.32	151
N(9)—H(9')...N(6)	2.6703	2.31	106
N(10)—H(10')...O(9) ⁱ	2.9467	2.11	164
O(17)—H(17A)...O(5) ⁱⁱ	2.7168	1.95	155
O(18)—H(18)...O(13) ⁱⁱⁱ	2.6308	1.84	162
O(23)—H(23A)...O(2)	2.6828	1.87	170
O(27)—H(27)...O(25)	2.7654	1.98	162
C(7)—H(7)...O(13)	2.7789	2.35	105
C(9)—H(9)...O(14)	2.7856	2.36	105
C(18)—H(18B)...O(16)	2.8189	2.47	101
C(26)—H(26)...O(1) ^{iv}	3.1833	2.34	144
C(26)—H(26)...O(9)	2.8182	2.42	103
C(37)—H(37B)...O(10)	3.1060	2.58	115
C(50)—H(50)...O(5)	2.8214	2.39	106
C(52)—H(52)...O(6)	2.8131	2.38	106
C(61)—H(61B)...O(8)	2.8617	2.50	102
C(69)—H(69)...O(1)	2.8265	2.43	104

C(69)—H(69)...O(9) ⁱ	3.3506	2.50	146
C(77)—H(77)...O(6) ⁱ	3.4802	2.57	166
C(80)—H(80B)...O(4)	2.9624	2.57	105

Table 4.1: Selected hydrogen bonding distances (Å) and bond angles (°) in **4**+Cu(II) Complex.

In the case of **4**, it could be imagined that metal-carboxylate interactions offer a beneficial cooperative effect, along with other stabilizing non-covalent interactions, to form interesting supramolecular structures. Thus, we started with the determination of solution-phase morphology of **4**, followed by investigating the effect of metal ions, in the solution phase, in generating metallopeptide ensembles.

4.4.2. Solution phase self-assembly of 4: The propensity of peptide conjugate **4** to self-assemble was studied. It was dissolved in 50% methanol-water at a concentration of 1 mM and unlike FF dipeptide that forms nanotube, **4** lead to instantaneous formation of spherical vesicles with a diameter of 350-650 nm, as visualized using atomic force microscopy (AFM) (Figure 4.4) and dynamic light scattering (DLS) spectrum (Figure 4.4 c). Spherical nature of the assemblies could be attributed to the crescent-shaped structural design of this conjugate. The vesicles spherical morphology was further analyzed using scanning electron microscopy (SEM) and

transmission electron microscopy (TEM) (Figure 4.4). Stability of these soft structures was also probed by subjecting it to ion beam manipulation (Figure 4.4f). A focused ion beam (FIB) system, using a gallium ion beam, site-selectively machined a spherical particle, at an operating voltage of 15.00 KV. This experiment revealed a solid inner core in the soft structure, suggesting formation of compact structures that are able to withstand high energy of ion beams, for almost 5 min, without any loss of morphological integrity.¹⁴

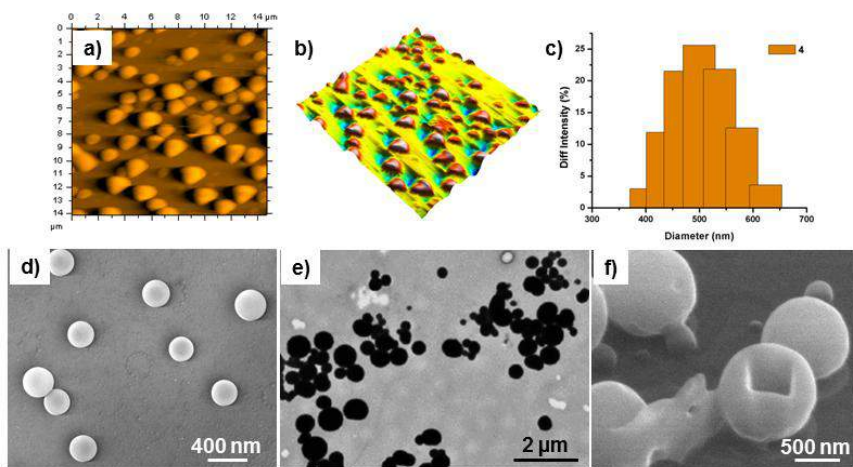


Figure 4.4: Microscopy analysis of **4** (a-b) AFM micrographs. (c) DLS spectrum showing the spherical structure size distribution. (d) SEM image. (e) TEM image. (f) FIB-SEM image of the sphere after ion beam damage revealing the inner surface (1 mM, 50% aqueous methanol) on the silicon wafer.

It is known that aromatic amino acid side-chains interact during peptide aggregation process to form parallel-stacked or T-shaped geometries, leading to the formation of hydrophobic microenvironments by excluding water. Moreover, aromatic-aromatic interactions further help short peptides, such as FF, to rapidly and efficiently access energetically favored conformations.¹⁵ The mixed solvent used in this case, due to solubility constraints, may also exert some effect in stabilizing FF dipeptide side-chain interactions, as stacked arrangements are more stable in water, while amphiphilicity of methanol interferes with the stabilization of both stacked and T-shaped geometries, thereby attenuating aromatic-aromatic interactions.¹⁶

4.4.3. Interaction of 4 with copper ions:

Cu(II) ions form stable four-, five- and six-coordinate complexes. Cu(II) complexes show their potential use as anti-inflammatory,¹⁷ antimicrobial,¹⁸ antitumor agents,¹⁹ enzyme inhibitors, and chemical nucleases, generally bind through nitrogen of the ligands. Conjugate **4** offers pyridyl ring nitrogen as well as free carboxylate groups as probable metal binding sites. Samples were prepared by co-incubating **4** solution (1 mM, 0.5 mL, MeOH) with CuCl₂·2H₂O solution (1 mM, 0.5 mL, H₂O), followed by microscopy evaluation. The minor changes appeared within 2 h of mixing, which became

prominent within 12 h and confirmed by SEM and TEM (Figure 4.5). The images clearly showed initiation of vesicle coalescence by metal ions, leading to the formation of larger-sized vesicles upon fusion in 24 h (Figure 4.5b). The monitoring was continued for 120 h through DLS measurements. The size of spherical structures increased up to $\sim 3.4 \mu\text{m}$ in 120 h upon copper interaction. Notably, the presence of copper ions in vesicles was confirmed by energy-dispersive X-ray spectroscopy (EDX) measurements (Figure 4.5d).

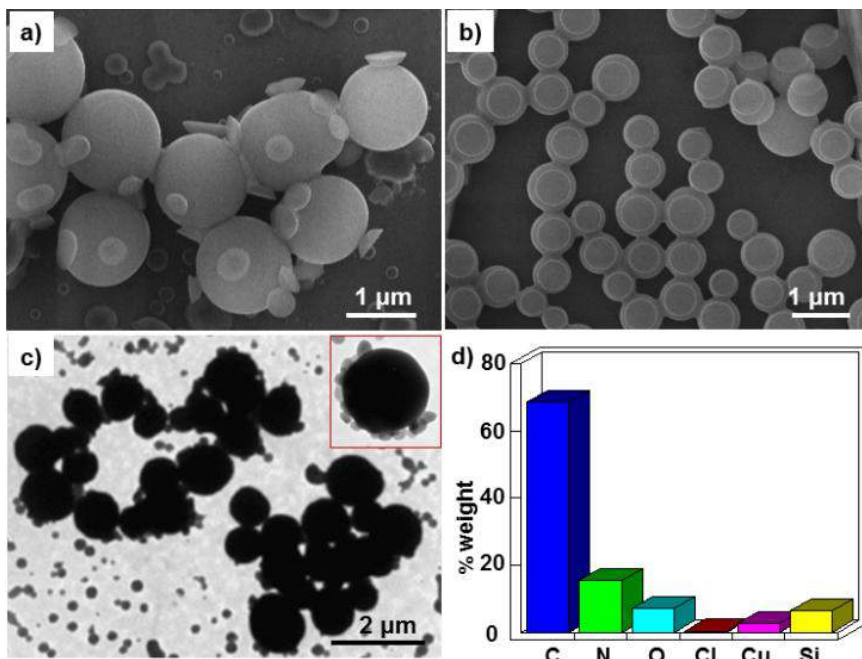


Figure 4.5: Microscopic images of **4**+Cu(II) complex. (a, b) SEM images on the silicon wafer after 12 h and 24 h respectively. (c) TEM image (inset: magnified view of a metal-bound spherical structure). (d) EDX spectrum after 24 h.

One of the hallmarks of Cu(II) interaction was the coalescence of self-assembled structures. As stacking predominate Phe-Phe interactions, phenyl rings would prefer to be buried inside spherical structures. Thus, it is likely that many free carboxylic groups and pyridyl ring nitrogens in **4** would possibly be exposed at the surface of spherical structures for metal ion binding.²⁰ This was also confirmed by single crystal analysis that Cu(II) ions would enable metal ion-mediated interactions to stitch together smaller spherical structures into a large aggregate structure.

4.4.4. Interaction of **4 with silver ions:**

Ag(I) ions generally interact through nitrogen of the ligands²¹ and Ag(I) complexes exhibit biological activity in many cases.²² They are also known to trigger conformational changes in self-assembled peptides.²³ As pyridyl nitrogen of **4** could be an interesting metal binding site for Ag(I), samples were prepared in presence of AgNO₃ as described before for copper ions. We were able to observe changes in morphology 12 h after the addition of metal ions (Figure 4.6a). Interestingly, coalescence of spherical vesicles was observed again, where soft structures of **4** exhibited formation of fused structures, as evidenced by SEM and TEM micrographs

(Figure 4.6b, 4.6c). As this morphology change was different compared to copper-mediated morphology, it is likely that Ag(I) coordination, in this case, is distinct to Cu(II) interactions.²⁴

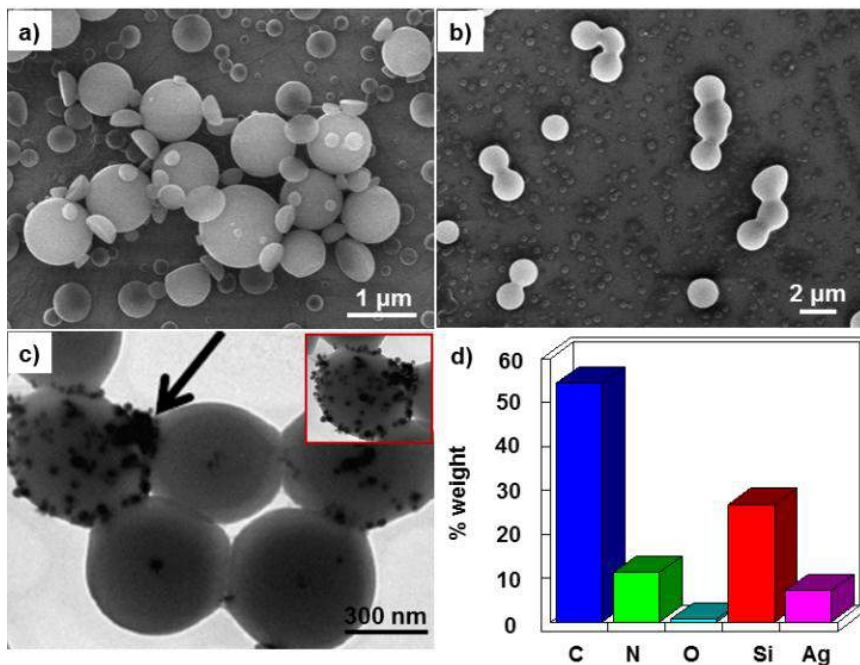


Figure 4.6: Microscopic images of **4**+Ag(I) complex. (a, b) SEM images on the silicon wafer after 12 h and 24 h respectively. (c) TEM image (inset: magnified view of a Ag(I)-mediated soft spherical structures). (d) EDX spectrum after 24 h.

4.4.5. Interaction of **4** with Au(III) ions:

Chloroauric acid (HAuCl_4) protonates pyridyl ring with counter anion AuCl_4^- ion balancing overall charge.²⁵ Latter possesses square-planar geometry, relatively diffuse charge distribution and

a weak interaction with solvent (water) molecules, with nearest solvent molecules occupying two orthogonal quasi-elliptical curved surfaces.²⁶ Dissolving **4** with HAuCl_4 also showed morphological changes where spherical structures were found linked in a network-like fashion within 12 h incubation (Figure 4.7).

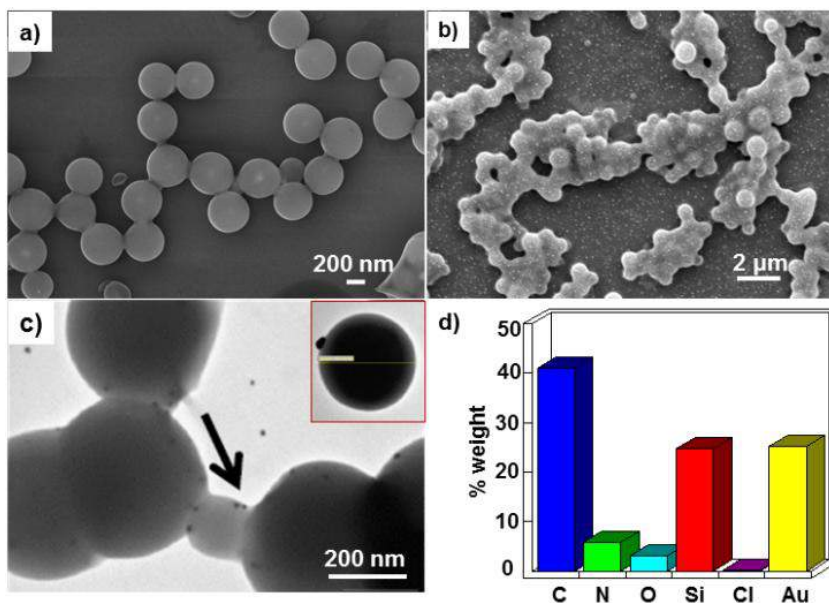


Figure 4.7: Microscopic images of **4**+Au(III) complex. (a, b) SEM images on Si wafer after 12 h and 24 h respectively. (c) TEM image, (inset: magnified view of a spherical structure). (d) EDX spectrum after 24 h.

Given the anionic nature of AuCl_4^- , it is likely that carboxylate anions will not have any role in coordination. Thus, observed coalescence could be attributed to pyridyl nitrogen coordination of Au(III). Indeed, several groups have reported the formation of Au(III) coordination complexes using pyridyl and phenanthrolyl ligands.²⁷ Vesicles linked in a network-like fashion were confirmed by various microscopy methods and EDX analysis data, which clearly suggests the formation of a metal-peptide framework.

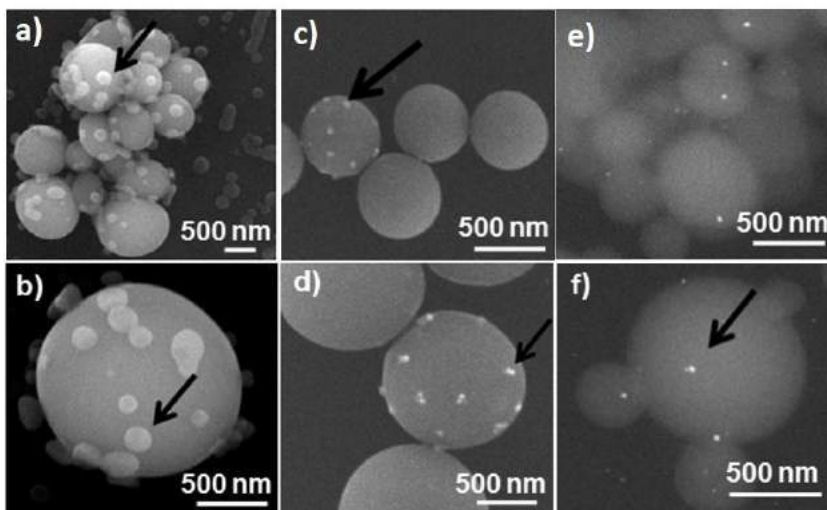


Figure 4.8: SEM images on copper grid after 12 h (a, b) $4+\text{Cu(II)}$ complex. (c, d) $4+\text{Ag(I)}$ complex. (e, f) $4+\text{Au(III)}$ complex.

To further understand the role of the surface in these experiments, we repeated entire procedure by using copper grids (Figure 4.8). Same results were obtained in all three cases irrespective of surface.

There could be different interactions possibilities: in the case of Cu(II) ions, free carboxyl group side-chains in **4** could interact as suggested by solid state structure; but, this does not preclude solution interaction of pyridyl nitrogens with copper ions. In the case of Ag(I) and Au(III) ions, the interaction could possibly be supported by pyridyl nitrogen. Despite repeated attempts, we were unable to grow crystals with Ag(I) and Au(III) ions.

4.4.6. Dynamic light scattering analysis:

Effect of metal ions on vesicle coalescence was confirmed by DLS analysis using similar metal-peptide solutions used for microscopy studies.²⁸ The samples were prepared by mixing **4** (1 mL, 10 μ m, MeOH) with metal ion solutions (1 mL, 10 μ m, H₂O). It was observed that the peptide vesicles alone have a hydrodynamic diameter of \sim 350-650 nm (Figure 4.9a), which upon Cu(II) ions addition changes to \sim 1.2 μ m (Figure 4.9b) after 24 h incubation and it further matured to an average diameter of \sim 3.4 μ m after 120 h (Figure 4.9c). For Ag(I) ions, the average size of metallated vesicles changed to \sim 1 μ m after 24 h (Figure 4.9d) and matured to

an average diameter of 2.2 μm after 120 h (Figure 4.9e). A similar trend was also observed for Au(III) interactions (Figure 4.9f and 4.9g). Such a change in size may be ascribed to metal-mediated vesicle fusion process.

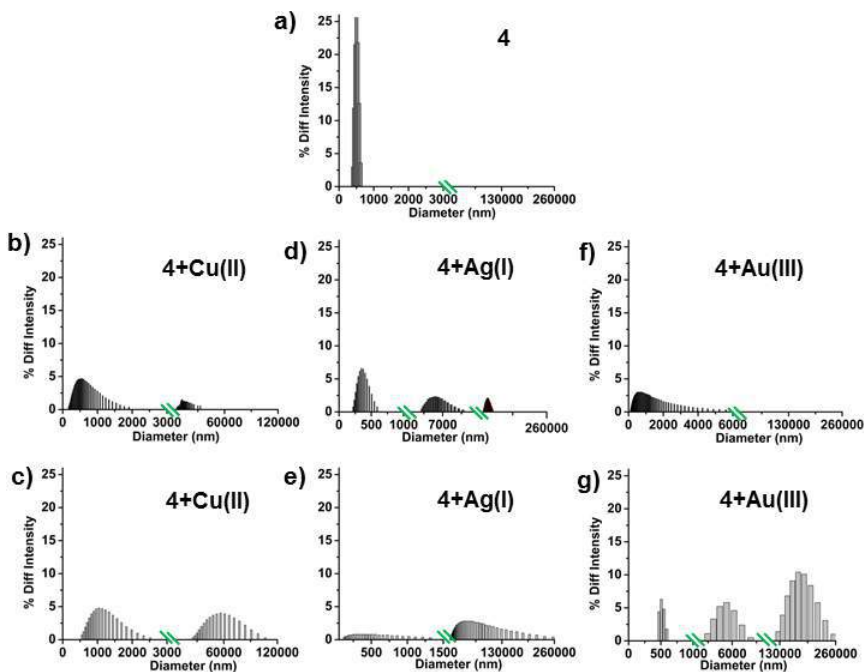


Figure 4.9: DLS spectra: (a) Size distribution of **4** (50% MeOH-H₂O). (b,d,f) Size distributions after 24 h. (c,e,f) Size distributions after 120 h.

4.4.7. Thiol displacement studies:

Au(III) ion binds very effectively with **4** to form network-like metal-peptide framework. As Au(III) has thiophilic binding

preference over nitrogen or oxygen centers,²⁹ we decided to treat **4**+Au(III) complex with 1-mercaptopropanoic acid (MPA) to achieve its displacement from the framework. Samples were prepared by mixing **4** (0.5 mL, 1 mM, MeOH) with HAuCl₄ solution (0.5 mL, 1 mM, H₂O), incubated for 12 h. This was followed by addition of MPA solution (0.5 mL, 10 mM, 50% methanol-water) and further incubation for 5 h (Figure 4.10). Notably, network-like structure disappeared confirming the crucial role of Au(III) ions in causing metalized vesicles to stick together.

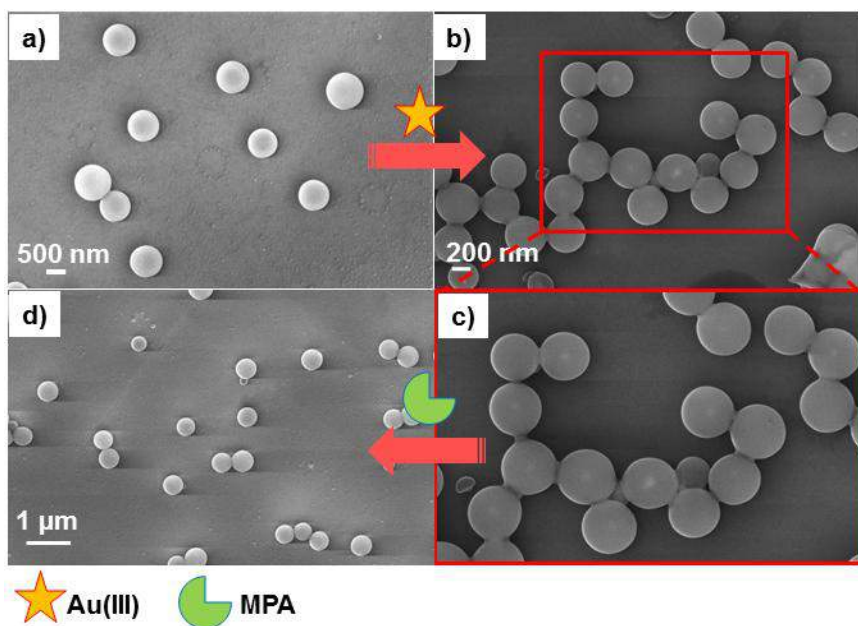


Figure 4.10: (a) SEM image of **4**. (b) SEM image of **4**+Au(III) complex after 12 h. (C) Magnified view of **4**+Au(III) complex. (d) SEM image of **4**+Au(III)+MPA after 5 h incubation.

4.4.8. UV-Vis Studies:

Spectrometric titrations: The UV-Vis absorption spectrum of **4** was dominated by strong absorption of pyridine ring and phenyl rings. The dicpicolinic acid absorbed at 215 nm and had a π - π^* transition absorbance at 270, 273 and 279 nm³⁰ but it was not easily recognizable because of many overlapping peaks of Phe-Phe peptide in the same region as phenylalanine also absorbed around 210 and 257 nm.³¹ The absorption spectra of **4** (0.1 mM, MeOH) revealed the absorption peak at 213 nm and 274 nm. The π - π^* transitions peaks are known to shift to longer wavelength (bathochromic shift) when metal coordination occur.³²

Spectrometric titrations with Cu (II) ions: CuCl₂ solution (0.5 mL, 10 μ M, MeOH) was taken in UV cuvette (1 mL) and used as the baseline. To above metal solution, 50 μ L injections of **4** (10 μ M, MeOH) were added and were stirred for 2-3 min prior to measurement of relative absorbance spectrum. While titrations, either incrementally added metal to peptide or peptide to metal solutions. In the spectrometric titration of CuCl₂ with **4**, the amount of free peptide started disappearing as indicated by the decrease in absorption of **4** and amount of metal coordinate peptide started to incline due to increase in absorption for the same (Figure 4.11).

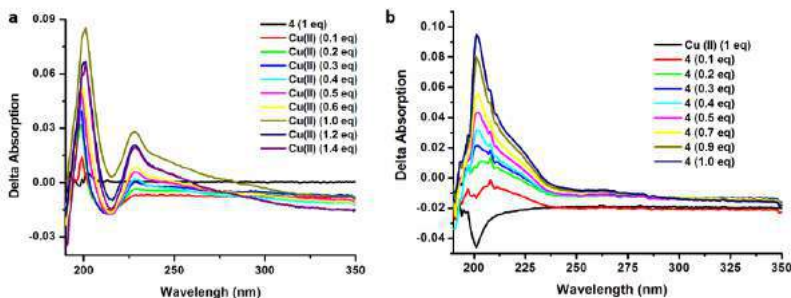


Figure 4.11: (a) 0.5 mL of CuCl_2 (10 μM , MeOH) was taken and used as the baseline. 50 μL injections of **4** (10 μM , MeOH) were added each time. (b) 0.5 mL of **4** (10 μM , MeOH) was taken and used as the baseline. 50 μL injections of CuCl_2 (10 μM , MeOH) were added each time.

Spectrometric titrations with Ag (I) ions: 0.5 mL of AgNO_3 solution (10 μM , MeOH) was taken in UV cuvette (1 mL) and used as the baseline. 50 μL injections of **4** (10 μM , MeOH) were added each time. Solutions were stirred for 2-3 min prior to measurement of relative absorbance spectrum. Spectrometric titrations were carried on in both ways: either incrementally added metal to peptide or peptide to metal solutions (Figure 4.12).

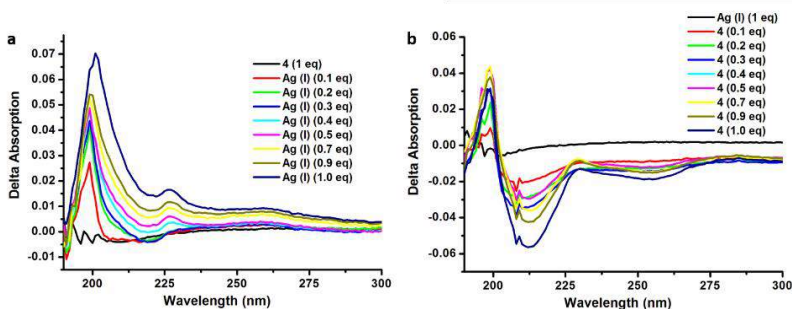


Figure 4.12: Spectrometric titrations (a) 0.5 mL of AgNO_3 (10 μM , MeOH) was taken and used as the baseline. 50 μL injections of **4** (10 μM , MeOH) were added each time. (b) 0.5 mL of **4** (10 μM , MeOH) was taken and used as the baseline. 50 μL injections of AgNO_3 (10 μM , MeOH) were added each time.

Spectrometric titrations with Au (III) ions: 0.5 mL of HAuCl_4 solution (10 μM , MeOH) was taken and used as the baseline. 50 μL injections of **4** (10 μM , MeOH) were added each time. Solutions were stirred for 2-3 min prior to measurement of relative absorbance spectrum. Titrations were performed both ways: either incrementally added metal to peptide or peptide to metal solutions (Figure 4.13).

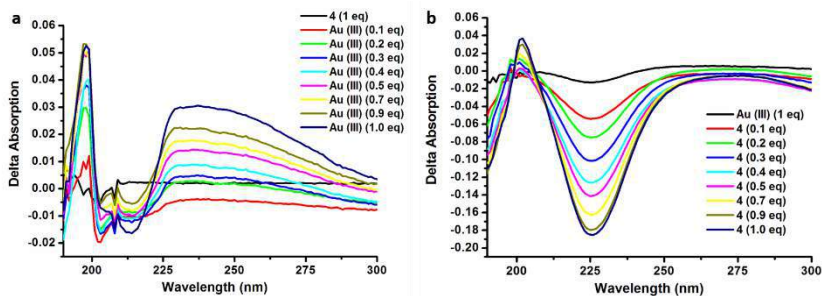


Figure 4.13: Spectrometric titrations (a) 0.5 mL of HAuCl_4 (10 μM , MeOH) was taken and used as the baseline. 50 μL injections of **4** (10 μM , MeOH) were added each time. (b) 0.5 mL of **4** (10 μM , MeOH) was taken and used as the baseline. 50 μL injections of HAuCl_4 (10 μM , MeOH) were added each time.

Peptide conjugate **4** afforded formation of spherical structures supported by H-bonding and π - π stacking interactions. Moreover, possible crescent-shape of monomers, engendered by pyridyl linker, further assisted self-organization of **4** to maximize

non-covalent interactions. Based on the occurrence of these forces, a model could be proposed to depict the formation of spherical vesicles from crescent-shaped conjugate (Figure 4.14). Observation of coalescence upon metal ion addition was attributed to metal-coordination, which could possibly bring these soft peptide-based structures in close proximity.

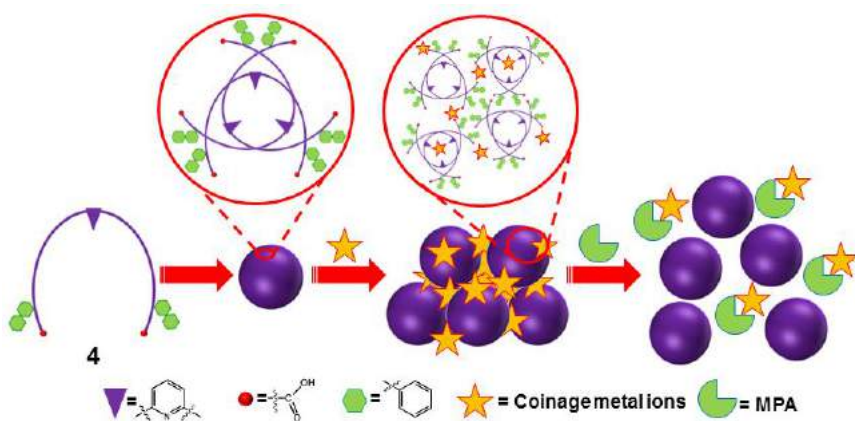


Figure 4.14: Proposed model of metal-peptide interactions

As seen in Au experiment, exogenous addition of MPA could revert coalescence perhaps by complexing metal ions thus releasing spherical structures.

4.4.9. Catalytic Studies:

Acid rain, photochemical smog, ozone depletion³³ and global warming are major environmental concerns which need to be attended first hand. The main reasons for such environmental crisis are due to pollutants generated in coal combustion process such as NO_x, CO, SO₂ to name a few. The high solubility of SO₂ in water had made its removal process easy through wet flue gas desulfurization (WFGD). But due to the weak solubility of NO in water, it has become the major concern for environmental scientists. Catalytic oxidation of NO to NO₂ can be used to remove excess of NO from the environment as NO₂ is highly soluble in water and could be removed easily by WFGD method.

Catalytic oxidation of NO to NO₂ has been carried out efficiently by noble metals (Pt and Pd).³⁴ But being less available and a high cost of noble metals, these could not be used as the potential catalyst in industry for catalytic oxidation of NO. Till date many transition metal catalysts have been synthesized to address the issue.³⁵ Copper ion mediated self-assembling peptides, known to form MPFs, could be a new catalyst for efficient and environmentally friendly way to oxidize NO to NO₂.

Sample preparation for NO oxidation: **4** (0.5 g, mmol) and CuSO₄.5H₂O (0.66 g, mmol) were dissolved in methanol and slowly evaporated to get MPFs. The crystals (0.5 g) were dried

under high vacuum and crushed in power for making a pellet for catalytic studies.

Reaction conditions:

Weight of the sample	0.5 g
Temperature	25 °C
Total feed flow rate	37.5 standard cc per minute (sccm)
NO flow rate	7.5 cc/min
O ₂ concentration	20%.

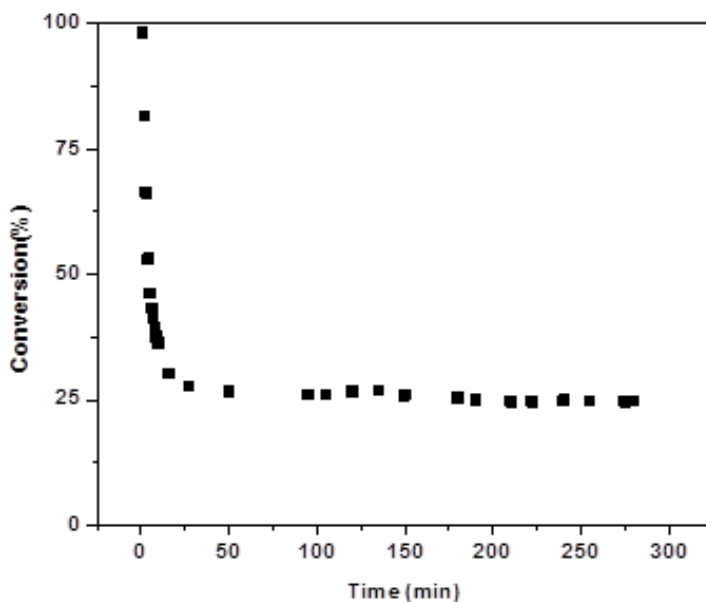


Figure 4.15: NO conversion efficiency of MPF [4+Cu(II)] at 25°C

The catalytic activity of MPF (**4**+Cu(II)) was studied at room temperature. NO flow rate was set 7.5 cc/min along with 20% O₂ concentration. The catalyst was found to convert 25% of NO to NO₂ under given conditions (Figure. 4.15).

4.5. Conclusion

Conjugate **4** was designed having a crescent-type of structure, synthesized and studied for its interaction with metal ions in the solid state and in solution. Crystal analysis of copper complex of **4** revealed M₂L₂ coordination, *via* carboxylate groups, to afford a Cu(II)-supported paddle-wheel structure. Lattice structure offered insight into the further interaction of these dinuclear units via noncovalent interactions. Solution phase self-assembly peptide conjugate and metal ion complexation revealed that ensembles of **4** beautifully coalesced in presence of metal ions to form large sized vesicles. Metal coordination played an important role in connecting spherical structures and exploits an interesting interfacial interaction to provide entry into novel metallopeptide materials. Further, copper MPF was explored as a catalyst for oxidation of NO.

4.6 References

- 1 (a) Pack, D. W.; Hoffman, A. S.; Pun S.; Stayton P. S. *Nat. Rev. Drug Discov.*, **2005**, *4*, 581–593. (b) Guo, X.; Szoka, F. C. *Acc. Chem. Res.*, **2003**, *36*, 335–341. (c) Rabotyagova, O. S.; Cebe, P.; Kaplan, D. L. *Biomacromolecule* **2011**, *12*, 269–289. (d) Brodin, J. D.; Ambroggio, X. I.; Tang, C.; Parent, K. N.; Baker, T. S.; Tezcan, F. A. *Nat. Chem.* **2012**, *4*, 375–382. (e) Branco, M. C.; Schneider, J. P. *Acta Biomater.* **2009**, *5*, 817–831. (f) Hirst, R.; Escuder, B.; Miravet, J. F.; Smith, D. K. *Angew. Chem., Int. Ed.* **2008**, *42*, 8002–8018. (g) Banwell, E. F.; Abelardo, E. S.; Adams, D. J.; Birchall, M. A.; Corrigan, A.; Donald, A. M.; Kirkland, M.; Serpell, L. C.; Butler, M. F.; Wollfson, D. N. *Nat. Mater.* **2009**, *7*, 596–600. (h) Al-Ahmady, Z. S.; Al-Jamal, W. T.; Bossche, J. V.; Bui, T. T.; Drake, A. F.; Mason, A. J.; Kostarelos, K. *ACS Nano*. **2012**, *6*, 9335–9346.
- 2 (a) Mart-Gastaldo, C.; Warren, J. E.; Stylianou, K. C.; Flack, N. L. O.; Rosseinsky, M. J. *Angew. Chem., Int. Ed.* **2012**, *51*, 11044–11048. (b) Martí-Gastaldo, C.; Antypov, D.; Warren, J. E.; Briggs, M. E.; Chater, P. A.; Wiper, P. V.; Miller, G. J.; Khimyak, Y. Z.; Darling, G. R.; Berry, N. G. *Nat. Chem.* **2014**, *6*, 343–351.
- 3 Manton, A.; Massüger, L.; Rabu, P.; Palivan, C.; McCusker, L. B.; Taubert, A. *J. Am. Chem. Soc.* **2008**, *130*, 2517–2526.
- 4 Ikezoe, Y.; Washino, G.; Uemura, T.; Kitagawa, S.; Matsui, H. *Nat. Mater.* **2012**, *11*, 1081–1085.
- 5 (a) Berl, V.; Huc, I.; Khoury, R. G.; Krische, M. J.; Lehn, J. M. *Nature*, **2000**, *407*, 720–723. (b) Berl, V.; Huc, I.; Khoury, R. G.; Lehn, J. M. *Chem. Eur. J.* **2001**, *7*, 2810–2820.
- 6 Jiang, H.; Léger, J. M.; Dolain, C.; Guionneau, P.; Huc, I. *Tetrahedron* **2003**, *59*, 8365–8374.

- 7 (a) Reches, M.; Gazit, E. *Science* **2003**, *300*, 625–627. (b) Ischakov, R.; Alder-Abramovich, L.; Buzhansky, L.; Shekhter, T.; Gazit, E. *Bioorg. Med. Chem.* **2013**, *21*, 3517–3522. (c) Ghosh, S.; Alder-Abramovich, L.; Gazit, E.; Verma, S. *Tetrahedron* **2013**, *69*, 2004–2009. (d) Hill, R. J. A.; Sedman, V. L.; Allen, S.; Williams, P. M.; Paoli, M.; Alder-Abramovich, L.; Gazit, E.; Eaves, L.; Tandler, S. J. B. *Adv. Mater.* **2007**, *19*, 4474–4479. (e) Reches, M.; Gazit, E. *Nat. Nanotechnol.* **2006**, *1*, 195–200. (f) Alder-Abramovich, L.; Kol, N.; Yanai, I.; Barlam, D.; Shneck, R. Z.; Gazit, E.; Rouso, I. *Angew. Chem., Int. Ed.* **2010**, *49*, 9939–9942. (g) Alder-Abramovich, L.; Aronov, D.; Beker, P.; Yevnin, M.; Stempler, S.; Buzhansky, L.; Rosenman, G.; Gazit, E. *Nat. Nanotechnol.* **2009**, *4*, 849–854. (h) Hauser, C. A.; Zhang, S. *Nature* **2010**, *468*, 516–517.
- 8 Görbitz, H. C. *Chem. Eur. J.* **2001**, *7*, 5153–5159.
- 9 (a) Mondal, S.; Barman, A. K.; Verma, S. *CHIMIA* **2012**, *66*, 930–935. (b) Gour, N.; Braman, A. K.; Verma, S. *J. Pept. Sci.* **2012**, *18*, 405–412.
- 10 Zhang, D. W.; Zhao, X.; Hou, J. L.; Li, T. *Chem. Rev.* **2012**, *112*, 5271–5316.
- 11 (a) Pichon, A.; Fierro, C. M.; Nieuwenhuyzen, M.; James, S. L. *CrystEngComm.* **2007**, *6*, 449–451. (b) Zhao, J. S.; Zhang, R. L.; Yang, S. Y.; Ng, S. W. *Acta Cryst.* **2004**, *e60*, m264–m266. (c) Xia, H. T.; Liu, Y. F.; Li, S. A. *Acta Cryst.* **2006**, *e62*, m2653–m2655. (d) Kong, L. L.; Huo, L. H.; Gao, S.; Zhao, J. G. *Acta Cryst.* **2005**, *e61*, m2289–m2290.
- 12 (a) Otero, A.; Lara-Sánchez, A.; Fernández-Baeza, J.; Alonoso-Moreno, C.; Tejada, J.; Castro-Osma, A.; Márquez-Segovia, I.; Sánchez-Barba, L. F.; Rodríguez, A. M.; Gómez, M. V. *Chem. Eur. J.* **2010**, *16*, 8615–8619. (b) Nishio, M. *CrystEngComm.* **2004**, *6*, 130–158. (c) Kumar, J.; Purohit, C. S.; Verma, S. *Chem. Commun.* **2008**, 2526–2528. (d) Bracco, S.; Comotti, A.; Valsesia, P.; Beretta, M.; Sozzani, P. *CrystEngComm.* **2010**, *12*, 2318–2321.

- 13 (a) Cook, T. R.; Zheng, Y. R.; Stang, P. J. *Chem. Rev.* **2013**, *113*, 734–777. (b) Spokoyny, M.; Kim, D.; Sumrein, A.; Mirkin, C. A. *Chem. Soc. Rev.* **2009**, *38*, 1218–1227. (c) Clever, G. H.; Kawamura, W.; Tashiro, S.; Shiro, M.; Shionoya, M. *Angew. Chem., Int. Ed.* **2012**, *51*, 2606–2609. (d) Carné-Sánchez, A.; Imaz, I.; Cano-Sarabia, M.; D. A. MasPOCH, *Nat. Chem.*, 2013, **5**, 203–211.
- 14 Joshi, K. B.; Verma, S. *Angew Chem., Int. Ed.* **2008**, *47*, 2860–2863.
- 15 (a) Gazit, E. *FEBS Journal* **2005**, *272*, 5971–5978. (b) Gazit, E. *FASEB Journal* **2002**, *16*, 77–83. (c) Waters, M. L. *Curr. Opin. Chem. Biol.* **2002**, *6*, 736–741. (d) Gloaguen, E.; Loquais, Y.; Thomas, J. A.; Pratt, D. W.; Mons, M. *J. Phys. Chem. B* **2013**, *117*, 4945–4955.
- 16 Chelii, R.; Gervasio, F. L.; Procacci, P.; Schettino, V. *J. Am. Chem. Soc.* **2002**, *124*, 6133–6143.
- 17 Chaviara, T.; Charistidis, P. C.; Papageorgiou, A.; Chrysogelou, E.; Hadjipavlou-Litina, J.; Bolos, C. A. *J. Inorg. Biochem.* **2005**, *99*, 2102–2109.
- 18 Djoko, K. Y.; Paterson, B. M.; Donnelly, P. S.; McEwan, A. G. *Metallomics* **2014**, *6*, 854–863.
- 19 (a) Gokhale, N. H.; Padhye, S. S.; Psdhye, S. B.; Anson, C. E.; Powell, A. K. *Inorg. Chim. Acta.* **2001**, *319*, 90–94. (b) Trávníček, Z.; Maloň, M.; Šindelář, Z.; Doležal, K.; Rolčík, J.; Kryštof, V.; Strnad, M.; Marek, J. *J. Inorg. Biochem.* **2001**, *84*, 23–32. (c) Marín-Hernández, A.; Gracia-Mora, I.; Ruiz-Ramírez, L.; Moreno-Sánchez, R. *Biochem. Pharm.* **2003**, *65*, 1979–1989. (d) Barceló-Oliver, M.; Garcia-Raso, Á.; Terrón, Á.; Molins, E.; M. J. Prieto, V. Moreno, J. Martínez, V. Lladó, I. López, and A. Gutiérrez, *J. Inorg. Biochem.* **2007**, *101*, 649–659.
- 20 Butterfield, S. M.; Patel, P. R.; Waters, M. L. *J. Am. Chem. Soc.* **2002**, *124*, 9751–9755.

- 21 Hu, T.; Mak, T. C. W. *Eur. J. Inorg. Chem.* **2013**, 5476–5486.
- 22 (a) Gerasimchuk, N.; Gamian, A.; Glover, G.; Szponar, B. *Inorg. Chem.* **2010**, 49, 9863–9874. (b) Fan, F. F.; Bard, A. J. *J. Phys. Chem. B* **2002**, 106, 279–287.
- 23 Dublin, S. N.; Conticello, V. P. *J. Am. Chem. Soc.* **2008**, 130, 49–51.
- 24 Halder, P.; Zangrando, E.; Paine, T. P. *Dalton Trans.* **2009**, 5386–5394.
- 25 (a) Spatz, J. P.; Sheiko, S.; Moller, M. *Macromolecule* **1996**, 29, 3220–3226. (b) Spatz, J. P.; Mossmer, S.; Hartmann, C.; Moller, M. *Langmuir* **2000**, 16, 407–415. (c) Li, X.; Zhao, S.; Zhang, S.; Kim, D. H.; Knoll, W. *Langmuir* **2007**, 23, 6883–6888. (d) Sidorov, S. N.; Bronstein, L. M.; Kabachii, Y. A.; Valetsky, P. M.; Soo, P. L.; Maysinger, D.; Eisenberg, A. *Langmuir* **2004**, 20, 3543–3550.
- 26 Ye, Q.; Zhou, J.; Zhao, T.; Zhao, H.; Chu, W.; Sheng, Z.; Chen, X.; Marcelli, A.; Luo, Y.; Wu, Z. *J. Phys. Chem. B* **2012**, 116, 7866–7873.
- 27 Hudson, Z. D.; Sanghvi, C. D.; Rhine, M. A.; Ng, J. J.; Bunge, S. D.; Hardcastle, K. I.; Saadein, M. R.; MacBeth, C. E. *Dalton Trans.* **2009**, 7473–7480.
- 28 Rodina, T. A.; Ivanov, A. V.; Gerasimenko, A. V.; Loseva, O. V.; Antzutkin, O. N.; Sergienko, V. I. *Polyhedron* **2012**, 40, 53–64.
- 29 (a) Tunny, J. M.; Blake, A. J.; Davies, E. S.; McMaster, J.; Wilson, C.; Garner, C. D. *Polyhedron* **2006**, 25, 591–598. (b) Jin, H.; Huang, W.; Zheng, Y.; Zhou, Y.; Yan, D. *Chem. Eur. J.* **2012**, 18, 8641–8646.
- 30 Xie, J. R.-H.; Smith Jr, V. H.; Allen, R. E. *Chem. Phys.* **2006**, 322, 254–268.
- 31 Barazzouk, S.; Daneault, C. *Nanomaterials* **2012**, 2, 187–205.
- 32 (a) Jørgensen, C. K. *Adv. Chem. Phys.* **1963**, 5, 33–146. (b) Sone, K.; Krumholz, P.; Stammreich, H. *J. Am. Chem. Soc.* **1955**, 77, 777–780. (c) Coppock, M. B.; Kapelewski, M. T.; Youm, H. W.; Levine, L. A.; Miller,

- J. R.; Myers, C. P.; Williams, M. E. *Inorg. Chem.* **2010**, *49*, 5126–5133. (d) Coppock, M. B.; Miller, J. R.; Williams, M. E. *Inorg. Chem.* **2011**, *50*, 949–955.
- 33 (a) Yung, M. M.; Holmgreen, E. M.; Ozkan, U. S. *J. Catal.* **2007**, *247*, 356–367. (b) Peng, Y.; Peng, H.; Liu, W.; Xu, X.; Liu, Y.; Wang, C.; Hao, M.; Ren, F.; Li, Y.; Wang, X. *RSC Adv.* **2015**, *5*, 42789–42797. (c) Liu, J.; Song, W.; Xu, C.; Liu, J.; Zhao, Z.; Wei, Y.; Duan, A.; Jiang, G. *RSC Adv.* **2015**, *5*, 104923 – 104931.
- 34 (a) Auvray, X.; Olsson, L. *Appl. Catal. B* **2015**, *168*, 342–352. (b) Weiss, B. M.; Iglesia, E.; *J. Catal.* **2010**, *272*, 74–81.
- 35 (a) Chen, H.; Wang, Y.; Lv, Y. K. *RSC Adv.* **2016**, *6*, 54032–40. (b) Lin, F.; He, Y.; Wang, Z.; Ma, Q.; Whiddon, R.; Zhu, Y.; Liu, J. *RSC Adv.* **2016**, *6*, 31422–31430.

Chapter 5A

**Soft Structure Formation and Cancer Cell
Transport Mechanisms of a Folic acid-
dipeptide Conjugate**

(Published in *J. Pept. Sci.* **2015**, 21, 248)

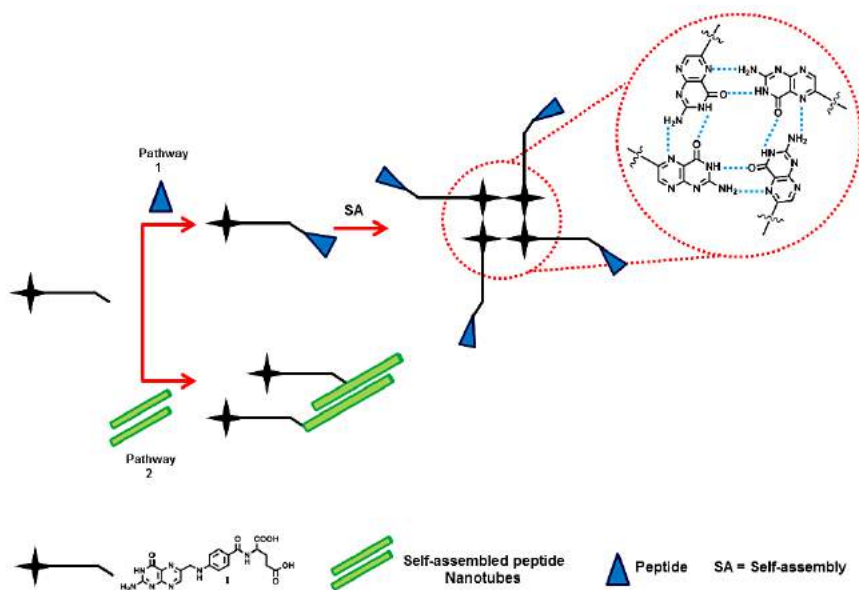
5A.1 Introduction

Folic acid-conjugated imaging agents and candidate drugs have evoked considerable interest over the years owing to their ability to enter cancer cells, through high-affinity interaction with folate receptor (FR) protein. Folate receptors, particularly FR α , exhibit hyperactivity in several cancer cells such as breast, brain, lungs, cervical, and renal carcinomas¹ and offer key entry points supporting active folate intake in cancer cells.² Subsequent to FR binding in cancer cells, folate conjugates are transported inside cells *via* endocytosis.³ Chemical functionalities in folic acid play key roles in high-affinity FR binding⁴, and once folate-conjugates enter cells, enzymatic transformations release bioactive molecules inside the cell. Increased involvement of FRs in cancer cells makes this Trojan horse strategy very useful for delivery of drugs and bioactives, in cancer cells.⁵ Over a period of time, many such conjugates have entered different stages of clinical studies to deliver chemotherapeutic drugs to target cells.⁶ However, the main impediment of such conjugates, which limits their widespread use, concerns the lack of conjugate stability and cytotoxicity.

From the standpoint of supramolecular chemistry, folic acid consists of a heterocyclic pterin skeleton, which affords self-assembled structures belonging to cholesteric and hexagonal

mesophases, under mild alkaline conditions.⁷ Suitably disposed donor-acceptor sites in pterin skeleton drive hydrogen bond assisted self-recognition event, in a manner analogous to guanine tetramer formation, and it has been shown that the presence of monovalent cations imparts stability to the cholesteric phases. A recent study demonstrated that a change in monovalent cations resulted in enhanced folic acid tetramer rigidity, as a result of favorable stacking interactions and quadruplex elongation.⁸

Given our ongoing interest in peptide soft structures⁹ and bionanoconjugation based on guanine tetrad formation¹⁰, we decided to investigate whether bottom-up approach with the folic acid containing peptide building blocks will reveal interesting structural features. One could approach the design of folic acid conjugates *via* two different routes: firstly, by making folic acid conjugated peptides, followed by their self-assembly; or through post-synthetic modification¹¹; of *in situ* assembled peptide nanotubes by folic acid (Scheme 1). The former approach is perhaps better as it offers superior control over the gross morphology of soft structures and the possibility of additional chemical modifications to create a multivalent, folate displaying building block.

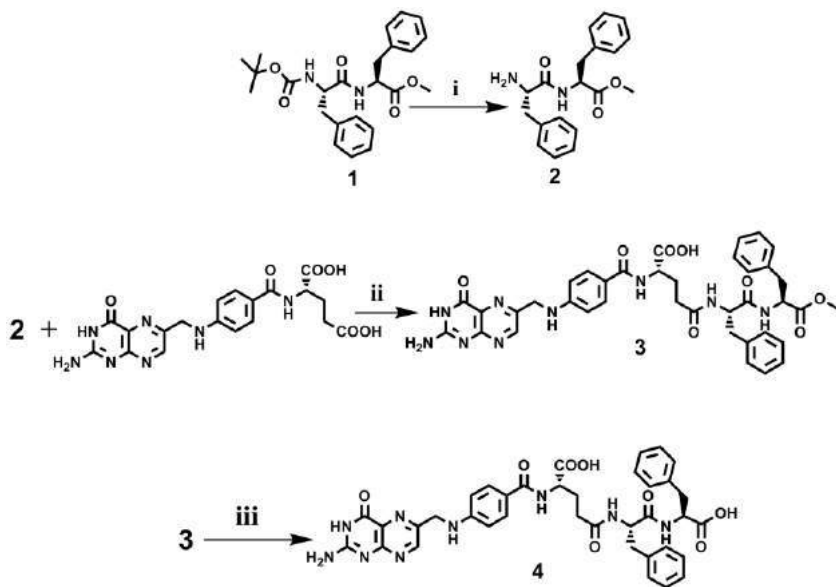


Scheme 1: Two approaches for the design of folic acid and diphenylalanine dipeptide conjugate (inset: hydrogen bonded pterin tetrad)

We decided to employ Phe-Phe dipeptide for the synthesis of a folic acid-conjugated building block (Scheme 2), as both dipeptide and folic acid demonstrate remarkable ability to self-assemble in solution^{7a-b, 8a-b, 12}. Thus, we envisaged that it would be intriguing to study how the proposed covalent conjugation affects self-assembly and gross morphology. We also decided to undertake cytotoxicity assay for the conjugate and the possibility of following its uptake in various cancer cell lines.

5A.2. Synthesis and Characterization:

Conjugate **3** and **4** were prepared by standard solution phase peptide synthesis. Scheme 2 shows various synthetic steps:



Scheme 2: Synthetic scheme for peptide **4**: (i) 75% TFA-DCM, 4 h, N₂ atmosphere. (ii) DCC, pyridine, dark. (iii) 1 N HCl, 6 h.

L-Phenylalanine-L-phenylalanine methyl ester folic acid conjugate (3): Folic acid (250 mg, 0.556 mmol), **2** (184 mg, 0.556 mmol), and DCC (128 mg, 0.614 mmol) were dissolved in DMSO (5 mL) in presence of dry pyridine (10 μ L). The mixture was stirred overnight, in the dark, at room temperature under nitrogen

atmosphere. Afterward, the mixture was diluted with deionized water (10 mL) and centrifuged at 1000 rpm for 30 min to separate insoluble dicyclohexylurea. The supernatant was collected and washed with diethyl ether to give a yellow precipitate, which was filtered and dried. The crude compound was further purified by silica gel column chromatography eluting with methanol-dichloromethane, to isolate a pure yellow-coloured compound **3** (180 mg, 72% yield). HRMS (M+H)⁺ for C₃₈H₄₀N₉O₈: 750.3000 (Calcd.), 750.3000 (Anal.), ¹H NMR (500 MHz, d₆-DMSO, TMS, δ ppm): 1.17-1.22 (m, 4H), 1.45-1.75 (m, 4H), 2.46 (s, 3H), 3.31 (s, 2H), 3.45-3.52 (m, 3H), 6.59-7.62 (m, 14H), 7.91 (s, 3H), 8.61 (s, 3H), 9.05 (s, 1H), 11.40 (s, 1H); ¹³C NMR (125 MHz; d₆-DMSO, δ ppm): 25.7, 34.6, 36.7, 42.4, 46.4, 48.3, 52.2, 52.7, 54.1, 54.9, 111.7, 121.7, 126.7, 127.0, 128.5, 128.7, 129.6, 149.0, 149.2, 151.3, 152.8, 154.4, 158.9, 166.9, 171.9, 172.2, 174.3, 174.4.

L-Phenylalanine-L-phenylalanine folic acid conjugate (4): Conjugate 3 (100 mg) was dissolved in 15 mL of 1 N HCl and stirred for 6 h. The residue was filtered and washed with diethyl ether/ acetone (70:30) to achieve yellow precipitates of 4, which was filtered and dried (80 mg, 80% yield). HRMS (M-H)⁻ for C₃₇H₃₆N₉O₈: 734.2687 (Calcd.), 734.2689 (Anal.), ¹H NMR (500

MHz, d₆-DMSO, TMS, δ ppm): 1.68-1.80 (m, 4H), 2.03-3.51 (m, 4H), 4.50 (s, 3H), 6.20-7.63 (m, 14H), 7.90-7.96 (m, 1H), 8.21 (m, 2H), 8.45-8.48 (m, 3H), 8.69-8.86 (s, 1H), 9.02 (s, 1h), 10.60 (s, 1H); ¹³C NMR (125 MHz; d₆-DMSO, δ ppm): 25.84, 30.44, 36.06, 39.35, 47.17, 53.07, 57.45, 59.69, 116.51, 132.07, 132.20, 133.23, 133.52, 134.39, 147.16, 148.04, 148.08, 148.08, 148.97, 150.04, 150.21, 158.44, 163.65, 167.56, 167.70.

5A.3. Microscopy Studies:

Field Emission Scanning Electron Microscopy (FE-SEM): 10 μ L aliquots of samples (1 mM and 10 μ M solutions of conjugates **3** and **4**) were deposited on a silicon wafer (100) and allowed to dry at room temperature. Subsequently, the samples were dried in vacuo for 30 min prior to imaging. Samples were dried in vacuo for 30 min prior to imaging. Samples were gold-coated and SEM images acquired on FEI Quanta 200 microscope (Zeiss Supra 40 VP, Germany), equipped with a tungsten filament gun, operating at WD 3 mm and an operating voltage of 10 kV.

Dynamic Light Scattering (DLS): The solution of **3** at 10 μ M concentration was prepared in HPLC water and sonicated for 10 min. Particle size distribution of **3** was measured using dynamic

light scattering analyzer at a wavelength 657 nm, with Delsa Nano C Particle analyzer (Beckman Coulter, USA) and at 25 °C.

5A.4. Cell assays:

Materials and methods: 3-(4, 5-Dimethylthiazol-2-yl)-2, 5-diphenyltetrazolium bromide (MTT), trypsin-EDTA, Dulbecco's modified eagle's medium (DMEM), penicillin-streptomycin antibiotic, bisBenzimide H 33258 and gelatin (from cold water fish skin) were purchased from Sigma-Aldrich (Bangalore, India) and used without further purification. Dimethyl sulphoxide (DMSO) was obtained from Merck (Bangalore, India). Fetal bovine serum and CellMask™ Deep Red Plasma Membrane stain was purchased from Gibco® Life Technologies (Bangalore, India).

Cell lines: HeLa cell (immortal cervical cancer cell line), MCF7 (breast cancer cell line) and H460 (lung cancer cell line), were purchased from National Center for Cell Sciences Pune, India. It is a national repository of cell lines in India. *In vitro* studies were performed to assess the biocompatibility of **3**.

In vitro cell viability/cytotoxicity studies: Cytotoxicity studies were done with sterilized solution of **3** at a concentration 0.25, 0.5 and 1 μ M in the cell medium to determine if it could be used for biological applications.

MTT assay: *In vitro* biocompatibility studies of **3** were carried out with HeLa cells by MTT assay (Mosmann, 1983)¹³. Cells were maintained with Dulbecco's minimum essential medium supplemented with 10% fetal bovine serum in a humid incubator (37 °C and 5% CO₂). Cells (10⁴ cells/ well) were plated onto 96-well glass-bottom tissue culture plates at an initial confluence of 70%. After 8 h, **3** was added to a final concentration of 0.25, 0.5 and 1 µM and the wells including the control wells (*i.e.* only cells) were, incubated for ~17 h at 37 °C, in 5% CO₂ humidified incubator followed by removal of media. MTT in DMEM medium (0.5 mg/mL) was prepared and stored in the dark environment. After discarding the old media, 200 µL of freshly prepared MTT solution was added to each of the cell-containing wells followed by incubation for 4-5 h. After incubation, basal DMEM (having MTT) was removed and 200 µL of DMSO was added. The viability of cells was determined by measuring their absorbance at 570 nm. The optical density of absorbance is directly proportional to the number of live cells. All *in vitro* cytotoxicity experiments were performed in quintuplicate and the best three were taken to quantitate.

Cell uptake studies: Cells (10⁴ cells/well) were seeded on a sterilized glass cover slip (13 mm, 0.2% gelatin-coated) for 10 h. To study cellular uptake of **3** by confocal laser scanning

microscopy, a solution of **3** (1 μ M) was added to the cell culture media which was incubated for \sim 17 h at 37 $^{\circ}$ C with 5% CO₂ humidified incubator. After incubation cells were washed thrice with PBS buffer and fixed with 4% formaldehyde solution for 20 min. After washing, cells were stained with deep red plasma membrane dye and washed again with PBS buffer. Coverslips were then mounted on slides coated with buffered mounting medium to prevent fading and drying. Samples were observed under confocal laser scanning microscope (CLSM, Leica sp5, Germany).

Flow cytometry data: HeLa cells (10⁴ cells per well) were grown as described above and the cells were incubated with **3** (10 μ M in sterilized water, 1 mL) for 17 h. After the incubation, cells were washed with PBS buffer (pH 7.4) and trypsinized by using 0.25% Trypsin-EDTA. The cells were then resuspended in PBS (pH 7.4) and analyzed by flow cytometry. The experiments were done in triplicate.

For elucidation of the mechanism of particles of **3** in the present work, different cell lines (MCF7, HeLa and H460) were preincubated for 1 h with inhibitors of endocytosis and macropinocytosis followed by incubation with **3** for 17 h afterward. After exposure of cells to **3**, the cells were trypsinized by using

0.25% Trypsin-EDTA after PBS (pH 7.4) wash. The cells were suspended in PBS (pH 7.4) and analyzed by flow cytometry. The experiments were done in triplicate.

5A.5. Results and discussions:

We designed and synthesized conjugates **3** and **4** from folic acid and diphenylalanine dipeptide using a standard protocol involving DCC coupling method (Scheme 2). **3** and **4** were characterized with the help of spectral techniques and their purity established. A number of concentration ranges were assessed for solution-phase self-assembly study of **3**, under aqueous conditions. After some experimentation with respect to solubility characteristics, we recorded SEM micrographs at two difference concentrations (1 mM and 10 μ M). Worm-like, short self-assembled structures were observed (Figure 5A.1a, b), which clearly looked very different from the well-established nanotubular morphology observed for diphenylalanine dipeptide alone. This suggests that not only self-assembly of **3** is concentration dependent, but the two components influence and modulate self-assembly behavior of the conjugate.^{8b} Difference observed with the present conjugate may be ascribed to the number of molecules in stacked orientation and to the possibility of solvent intervention during the H-bond formation.

DLS experiments were performed with 10 μ M aqueous solutions of sample **3**, revealing the hydrodynamic cross-section in the range of ~550-700 nm (Figure 5A.1c). Self-assembly study for **4** also revealed the formation of similar worm-like morphologies under aqueous conditions (Figure 5A.1d). Notably, both **3** and **4** showed similar gross morphological features, despite the presence of an additional hydrogen bonding site in **4**. Folic acid units are proposed to exist as tetramers (Figure 5A.2a, b). Tetrameric ensembles of folic acid are known to self-assemble, with the help of eight intermolecular hydrogen bonds, to form stacked, columnar structures.^{8b} Incidentally, diphenylalanine dipeptide is also known to form hollow nanotubes due to π - π stacking and H-bonding interactions. Thus, it could be surmised that a combination of non-covalent interactions in **3** and **4** govern final morphologies of these conjugates. A proposed model for various interactions is given in Figure 5A.2.

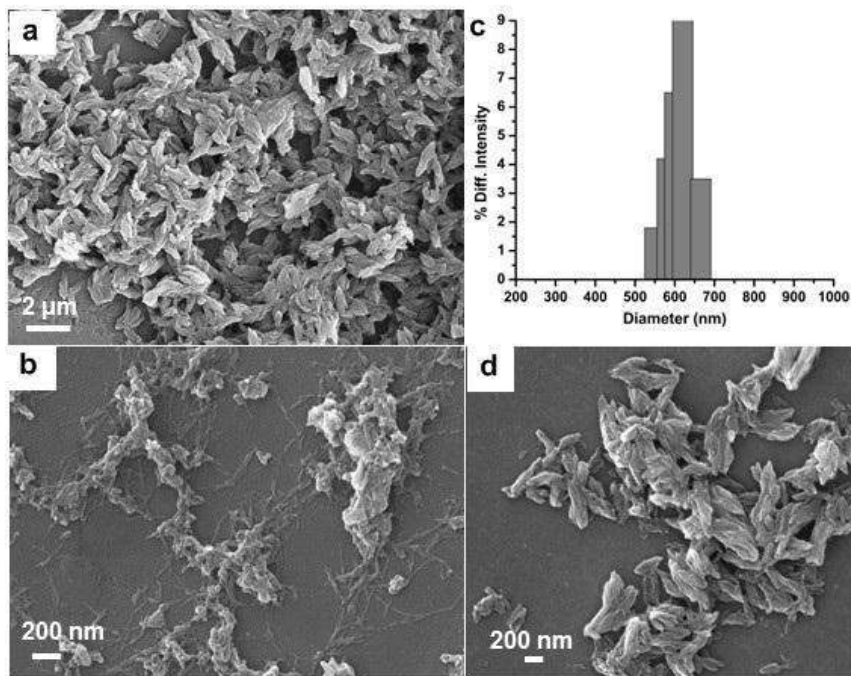


Figure 5A.1: Microscopy analysis on Si(100) wafer in water: (a) 1 mM of **3**; (b) 10 μM concentration of **3**; (c) DLS analysis of **3** at 10 μM; (d) SEM image of **4** at 10 μM.

The experiments were carried out with **3** due to solubility constraints of conjugate across microscopy and cell culture studies. As the premise of this study was to check the effect of folic acid conjugation in dipeptide self-assembly uptake, we decided to first

work with three concentrations (0.25, 0.5 and 1 μM) to find out the toxicity of **3** towards cancer cell lines.

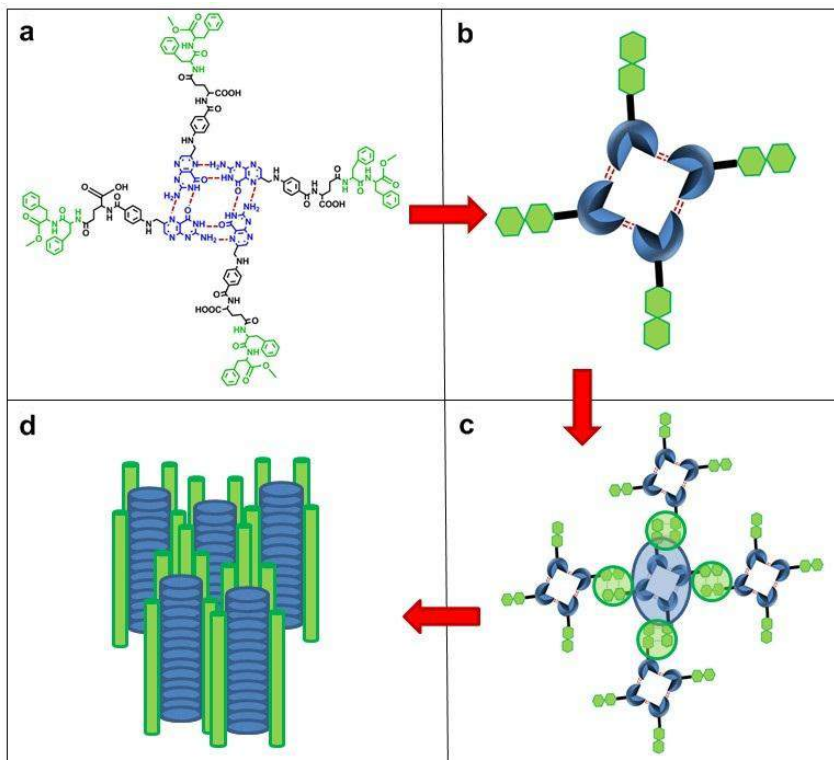


Figure 5A.2: Hypothetical model showing FA-guided self-assembly for **3** and **4**. (a) Proposed core tetramer of folic acid units; (b) model tetramers formed by the Phe-phe conjugates; (c) proposed interactions between various tetramer units and Phe-phe units; (d) stacked, columnar self-assembled structures.

MTT assay study: *In vitro* cytotoxicity of **3** was studied on HeLa cells by MTT assay with different concentrations ranges (0.25, 0.5

and 1 μM), to investigate the effect of these particles on cell viability.

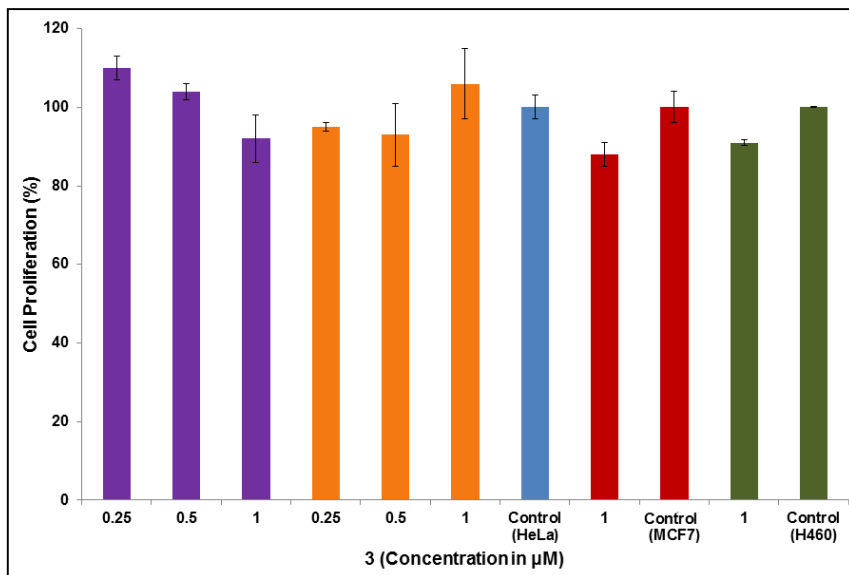


Figure 5A.3: *In vitro* biocompatibility assay of **3** at different concentrations in HeLa cells (17 h incubation) [purple bars (powder sample), orange bars (sample in HPLC water)]; MCF7 (red bars, the sample in HPLC water) and H460 (green bars, the sample in HPLC water) cancer cells.

Samples were prepared in DMEM by two methods: (i) powder sample was dissolved in the medium; (ii) solution was prepared in HPLC grade water, followed by dilution with DMEM. It was observed that cell proliferation percentages for **3** were nearly similar to that of non-treated cell control *i.e.* they are biocompatible (Figure 5A.3, purple and orange bars). Since both sample

preparations showed nontoxic behavior; we opted for the sample prepared in HPLC water, followed by dilution, for further studies. MTT assay was also carried out with MCF7 and H460 cancer cell lines, which confirmed non-cytotoxic nature of **3** (Figure 4A.3, red and green bars).

5A.5.1. Cellular uptake Study:

The conjugate **3** was designed in such a way so that it could bind to and exploit cellular entry-mediated by FR receptors in cancer cells.^{14a-b} Notably, **3** also exhibits fluorescence emission making it conveniently monitored by fluorescence microscopy methods. The non-toxic and biocompatible nature of conjugate **3** motivated us to further investigate uptake and internalization of **3** in various cancer cell lines (HeLa cells, H460 cells and MCF7 cells).

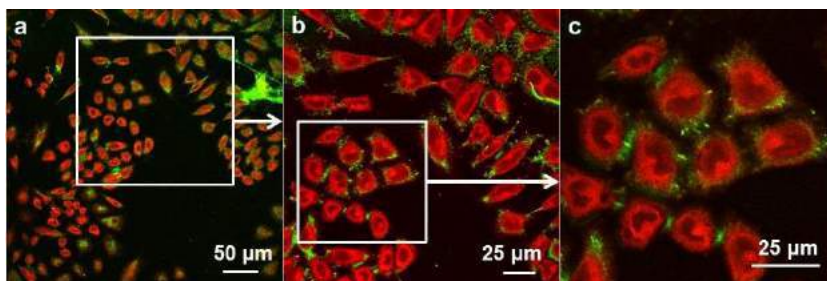


Figure 5A.4: (a) Confocal microscopy images showing uptake of **3** in HeLa cells; (b, c) Magnified view. HeLa cells were stained with deep red plasma

membrane dye, which exhibits red emission ($\lambda_{em} = 633$ nm); green emission ($\lambda_{em} = 488$ nm) in a-c is ascribed to **3**.

HeLa cells were incubated with **3** (1 μ M in cell medium) for 17 h and observed under confocal microscopy, clearly suggesting uptake of **3** by HeLa cells (Figure 5A.4).

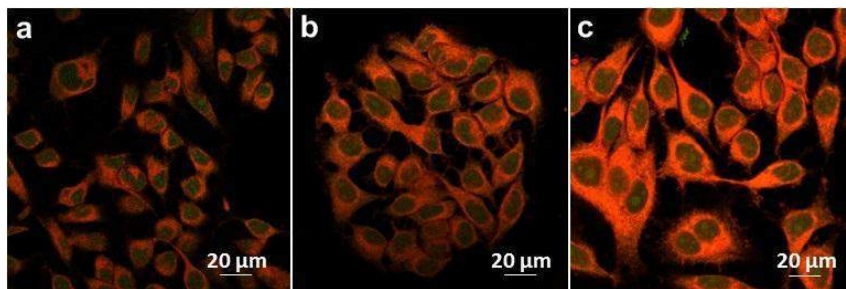


Figure 5A.5: (a) Confocal microscopy images showing uptake of **3** in H460 cells; (b,c) Magnified view. H460 cells were stained with deep red plasma membrane dye, which exhibits red emission ($\lambda_{em} = 633$ nm); green emission ($\lambda_{em} = 488$ nm) in a-c is ascribed to **3**.

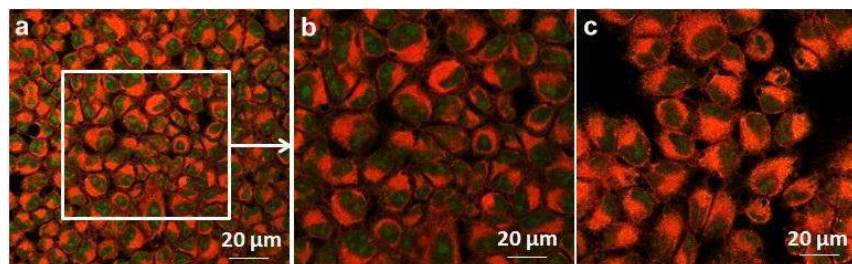


Figure 5A.6: (A) Confocal microscopy images showing uptake of **3** in MCF7 cells; (B, C) Magnified view. MCF7 cells were stained with deep red plasma membrane dye, which exhibits red emission ($\lambda_{em} = 633$ nm); green emission ($\lambda_{em} = 488$ nm) in A-C is ascribed to **3**.

Further, H460 cells (Figure 5A.5), MCF7 cells (Figure 5A.5) were incubated with **3** (1 μ M in cell medium) for 17 h and observed under confocal microscopy, suggesting uptake of **3**.

5A.5.2. Elucidation of uptake mechanism:

Flow cytometry was used to determine the probable mechanism of uptake of **3** (10 μ M) in cancer cells. This technique offers simultaneous measurement and analysis of multiple physical characteristics of single cells, as they pass through a beam of light in a fluid stream. It is commonly used for cell counting and sorting, biomarker detection and in clinical studies. Of the many properties that can be measured such as relative size, relative granularity, and relative fluorescence intensity, we decided to use the later for our experiments. In these analyses, optical information is known as forward scatter (FSC) and side scatter (SSC) are collected. FSC essentially provides information correlating cell size. SSC, light scattering of the cell at 90° angle, provides information on cell granularity. FSC vs. SSC plot is a basic method of visualizing flow cytometric data and the upper right quadrant (*i.e.* Q2), provides information about cells positive for **3**, whereas cells negative for **3** are found in the bottom left quadrant (Q3). For this purpose, a positive control experiment was carried out with HeLa cells (Figure 5A), H460 (Figure S1) and MCF7 cell lines (Figure S2), in

presence of **3**, which suggested that cells internalized **3** and displayed an increase in cell size.

Uptake mechanism of **3** by various cancer cells was probed by using different inhibitors, such as filipin III (1 $\mu\text{g/mL}$), chlorpromazine (5 $\mu\text{g}/100\text{ }\mu\text{L}$), cytochalasin-D (5 μM), rottlerin (25 $\mu\text{g/mL}$), nocodazole (20 μM) and genistein (100 μM), which selectively interfere with various endocytic pathways. Filipin-III and genistein are known to inhibit caveolae-mediated endocytosis, chlorpromazine inhibits clathrin-mediated endocytosis, rottlerin is a selective inhibitor of macropinocytosis, while cytochalasin D inhibits actin polymerization, thus inhibiting both phagocytosis and macropinocytosis.

Uptake of **3** in HeLa (Figure 5A.7) and H460 (lung cancer cells) (Figure 5A.8), in the presence of all inhibitors, was analyzed by flow cytometry. In both of these cell lines, rottlerin leads to the maximum decrease in the percentage of the cell population (Q2) with internalized particles of **3** as compared to the positive control, which showed partial to complete inhibition. This suggests that internalization occurs perhaps through a macropinocytosis-mediated pathway for HeLa cells and H460 cells.

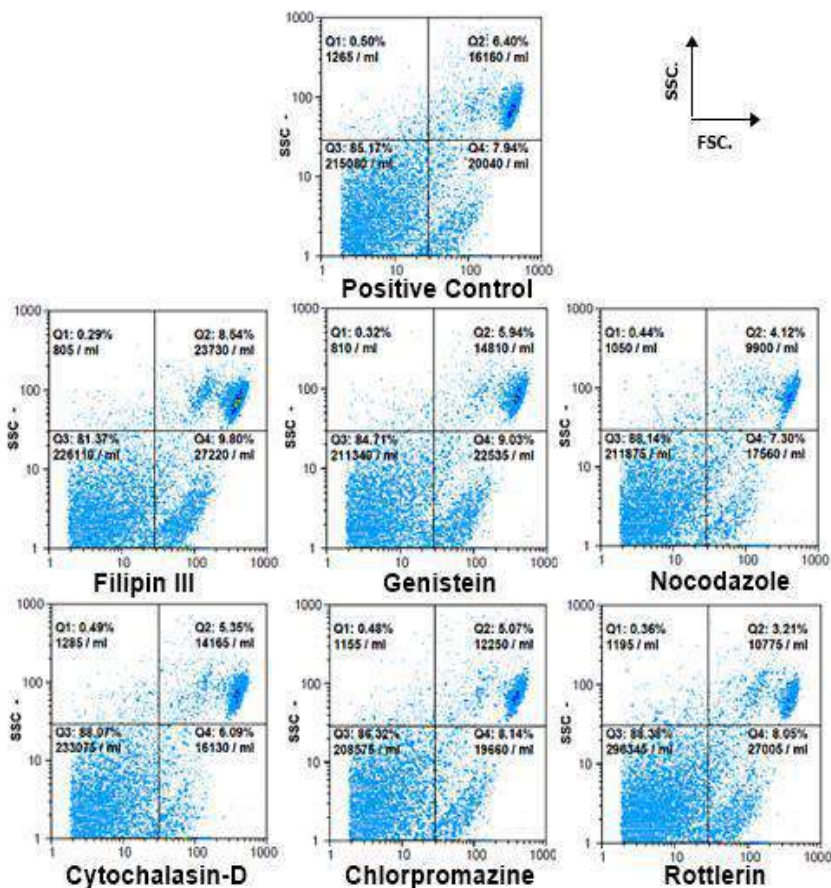


Figure 5A.7: Flow cytometry assay of HeLa cells preincubated for 1 h with endocytic inhibitors, which were treated with **3** for 17 h: (A) no inhibitor; (B) filipin III; (C) genistein; (D) nocodazole; (E) cytochalasin D; (F) chlorpromazine; (G) rottlerin (highlighted Q2).

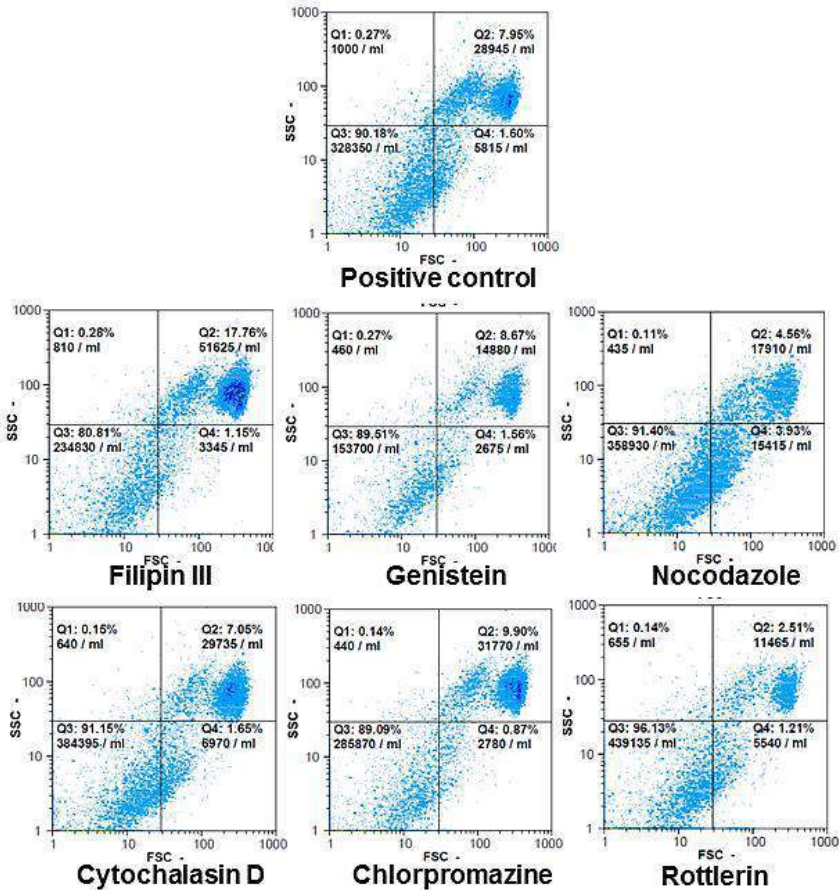


Figure 5A.8: Flow cytometry assay: H460 cells treated with **3** (positive control) and different inhibitors (Filipin III, Genistein, Nocodazole, Cytochalasin D, Chlorpromazine, Rottlerin) showing the percentage of cell uptake. H460 cells were preincubated for 1 h with inhibitors which were treated with **3** particles for 17 h.

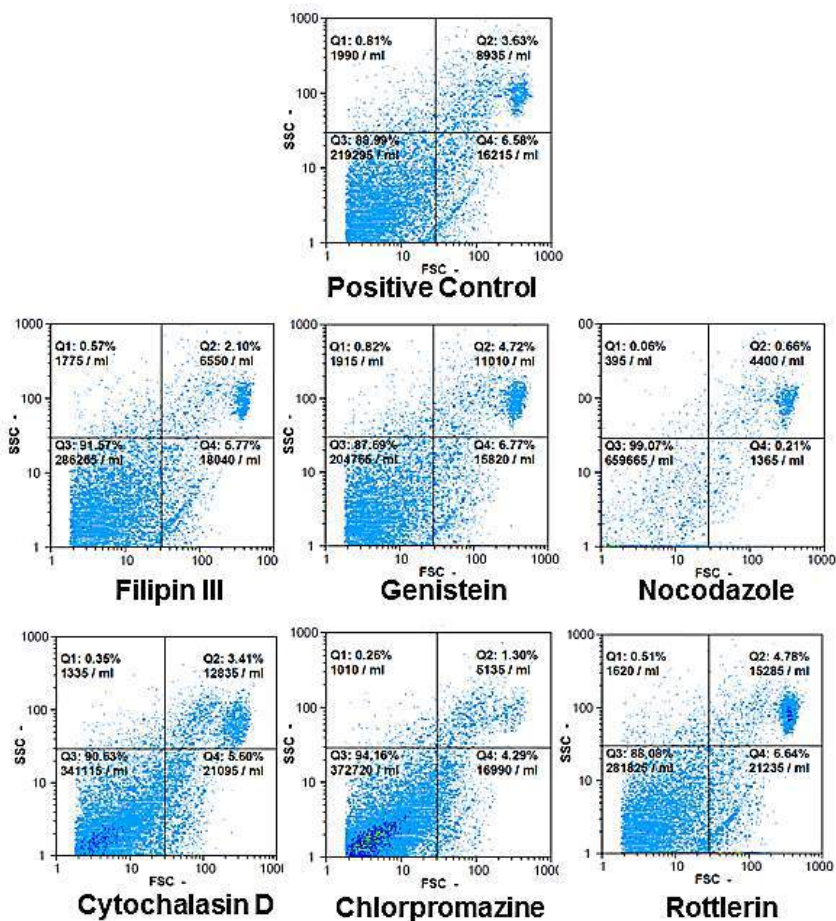


Figure 5A.9: Flow cytometry assay: MCF7 cells treated with **3** (positive control) and different inhibitors (Filipin III, Genistein, Nocodazole, Cytochalasin D, Chlorpromazine, Rottlerin) showing the percentage of cell uptake. MCF7 cells were preincubated for 1 h with inhibitors which were treated with **3** particles for 17 h.

However, in the case of MCF-7 cell line, chlorpromazine and nocodazole inhibited internalization of **3**, which suggests a probable role of clathrin-mediated endocytosis in the uptake process by these cells (Figure 5A.9). Thus, it appears that different cell lines used different endocytotic pathways for the transport of **3** particles.^{15a-d} In addition, there are numerous reports for folate conjugates following multiple pathways for cellular entry thus suggesting that entry *via* folate receptor is not a unique pathway for cell uptake^{16a-b} and mono-or multivalency of folate conjugates have little effect on the rate of cell internalization, despite the fact that multivalent folate conjugates are taken up via different endocytic pathways.¹⁷

5A.6. Conclusion

Folic acid diphenylalanine derivatives were synthesized and studied for their self-assembled behavior. A new morphological structure was obtained as compared to folic acid and diphenylalanine peptide alone. Further, MTT assay showed biocompatible nature and stable behavior of these derivatives. **3** could be used as potential drug delivery vehicle, with further modifications to optimize required properties, as the cellular uptake studies and uptake mechanism studies confirmed internalization of

3 in three different cancer cell lines. Uptake in HeLa and H460 cells was ascribed to macropinocytosis-mediated pathway, based on rottlerin interference. In the case of MCF7 cell line, chlorpromazine and nocodazole inhibited internalization of the peptide, which suggested a probable role of clathrin-mediated endocytosis in the uptake process in this cell line.

5A.7. References

1. (a) Kamaly, N.; Kalber, T.; Thanou, M.; Bell, J. D.; Miller, A. D. *Bioconjug. Chem.* **2009**, *20*, 648–655; (b) Xia, W.; Low, P. S. *J. Med. Chem.* **2010**, *53*, 6811–6824.
2. Chen, C.; Jiyan, K.; Edward, Z. X.; Wei, Y.; Joseph, S. B.; Jun, L.; Eu-Leong, Y.; Eric, X. H.; Karsten, M. *Nature* **2013**, *500*, 486–489.
3. (a) Sudimack, J.; Lee, R. J. *Adv. Drug Deliv. Rev.* **2000**, *41*, 147–162. (b) Paulos, C. M.; Reddy, J. A.; Leamon, C. P.; Turk, M. J.; Low, P. S. *Mol. Pharmacol.* **2004**, *66*, 1406–1414.
4. Wang, S.; Low, P. S. *J. Control. Release* **1998**, *53*, 39–48.
5. (a) Xiaofeng, W.; Wenlie, L.; Na, M.; Fang, L.; Zhenyu, L.; Longhua, G.; Bin, Q.; Guonan, C. *Chem. Commun.* **2012**, *48*, 6184–6186; (b) Cooper, M. A. *Nat. Rev. Drug Discov.* **2002**, *1*, 515–528; (c) Nien-Chu, F.; Fong-Yu, C.; Ja-an, A. H.; Chen-Sheng, Y. *Angew. Chem., Int. Ed.* **2012**, *51*, 8806–8810.
6. (a) Li, J.; Sausville, E. A.; Klein, P. J.; Morgenstern, D.; Leamon, C. P.; Messmann, R. A.; LoRusso, P. J. *Clin. Pharmacol.* **2009**, *49*, 1467–1476; (b) Leamon, C. P.; Reddy, J. A.; Vlahov, I. R.; Westrick, E.; Dawson, A.;

- Dorton, R.; Vetzal, M.; Santhapuram, H. K.; Wang, Y. *Mol. Pharma.* **2007**, *4*, 659–667.
7. (a) Bonazzi, S.; DeMoraes, M. M.; Gottarelli, G.; Mariani, P.; Spada, G. P. *Angew. Chem., Int. Ed. Engl.* **1993**, *32*, 248–250. (b) Ciuchi, F.; Nicola, G. D.; Franz, H.; Gottarelli, G.; Marisni, P.; Bassi, M. G. P.; Spada, G. P. *J. Am. Chem. Soc.* **1994**, *116*, 7064–7071.
8. (a) Federiconi, F.; Mattioni, M.; Baldassarri, E. J.; Ortore, M. G.; Mariani, P. *Eur. Biophys. J.* **2011**, *40*, 1225–1235. (b) Xing, P.; Chu, X.; Ma, M.; Li, S.; Hao, A. *Phys. Chem. Chem. Phys.* **2014**, *16*, 8346–8359.
9. (a) Thomas, A.; Shukla, A.; Sivakumar, S.; Verma, S. *Chem. Commun.* **2014**, *50*, 15752–15755; (b) Kaur, G.; Alder-Abramovich, L.; Gazit, E.; Verma, S. *RSC Adv.* **2014**, *4*, 64457; (c) Ghosh, S.; Alder-Abramovich, L.; Gazit, E.; Verma, S. *Tetrahedron*, **2013**, *69*, 2004–2009; (d) Barman, A. K.; Verma, S. *RSC Adv.* **2013**, *3*, 14691–14700; (e) Mishra, N. K.; Joshi, K. B.; Verma, S. *Mol. Pharm.* **2013**, *10*, 3903–3912; (f) Barman, A. K.; Chaturbedi, A.; Subramaniam, K.; Verma, S. *J. Nanopart. Res.* **2013**, *15*, 2083; (g) Modal, S.; Barman, A. K.; Verma, S. *Chimia* **2012**, *66*, 930–935; (h) Gour, N.; Barman, A. K.; Verma, S. *J. Pept. Sci.* **2012**, *18*, 405–412; (i) Barman, A. K.; Verma, S. *Chem. Commun.* **2010**, *46*, 6992–6994. (j) Joshi, K. B.; Verma, S. *Angew Chem., Int. Ed.* **2008**, *47*, 2860–2863.
10. Singh, P.; Venkatesh, V.; Nagapradeep. N.; Verma, S.; Bianco, A. *Nanoscale* **2012**, *4*, 1972–1974.
11. Castillo, J. J.; Rindzevicius, T.; Wu, K.; Schmidt, M. S.; Janik, K. A.; Boisen, A.; Svendsen, W.; Rozlosnik, N.; Castillo-León, J. *J. Nanopart. Res.* **2014**, *16*, 2525.
12. (a) Reches, M.; Gazit, E. *Science*, **2003**, *300*, 625–627; (b) Adler-Abramovich, L.; Aronov, D.; Beker, P.; Yevnin, M.; Stempler, S.;

- Buzhansky, L.; Rosenman, G.; Gazit, E. *Nat. Nanotechnol.* **2009**, *4*, 849–854; (c) Santhanamoorthi, N.; Kolandaivel, P.; Adler-Abramovich, L.; Gazit, E.; Filipek, S.; Viswanathan, S.; Strzelczyk, A.; Renugopalakrishnan, V. *Adv. Mat. Lett.* **2011**, *2*, 100–105. (d) Yan, X.; Zhu, P.; Li, J. *Chem. Soc. Rev.* **2010**, *39*, 1877–1890. (e) Adler-Abramovich, L.; Reches, M.; Sedman, V. L.; Allen, S.; Tendler, S. J. B.; Gazit, E. *Langmuir* **2006**, *22*, 1313–1320.
13. Mosmann, T.; *J. Immunol. Meth.* **1983**, *65*, 55–63.
14. (a) Dong, S.; Cho, H. J.; Lee, Y. W.; Roman, M. *Biomacromolecules* **2014**, *15*, 1560–1567. (b) Yameen, B.; Choi, W. I.; Vilos, C.; Swami, A.; Shi, J.; Farokhzad, O. C. *J. Control. Release.* **2014**, *190*, 485–499.
15. (a) Vercauteren, D.; Vandenbroucke, R. E.; Jones, A. T.; Rejman, J.; Demeester, J.; Smedt, S. C. D.; Sanders, N. N.; Braeckmans, K. *Mol. Ther.* **2010**, *18*, 561–569; (b) Sarkar, K.; Kruhlak, M. J.; Erlandsen, S. L.; Shaw, S. *Immunology* **2005**, *116*, 513–524; (c) Sami, H.; Maparu, A. K.; Kumar, A.; Sivakumar, S. *PLoS One* **2012**, *7*, e36195. (d) Schnitzer, J. E.; Oh, P.; Pinney, E.; Allard, J. *J. Cell. Biol.* **1994**, *127*, 1217.
16. (a) Dong, S.; Cho, H. J.; Lee, Y. W.; Roman, M. *Biomacromolecules* **2014**, *15*, 1560–1567. (b) Li, Y. L.; Cuong, N. V.; Hsieh, M. F. *Polymers* **2014**, *6*, 634–650.
17. Bandara, N. A.; Hansen, M. J.; Low, P. S. *Mol. Pharma.* **2014**, *11*, 1007–1013.

Chapter 5B

Dityrosine-folic acid Conjugate in Electrospun Nanofibers for Selective Cell Adhesion

5B.1. Introduction

Electrospun nanofibers are highly useful scaffolds that offer added scope for fine-tuning physical properties such as surface area and mechanical strength and chemical functionalization to afford materials for tissue engineering and drug delivery applications.¹ More specifically, such nanofibers have been used in filtration systems, protective clothing, medical prostheses, energy storage, space applications, nano-optoelectronics, wound healing, and tissue engineering scaffolds, etc.² Advantages of using polymer nanofibrous materials as tissue scaffolds are ascribed to their nontoxic nature and the possibility of creating structural features similar to extracellular matrices.³

Biological applications necessitate nanofibers that are biocompatible and present favorable interactions with cells, extracellular matrix, growth factors and other biomolecules. Exploration in this domain includes modification of hydrophobic/hydrophilic properties, the creation of a robust mesh-like structure enabling optimal fluid sorption, transport and delivery properties supporting the overarching aim to achieve cell interaction, adhesion and proliferation. It is desirable that biocompatible nanofibers also exhibit mechanical strength and

present a good enough surface area to allow for high volume cell attachment and favorable interactions.⁴ For example, poly(lactic-co-glycolic acid), a biodegradable polymer, has been extensively used in electrospinning to create scaffolds with appropriate physical and mechanical properties.⁵

FDA approved poly- ϵ -caprolactone (PCL) is a biocompatible synthetic polymer with potential uses in tissue engineering and regenerative therapies due to its affordability, biocompatibility, and mechanical strength.⁶ However, hydrophobicity and cell binding incapability of PCL demands attention before it could be developed as an advanced biomaterial. These issues were addressed by the incorporation of peptides and peptide amphiphiles along with PCL in electrospinning process.⁷ Fibrous networks derived from peptide-modified PCL displayed improved cell adhesion and proliferation.⁸

Folic acid (FA) is a vitamin crucial for DNA synthesis, cell division and replication and for the formation of red and white blood cells. As a strategy to achieve cell interaction and uptake, folate-drug conjugates exploit binding of folic acid to its cognate folate receptor (FR) protein present on the cell surface of many human cancers, through endocytosis uptake

mechanism.⁹ Recent applications in this direction include folic acid conjugated poly(ϵ -caprolactone)-polypeptide copolymer vesicles as antibacterial agents,¹⁰ polyethylenimine-graft-polycaprolactone-block-poly(ethylene glycol)-folate ternary copolymer for targeted siRNA delivery,¹¹ and folate-functionalized poly(ethylene glycol)-b-polycaprolactone (folate-PEG-b-PCL) for intracellular and prolonged delivery to retinal pigment epithelium cells,¹² to name a few.

Our interest in peptide conjugates and functional peptide self-assembly concerns the creation of soft compartments for cellular delivery and amyloid modeling.¹³ We recently described the synthesis of a folic acid-containing phenylalanine, which was further used to study self-assembly, gross morphology of ensuing supramolecular structures and their cell delivery properties.¹⁴ It was determined that covalent conjugation of folic acid to the dipeptide afforded predictable assemblies and that both macropinocytosis-mediated pathway and clathrin-mediated endocytosis were possibly involved in the cellular uptake process. In order to expand the applications of folate conjugated amino acids and peptides, we became interested in developing a new conjugate as an additive for electrospun PCL nanofiber mats to seek separation of cancer cells, given the propensity of

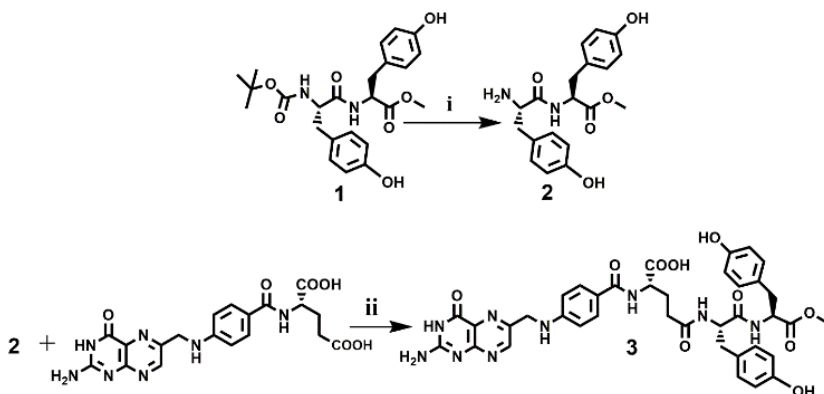
overexpression of folate receptors on certain cancer cells surfaces. This study is expected to serve as a step towards developing adaptive nanomats for detection and selective capture of FR-positive cancer cells.

5B.2. Experimental Section

5B.2.1. Materials: Poly- ϵ -caprolactone (PCL), average $M_n = 80,000$ used to synthesize electrospun mats was purchased from Sigma-Aldrich (Bengaluru, India). L-tyrosine (Tyr), N, N'-Dicyclohexylcarbodiimide (DCC) and trifluoroacetic acid (TFA) were purchased from Spectrochem Pvt. Ltd., Mumbai, India; *N*-tert-butoxy carbonyl (Boc anhydride), thionyl chloride, *N*-Hydroxybenzotriazole (HOBt) and folic acid (FA) were purchased from S. D. Fine-Chem Ltd., Mumbai, India; and used without further purification. Dichloromethane (DCM), methanol (MeOH), N, N-dimethylformamide (DMF), methanol, trimethylamine (TEA), pyridine were distilled according to standard procedures prior to use. Merck pre-coated TLC plates (TLC Silica gel 60 F254) were used for thin layer chromatography (TLC), and compounds were visualized with a UV light at 254 nm. 100-200 mesh silica gel (S. D. Fine-Chem Pvt. Ltd.) was used for chromatographic separations.

5B.2.2. Peptide conjugate synthesis:

Dityrosine conjugate **3** was prepared by standard solution phase peptide synthesis methodology (Scheme 1).



Scheme 1. Synthetic scheme for **3**: (i) 75% TFA–DCM, 4 h, N₂ atmosphere; (ii) N, N'-dicyclohexylcarbodiimide, pyridine (dark conditions).

Boc-L-tyrosyl-L-tyrosine methyl ester (1): N-(Boc)-L-Tyrosine (3 g, 10.7 mmol) and HOBt (1.44 g, 10.7 mmol) were dissolved in dry DMF (25 mL) under the nitrogen atmosphere. The reaction mixture was cooled to 0 °C and a solution of DCC (2.64 g, 12.7 mmol), dissolved in DCM was added in small portions. L-tyrosine methyl ester hydrochloride (2.50 g, 12.8 mmol) was further added to the reaction mixture followed by dropwise addition of triethylamine (7.44 ml, 53.3 mmol) after 45 min while stirring at 0 °C. The reaction mixture was further stirred for 24 h at room

temperature. DCU was removed by filtration and the filtrate was concentrated under reduced pressure. The residue was dissolved in ethyl acetate and the organic layer was washed with 1 N HCl (2×30 mL) and brine (30 mL). The organic layer was dried over anhydrous sodium sulfate and concentrated under reduced pressure. The crude compound was purified on a silica gel column by using DCM and MeOH to get pure **1** (1.90 g, 64% yield), R_f [7% MeOH in DCM] 0.5, HRMS ($M+Na$)⁺ for C₂₄H₃₀N₂O₇: 481.1951 (Calcd.), 481.1959 (Anal.), ¹H NMR (500 MHz, CDCl₃, TMS, δ ppm): 1.39 (s, 9H), 2.84-3.19 (m, 4H), 3.63 (s, 3H) 4.28 (t, 1H), 4.71 (t, 1H), 5.26 (m, 2H), 6.51-7.34 (m, 8H); ¹³C NMR (125 MHz; CDCl₃, δ ppm): 28.34, 37.05, 37.73, 52.57, 56.06, 60.59, 80.91, 115.76, 126.88, 130.38, 155.40, 155.84, 171.67, 171.79.

L-Tyrosyl-L-tyrosine methyl ester (2): **1** (1g) was dissolved in 75% TFA-DCM (10 mL) and stirred for 6 h under nitrogen atmosphere. After completion of the reaction, the solvent was evaporated *in vacuo* and the resulting solid was subsequently washed with diethyl ether (3×20 mL) to afford a white solid. The latter was dissolved in MeOH and passed through Dowex resin, followed by evaporation of fractions under reduced pressure to obtain pure **2** (0.822 g, 82.2% yield) which was used as such in the next step.

Folate L-Tyrosyl-L-tyrosine methyl ester (3): FA (0.25 g, 0.556 mmol), **2** (0.203 g, 0.556 mmol), and DCC (0.701 g, 3.39 mmol) were dissolved in DMF (5 mL), in the presence of dry pyridine (10 μ L). The mixture was stirred overnight at room temperature under nitrogen atmosphere and dark conditions. The resulting mixture was diluted with deionized water (10 mL) and centrifuged at 1000 rpm for 30 min to separate insoluble DCU. The supernatant was collected and washed with diethyl ether to afford a yellow precipitate which was filtered and dried. The crude compound was further dialyzed against distilled water for 48 h (0.167 g, 65% yield). HRMS ($M+H$)⁺ for C₃₈H₃₉N₉O₁₀: 782.2898 (Calcd.), 782.2897 (Anal.), ¹H NMR (500 MHz, d₆-DMSO, TMS, δ ppm): 2.04-3.34 (m, 8H), 3.63 (s, 3H, merged with residue peak with DMSO-d₆), 4.28 (m, 2H), 4.44 (m, 2H), 5.24 (s, 2H), 6.60-7.62 (m, 12H), 8.07-8.09 (m, 3H), 8.61-8.63 (m, 3H), 11.90 (s, 1H); ¹³C NMR (125 MHz; d₆-DMSO, δ ppm): 26.9, 31.17, 35.41, 42.59, 46.4, 52.39, 55.07, 65.42, 111.72, 121.85, 128.46, 129.50, 132.70, 136.93, 138.61, 142.21, 149.14, 151.33, 154.71, 161.19, 166.84, 173.30, 174.50.

5B.2.3. Cell Assays

Material and Methods: Dulbecco's modified eagle's medium (DMEM), 3-(4, 5-Dimethylthiazol-2-yl)-2, 5-diphenyltetrazolium

bromide (MTT), trypsin–EDTA, Penicillin–streptomycin and gelatin (from cold water fish skin) were purchased from Sigma-Aldrich (Bengaluru, India). Dimethyl sulfoxide (DMSO) was obtained from Merck (Bengaluru, India). Fetal bovine serum (FBS), DAPI (4,6-diamidino-2-phenylindole) and CellMask™ deep red plasma membrane stain were purchased from Gibco® Life Technologies.

Cell lines, culture conditions and treatments: HeLa cells (cervical cancer cells) and HEK 293 cells (Human embryonic kidney cells) were maintained at 37 °C, 5% CO₂ and 95% relative humidity in DMEM and DMEM with 100 mM sodium pyruvate medium respectively, supplemented with 10% heat-inactivated FBS, penicillin (100 U/ml) and streptomycin (100 U/ml). Cells were seeded for 24 h prior to treatment. All the treatments were performed at 37 °C and at a cell density allowing exponential growth.

MTT cell viability assay: *In vitro* biocompatibility studies of **3** were carried out with HeLa cells by MTT assay.¹⁵ Cells were maintained in DMEM, supplemented with 10% fetal bovine serum in a humid incubator (37 °C and 5% CO₂). Cells (10⁴ cells/well) were plated onto 96-well glass-bottom tissue culture plates. After 12 h, **3** was added to a final concentration of 0.01, 0.02, 0.08, 0.12

and 0.16 mM, to the wells and incubated for ~24 h. MTT in DMEM medium (0.5 mg/mL) was prepared and stored in a dark environment. After discarding the old media, 200 μ L of freshly prepared MTT solution was added to each of the cell-containing wells followed by incubation for 4 h. After incubation, basal DMEM (having MTT) was removed, and 200 μ L of DMSO was added. Cell viability was determined by measuring their absorbance at 570 nm. The optical density of absorbance is directly proportional to the number of live cells. All *in vitro* cytotoxicity experiments were performed in quintuplicate, and the three consistent readings were used.

Cell adhesion study:

Cells (10^4 cells/well) were seeded on a sterilized glass surface (13 mm, 0.2% gelatin-coated) for 24 h. To study the cell adhesion on **3**/PCL mats by confocal laser scanning microscopy (CLSM), HeLa cells were incubated on the **3**/PCL mat placed on a glass surface in the cell culture media for ~24 h, at 37 °C with 5% CO₂ humidified incubator. After incubation, cells were washed thrice with phosphate buffered saline (PBS) buffer and fixed with 4% formaldehyde solution for 15 min. After washing, cells were stained with deep red plasma membrane dye or DAPI and washed again with PBS buffer. Coverslips were then mounted on the slides

coated with buffered mounting medium to prevent fading and drying.

5B.2.4. Microscopy Studies

Optical Microscopy (OM): Electrospun mats (with and without **3**) were deposited on a glass surface. OM images were acquired on Leica DM2500M microscope, equipped with a bright and dark field imaging.

Fluorescence Microscopy (FM): The samples were examined under a fluorescent microscope (Leica DM2500M), provisioned with a Rhodamine filter N2.1 (absorption 540 nm/emission 625 nm) and I3 filter (absorption 370 nm /emission 450 nm).

Field Emission Scanning Electron Microscopy (FE-SEM): (a) Electrospun mats (with and without **3**) were deposited on a glass surface at 25 °C; (b) 10 μ L aliquots of peptide samples (1 mM solution) were deposited on a silicon wafer (100) and allowed to dry at room temperature. The samples were dried *in vacuo* for 30 min prior to imaging. Samples were gold-coated and SEM images acquired on FEI Quanta 200 microscope equipped with a tungsten filament gun, operating at a WD 4 mm and an operating voltage of 10 kV.

Confocal laser scanning microscopy (CLSM): Cell assays samples were observed under confocal laser scanning microscope (CLSM, LSM 780 NLO, Carl Zeiss GmbH).

Optical Profiler: Samples were scanned with Nanomap-D (Universal 3D Profilometer). The area scanned was 150x150 mm² with Z focusing range 0.1 nm to 10 mm.

5B.2.5. Electrospinning method: Electrospun fibrous mats were synthesized using 3/PCL polymer solution, on a Super ES-2 model electrospinning unit (E-Spin Nanotech Pvt. Ltd., SIBDI Innovation and Incubation Centre, IIT Kanpur). High voltage (10-30 kV) was applied on to 3/PCL, the flow rate of which was controlled and maintained by a syringe pump. When the applied voltage exceeded the critical limit, the former stretches, leading to solvent evaporation and deposition of 3/PCL in the form of nanofibers on a grounded collector.

5B.2.6. Contact angle measurements: The surface hydrophobicity was measured on Drop Shape Analyser DSA25 (Krüss Advancing), equipped with a high-resolution USB 3.0 camera for the drop shape analysis, was used at 25 °C and 65% relative humidity. 3/PCL were electrospun on a glass surface and ultrapure water was applied on different areas of the mats. The

experiments were performed in triplicate and the average of the data has been reported.

5B.3. Results and Discussion

5B.3.1. Solution phase self-assembly of **3:** Tyrosine is an important aromatic amino acid that serves as a versatile precursor for the biosynthesis of certain neurotransmitters and plays a key role in signal transduction through phosphorylation catalyzed by tyrosine kinases. We recently demonstrated that Tyr can afford formation of well-ordered assemblies, which could be influenced by parameters such as concentration, duration of aggregation, pH, etc., forming morphologies ranging from nanoribbons to branched, fern-like structures.¹⁶ These supramolecular structures could find potential applications such as biosensors, which lead us to surmise their potential use as molecular scaffolds in regenerative medicine by chemical modification via Tyr cross-linking.

With this as a backdrop, **3** was designed and synthesized by standard procedures and protocols using DCC coupling method (Scheme 1). A stock solution of **3** (5 mg/mL DMSO) was diluted with DCM to afford 1 mM final concentration, which was used to study self-assembly behavior. **3** afforded formation of fibrous networks as determined by scanning electron microscopy studies

on silicon wafers (100) (Figure 5B.1a, b). These structures were somewhat different from the ones obtained for pure Tyr suggesting a role of folic acid in giving rise to aggregate structures.

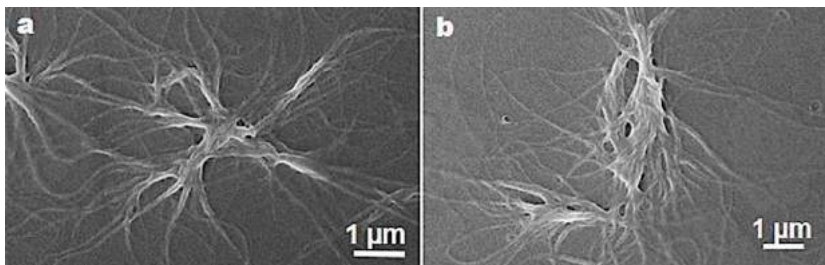


Figure 5B.1. (a, b) SEM images of **3** in (DMSO:DCM)

5B.3.2. Preparation of 3/PCL based mats: A stock solution of **3** (50 mg/mL DMSO) was prepared and diluted with 10% w/v PCL solution in DCM to afford a final concentration of 1 mg/mL. This solution was used for the synthesis of fibrous network containing mats using an electrospinning machine (Figure 5B.2). Three different concentrations of peptide/PCL solutions (**3**/PCL(I) = 1 mg/mL; **3**/PCL(II) = 2.5 mg/mL; and **3**/PCL(III) = 5 mg/mL, in 10% w/v PCL solution in DCM) were used to make three different mats through the electrospinning process.

Blend tip 20-G needle and a drum collector were used during the electrospinning process. The syringes were filled with

3/PCL solution and connected to the silicon tube of a connector. The solution was released at 1 mL/h by a pump operating at a voltage of 14 kV. Fibrous mat was synthesized on a glass surface attached to an aluminum foil wrapped around a drum collector (2000 rpm) at a distance of 14 cm from the needle present, at room temperature (25 °C). It was washed with absolute ethanol for 20 min and vacuum-dried prior to use. It was characterized through microscopy tools such as SEM, CLSM and FM to understand gross morphology (Figure 5B.2).

3/PCL mats showed notable changes in morphology (Figure 2d, 2e) and variation in fibers thickness (600 nm to 2.5 μ m) as compared to PCL control fibers (Figure 5B.3). The peptide self-assembled structures were uniformly distributed throughout on PCL fibers in the mats which were confirmed by fluorescence microscopy (FM) and confocal laser scanning microscopy (CLSM) (Figure 5B.2b, 5B.2c).

Surface hydrophobicity of mats was found to decrease with the addition of 1 mg peptide /mL of 10% w/v PCL solutions as compared to PCL control fibers (Figure 5B.4).

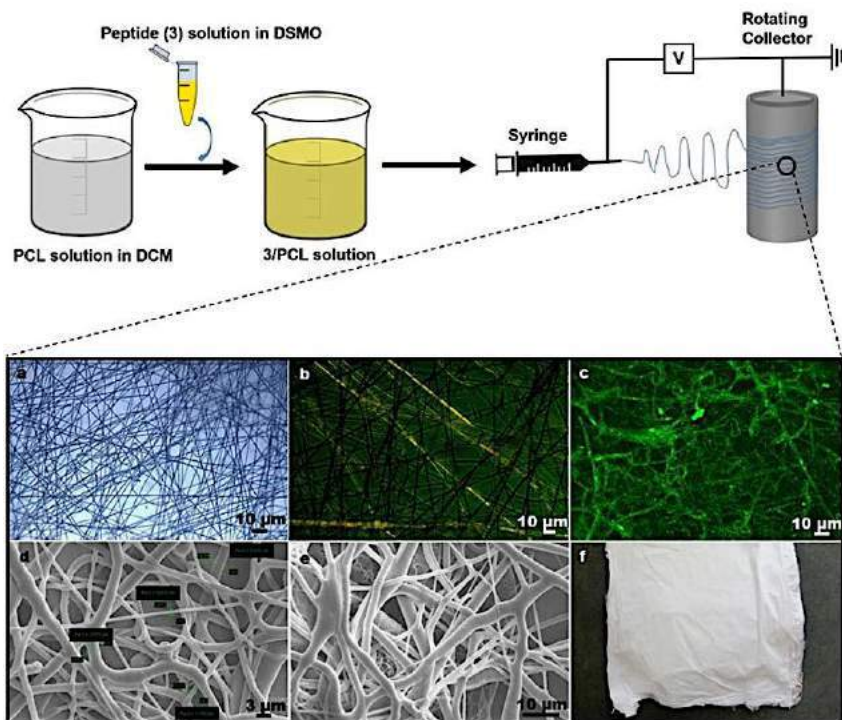


Figure 5B.2. Morphology of 3/PCL fibers and mat (1 mg/mL in 10% w/v PCL): (a) OM image, (b) FM image, (c) CLSM image, (d, e) SEM images, (f) Visual image of mat. Green emission ($\lambda_{\text{em}} = 488 \text{ nm}$) in b, c is ascribed to **3**.

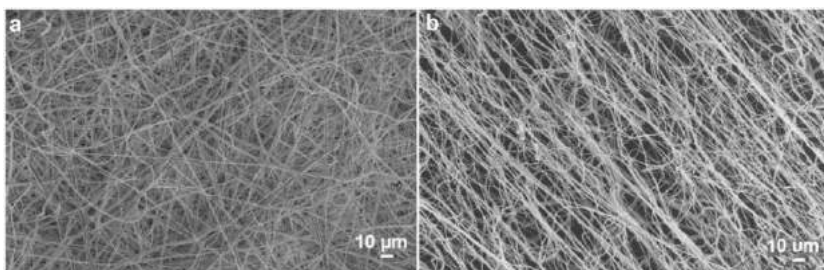


Figure 5B.3. (a,b) SEM image of PCL control mat.

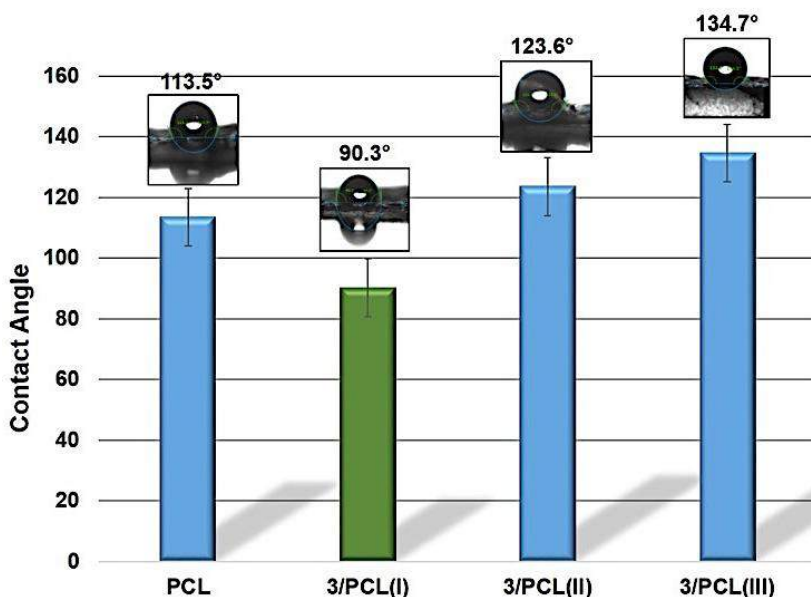


Figure 5B.4. Contact angles details of PCL and 3/PCL mats with different concentration of peptide (3/PCL(I), 3/PCL(II) and 3/PCL(III) were with concentration 1, 2.5 and 5 mg peptide/mL of 10% w/v PCL solution in DCM, respectively).

This probably occurred due to the polar nature of tyrosine and availability of H-bonding interactions. Further increase in peptide concentration led to an increase in the hydrophobicity of the mats. As 3/PCL(I) satisfied all required qualities for cell culture and cell adhesion, further study was carried out with 3/PCL(I) mats only.

5B.3.3. Cytotoxicity of 3: In order to test the biocompatibility of **3**, HeLa cells were grown in a medium containing five different concentrations of **3** (0.01, 0.02, 0.08, 0.12 and 0.16 mM) and its cytotoxicity measured using the established MTT assay. There was no statistically significant difference between control and treated sets ($p < 0.05$). As shown in Figure 5B.5, the peptide was nontoxic to HeLa cells up to 24 h incubation and hence, biocompatible.

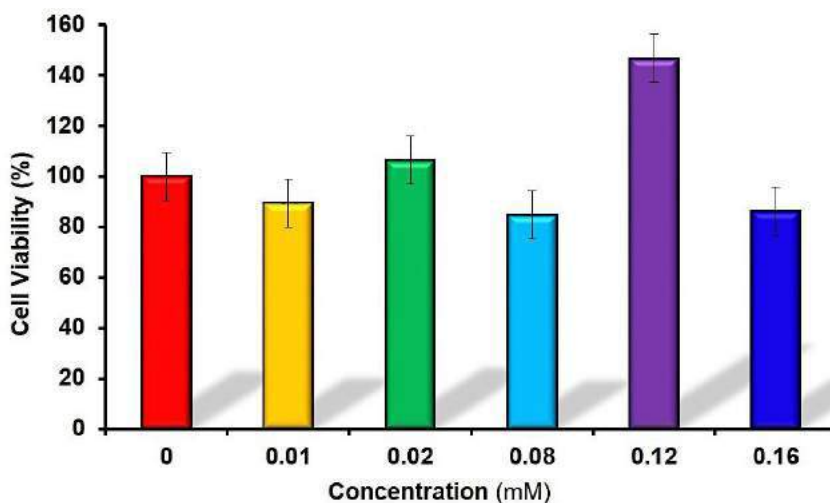


Figure 5B.5. Bar diagram viability of HeLa cells grown in various concentrations of **3**, as measured by MTT assay.

5B.3.4. Cell-adhesion properties of 3/PCL(I) mat: Cancerous cells have higher levels of folate receptor (FR) – the cell surface protein that binds to and promotes the cellular uptake of FA. Therefore, FR is often considered as a target for cancer diagnosis and therapeutics.¹⁷ For example, electrodes modified with folate conjugated peptide have been previously studied to successfully detect HeLa cancerous cells in very low concentration samples.¹⁸ Low cost and reliable early detection and diagnosis of cancer and other folate overexpressed infections would lead to increased chances of treatment and survival. To test such potential, the 3/PCL(I) mats were studied for their differential affinity toward cells that overexpress FR. HeLa cells – a human cervical cancer line with high FR expression – were seeded on a glass surface coated with 3/PCL(I) fibrous mat, or on a glass surface coated with PCL control mat.

Cells seeded and grown on a glass surface, coated with 0.2% gelatin, served as the control. These seeded cells were incubated at 37 °C in regular culture medium for 24 h, washed with PBS, fixed and the glass surfaces were analyzed using OM, SEM and CLSM. The 3/PCL fibrous mat favored better attachment and growth of HeLa cells (Figure 5B.6) as the adhered cells seem to have aligned along the direction of the 3/PCL(I) fibers (Figure

5B.7). It was noted that very few cells attached to the PCL control mat (Figure 5B.8) as compared to the **3**/PCL mat and the glass surface coated with gelatin (Figure 5B.8).

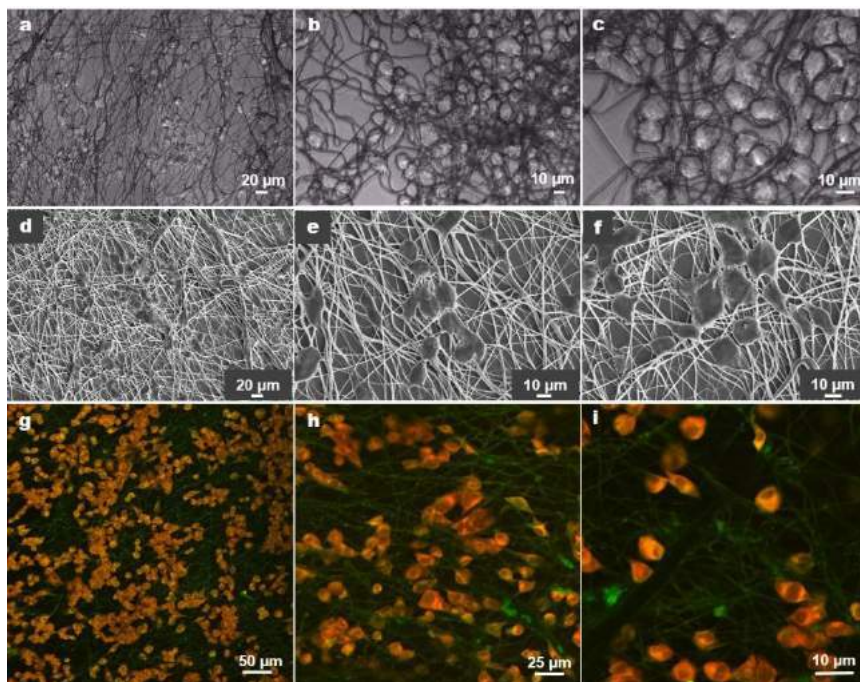


Figure 5B.6. Images showing HeLa cell adhesion on **3**/PCL mat (a-c) OM image, (d-f) SEM image, (g-i) CLSM images. Green emission ($\lambda_{em} = 488$ nm) in g–i is ascribed to **3** and HeLa cells were stained with deep red plasma membrane dye, which exhibits red emission ($\lambda_{em} = 633$ nm).

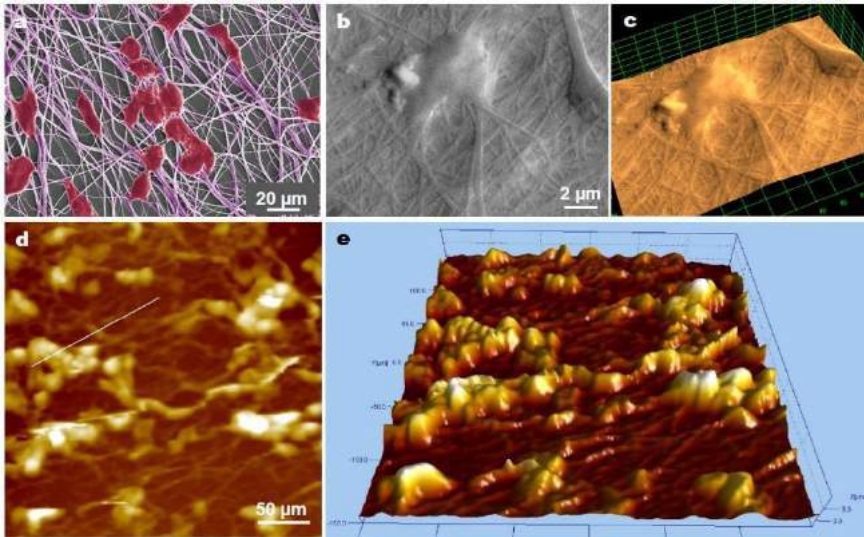


Figure 5B.7. HeLa cell adhesion study on 3/PCL mat (a) False-colored SEM image, (b, c) 3D SEM images, (d) Optical profile image, (e) 3D profile image.

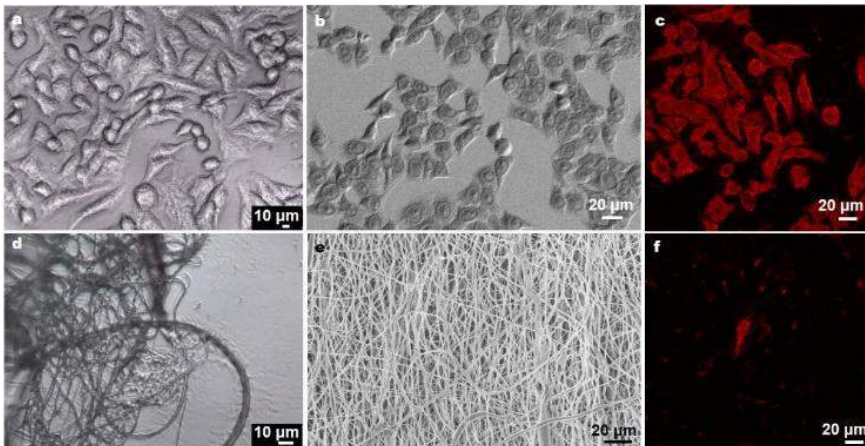


Figure 5B.8. (a-c) OM, SEM and CLSM images of HeLa cells on the glass surface with gelatin, respectively, (d-f) OM, SEM and CLSM images of PCL control mat with HeLa cells, incubated for 24 h.

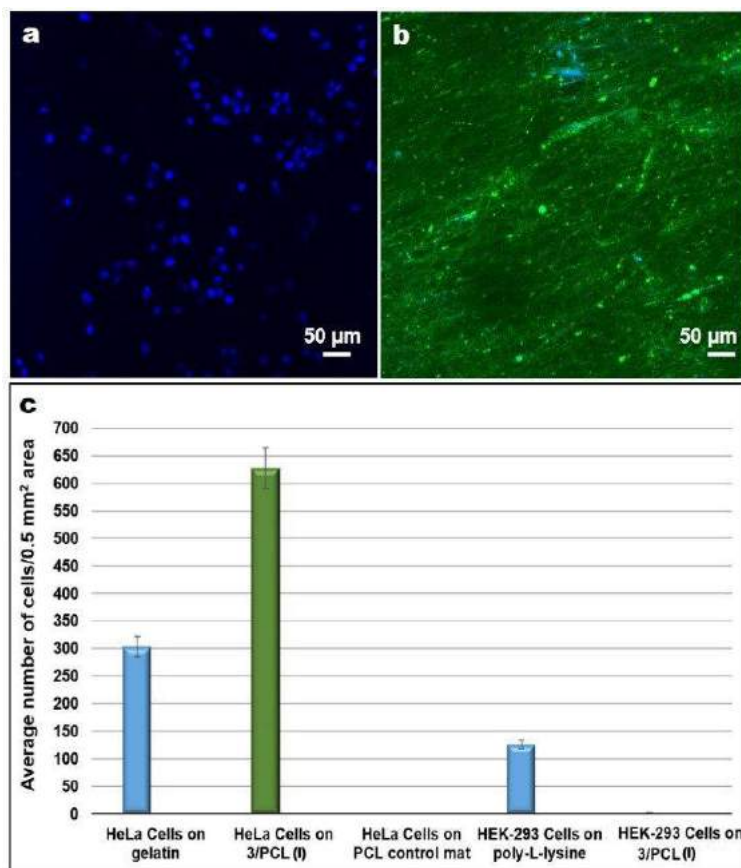


Figure 5B.9. (a) HEK 293 cells on the glass surface coated with poly-L-Lysine, (b) 3/PCL(I) mat after incubating seeded cells on the surface for 24 h, (c) an average number of cells (HeLa or HEK 293) on the glass slide, compared to the 3/PCL(I) mat and PCL alone. An average number of cells in 0.5 mm² were taken

each time. HEK 293 cells were stained with DAPI, which exhibits blue emission ($\lambda_{em} = 405$ nm) and green emission ($\lambda_{em} = 488$ nm) is ascribed to **3**.

To check if the observed adhesive property of HeLa cells is dependent on FR, equal number of HeLa cells or HEK 293 cells, a non-cancerous cell line derived from human embryonic kidney, with very low level FR expression, was seeded on to the **3**/PCL(I) mats, allowed to settle for 24 h at 37 °C, and the number of cells attached to the surface (0.5 mm²) were counted.

While the **3**/PCL(I) surface showed two-fold increase in the number of cells (623 cells/0.5 mm² area) as compared to the gelatin coated glass coverslip (300 cells/0.5 mm² area), the HEK 293 were hardly detected on the **3**/PCL(I) surface (Figure 5B.9) thus, establishing a selective affinity for the **3**/PCL(I) surface to FR positive cells. Number of cells in different conditions are summarized in the graph shown in Figure 5B.9c. It was revealed that **3**/PCL(I) mats selectively bound to folate overexpressed cells.

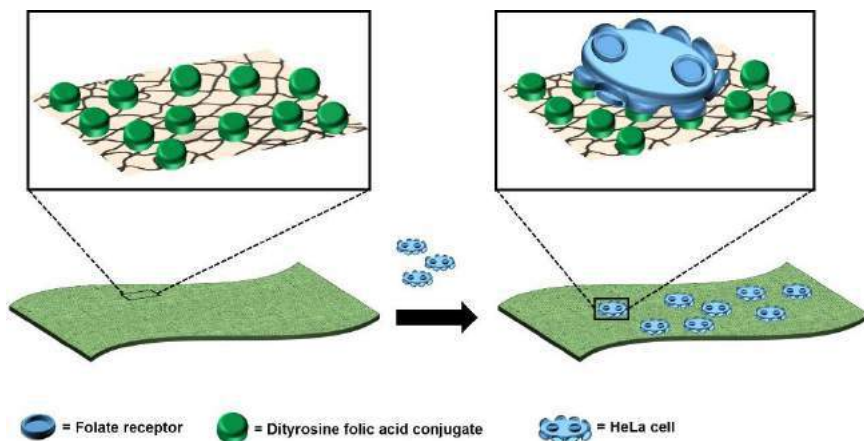


Figure 5B.10: Model showing capturing of HeLa cells over 3/PCL(I) mat.

5B.4. Conclusions

We have designed and synthesized a covalently linked Dityrosine-folic acid conjugate, followed by its use in creating electrospun mats with PCL. Hydrophilicity of these mats could be fine-tuned by choosing the correct ratio of peptide conjugate-PCL mixture, leading to the formation of homogenous fibers with folate display. The applicability of these recognition element functionalized mat was confirmed by analyzing selective adhesion and proliferation of HeLa cells (FR-positive cells) and the lack of adhesion of HEK 293 cells (FR negative cells). These nanomats can be engineered further

for selective detection and retention of specific cancerous cells and parasites, such as leishmania.

5B.5. References

1. (a) Sridhar, R.; Lakshminarayanan, R.; Madhaiyan, K.; Barathi, V. A.; Lim, K. H. C.; Ramakrishna, S. *Chem. Soc. Rev.* **2015**, *44*, 790–814. (b) Jin, M.; Yu, D. G.; Geraldles, C. F.; Williams, G. R.; Bligh, S. W. *Mol. Pharm.* **2016**, *13*, 2457–2465. (c) Jiang, T.; Carbone, E. J.; Lo, K. W. -H.; Laurencin, C. T. *Progr. Polym. Sci.* **2015**, *46*, 1–24.
2. (a) Kim, C.; Kim, Y. J.; Kim Y. A. *Solid State Commun.* **2004**, *132*, 567–571. (b) Zhang, Y.; Huang, Z. M.; Xu, X.; Lim, C. T.; Ramakrishna, S. *Chem. Mater.* **2004**, *16*, 3406–3409. (c) Berber, E.; Horzum, N.; Hazer, B.; Demir, M. M. *Fiber Polym.* **2016**, *17*, 760–768. (d) Martínez, S.; Amantia, D.; Knipping, E.; Aucher, C.; Aubouy, L.; Amici, J.; Zeng, J.; Francia, C.; Bodoardo, S. *RSC Adv.* **2016**, *6*, 57335–57345. (e) Ju, H. W.; Lee, O. J.; Lee, J. M.; Moon, B. M.; Park, H. J.; Park, Y. R.; Lee, M. C.; Kim, S. H.; Chao, J. R.; Ki, C. S.; Park, C. H. *Int. J. Biol. Macromol.* **2016**, *85*, 29–39. (f) Hassiba, A. J.; El Zowalaty, M. E.; Nasrallah, G. K.; Webster, T. J.; Luyt, A. S.; Abdullah, A. M.; Elzatahry, A. A. *Nanomedicine (Lond.)* **2016**, *11*, 715–737. (g) Xu, J.; Liu, C.; Hsu, P. C.; Liu, K.; Zhang, R.; Liu, Y.; Cui, Y. *Nano Lett.* **2016**, *16*, 1270–1275. (h) Yang, C.; Hu, L. W.; Zhu, H. Y.; Ling, Y.; Tao, J. H.; Xu, C. X. *J. Mater. Chem. B* **2015**, *3*, 2651–2659. (i) Zheng, Z.; Gan, L.; Zhai, T. *Sci. China Mater.* **2016**, *59*, 200–216. (j) Morello, G.; Camposeo, A.; Moffa, M.; Pisignano, D. *ACS Appl. Mater. Interfaces* **2015**, *7*, 5213–5218.

3. (a) Bhardwaj, N.; Kundu, S. C. *Biotechnol. Adv.* **2010**, *28*, 325–347. (b) Sun, B.; Jiang, X. J.; Zhang, S.; Zhang, J. C.; Li, Y. F.; You, Q. Z.; Long, Y. Z. *J. Mater. Chem. B* **2015**, *3*, 5389–5410. (c) Khadka, D. B.; Haynie, D. T. *Nanomedicine* **2012**, *8*, 1242–1262. (d) Durham, E.; Tronci, G.; Yang, X. B.; Wood, D. J.; Russell, S. J. *Elsevier*, **2015**, *ch. 3*, 45–66.
4. (a) Guarino, V.; Cirillo, V.; Ambrosio, L. *Expert Rev. Med. Devices.* **2016**, *13*, 83–102. (b) Butcher, A. L.; Offeddu, G. S.; Oyen, M. L. *Trends. Biotechnol.* **2014**, *32*, 564–570.
5. (a) Ru, C.; Wang, F.; Pang, M.; Sun, L.; Chen, R.; Sun, Y. *ACS Appl. Mater. Interfaces* **2015**, *7*, 10872–10877. (b) Cui, W.; Cheng, L.; Li, H.; Zhou, Y.; Zhang, Y.; Chang, J. *Polymer* **2012**, *53*, 2298–2305.
6. (a) Kamath, M. S.; Ahmed, S. S.; Dhanasekaran, M.; Santosh, S. W. *Int. J. Nanomed.* **2014**, *9*, 183–195. (b) Cipitria, A.; Skelton, A.; Dargaville, T. R.; Dalton, P. D.; Hutmacher, D. W. *J. Mater. Chem.* **2011**, *21*, 9419–9453. (c) Van der Schueren, L.; De Meyer, T.; Steyaert, I.; Ceylan, Ö.; Hemelsoet, K.; Van Speybroeck, V.; De Clerck, K. *Carbohydr. Polym.* **2013**, *91*, 284–293. (d) Suwantong, O. *Polymer. Adv. Tech.* **2016**, DOI: 10.1002/pat.3876.
7. (a) Collier, J. H.; Segura, T. *Biomaterials* **2011**, *32*, 4198–4204. (b) Nuansing, W.; Frauchiger, D.; Huth, F.; Rebollo, A.; Hillenbrand, R.; Bittner, A. M. *Faraday Discuss.* **2013**, *166*, 209–221. (c) Tayi, A. S.; Pashuck, E. T.; Newcomb, C. J.; McClendon, M. T.; Stupp, S. I. *Biomacromolecules* **2014**, *15*, 1323–1327.
8. (a) Hartman, O.; Zhang, C.; Adams, E. L.; Farach-Carson, M. C.; Petrelli, N. J.; Chase, B. D.; Rabolt, J. F. *Biomaterials* **2010**, *31*, 5700–5718. (b) Mota, A.; Sahebghadam, L. A.; Barzin, J.; Hatam, M.; Adibi, B.; Khalai, Z.; Massumi, M. *Cell J.* **2014**, *16*, 1–10. (c) Dettin, M.; Zamuner, A.; Roso, M.; Gloria, A.; Iucci, G.; Messina, G. M.; D'Amora, U.; Marletta, G.; Modesti,

- M.; Castagliuolo, I.; Brun, P. *PloS one* **2015**, *10*, e0137505. (d) Gharaci, R.; Tronci, G.; Davies, R. P.; Gough, C.; Alazragi, R.; Goswami, P.; Russell, S. *J. J. Mater. Chem. B* **2016**, DOI: 10.1039/C6TB01164K.
9. (a) Chen, C.; Ke, J.; Zhou, X.E.; Yi, W.; Brunzelle, J.S.; Li, J.; Yong, E.L.; Xu, H.E.; Melcher, K. *Nature*, **2013**, *500*, 486–489. (b) Xia, W.; Low, P.S. *J. Med. Chem.*, **2010**, *53*, 6811–6824. (c) Yang, S. J.; Lin, F. H.; Tsai, K. C.; Wei, M. F.; Tsai, H. M.; Wong, J. M.; Shieh, M. J. *Bioconjugate Chem.* **2010**, *21*, 679–689. (d) Lale, S. V.; Kumar, A.; Prasad, S.; Bharti, A. C.; Koul, V. *Biomacromolecules* **2015**, *16*, 1736–1752.
10. Wang, M.; Zhou, C.; Chen, J.; Xiao, Y.; Du, J. *Bioconjugate Chem.* **2015**, *26*, 725–734.
11. (a) Liu, L.; Zheng, M.; Librizzi, D.; Renette, T.; Merkel, O. M.; Kissel, T. *Mol. Pharm.* **2016**, *13*, 134–143. (b) Liu, L.; Zheng, M.; Renette, T.; Kissel, T. *Bioconjug Chem.* **2012**, *23*, 1211–1220.
12. Suen, W. L.; Chau, Y. *J. Control. Release.* **2013**, *167*, 21–28.
13. (a) Gour, N.; Barman, A. K.; Verma, S. *J. Pept. Sci.* **2012**, *18*, 405–412. (b) Thomas, A.; Shukla, A.; Sivakumar, S.; Verma, S. *Chem. Commun.* **2014**, *50*, 15752–15755. (c) Kaur, G.; Abramovich, L. A.; Gazit, E.; Verma, S. *RSC Adv.* **2014**, *4*, 64457–64465. (d) Mishra, N. K.; Joshi, K. B.; Verma, S. *Mol. Pharm.* **2013**, *10*, 3903–3912. (e) Barman, A. K.; Verma, S. *Chem. Commun.* **2010**, *46*, 6992–6994. (f) Gupta, A.; Krishna, K. V.; Verma S. *RSC Adv.* **2015**, *5*, 71785–71789.
14. Kaur, G.; Shukla, A.; Sivakumar, S.; Verma, S. *J. Pept. Sci.* **2015**, *21*, 248–255.
15. Mosmann, T. *J. Immunol. Methods* **1983**, *65*, 55–63.
16. Ménard-Moyon, C.; Venkatesh, V.; Krishna, K. V., Bonachera, F.; Verma, S.; Bianco, A. *Chem. Eur. J.* **2015**, *21*, 11681–11686.

17. Kelemen, L. E. *Int. J. Cancer*. **2006**, *119*, 243–250.
18. Castillo, J.J.; Svendsen, W.E.; Rozlosnik, N.; Escobar, P.; Martínez, F.; Castillo-León, J. *Analyst* **2013**, *138*, 1026–1031.

Chapter 5C

Folic acid Peptide Scaffolds for Electrochemical Capacitive Energy Storage

5C.1. Introduction

Energy storage or supercapacitor materials are green and clean alternatives for handling energy crisis in coming future.¹ Supercapacitor materials have been used in renewable energy harvesting appliances such as the wind, thermal and solar panels.² But, existing supercapacitor materials are very costly with limited cycle life, becoming environmental hazards itself. Carbon nanotubes and porous carbon materials have been explored in applications such as supercapacitors, gas adsorption for separation, catalyst support, ion exchange, as they have the advantage of chemical stability, high conductivity, high specific surface area and ability to interact with particles at the surface level as well as throughout the bulk.³ However, low energy density and wettability are their main limitations, resulting in low specific capacitance.⁴ The specific capacitance of carbon materials could be enhanced by various methods like activation, heteroatom doping, or addition of metal ions/nanoparticles.⁵ Among heteroatom-doped carbon materials, nitrogen-doped carbon materials are gaining attention due to ease in preparation, low cost and wide range of applications.⁶ Porous nitrogen-doped carbon materials generally display pyrrolic, pyridinic and quaternary nitrogen bonding designs in the main carbon lattice, exhibiting good surface potential with active

catalytic sites and superior conductivity due to the electronegativity difference between carbon and nitrogen.⁷

Vitamins, amino acid and peptides, containing nitrogen atoms in their skeleton, may be used as precursors for nitrogen-doped carbon materials, being environmentally safe, cheap and easy availability.⁸ Histidine-derived nitrogen-doped carbon materials have been studied for their electrochemical capacitive energy storage in the past.⁹ Folic acid as nitrogen-doped carbon material on $\text{Mg}(\text{OAc})_2 \cdot 4\text{H}_2\text{O}$ template has been used for supercapacitor studies.¹⁰ Nitrogen percentage of carbon materials can be enhanced by the addition of nitrogen containing additives capable of forming covalent or non-covalent interactions with carbon materials, such as urea, ammonia etc.¹¹ The hydrophobic nature of the pterin ring of folic acid results in poor solubility which can be reduced by addition of melamine in it. The hydrogen bonding capability of melamine with folic acid and solvent molecules results in higher solubility and wettability of complex.¹²

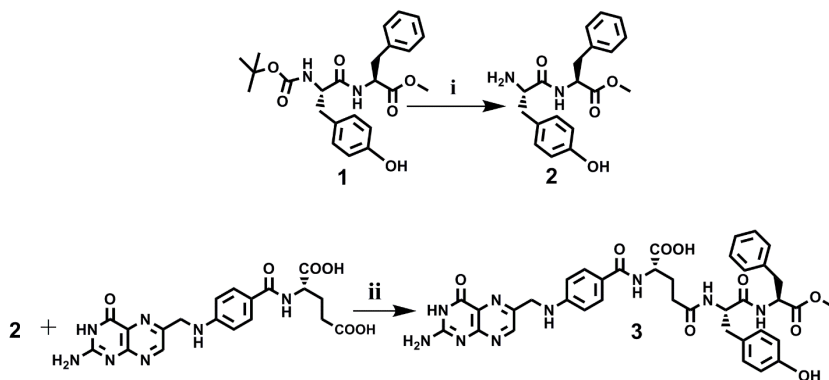
With prior knowledge of folic acid based peptides¹³, we designed and synthesized a folic acid based tyrosyl phenylalanine conjugated peptide which self-assembled into nanosheets. The co-assembly of the peptide with melamine was studied through various microscopic techniques. Porous nitrogen-doped carbon

materials were synthesized from peptide/melamine complex through its carbonization at 900 °C, which was tested for electrochemical capacitive performance in energy storage application.

5C.2. Experimental Section

5C.2.1. Materials: Folic acid (FA), L-phenylalanine (Phe), L-tyrosine (Tyr), N, N'-Dicyclohexylcarbodiimide (DCC) and trifluoroacetic acid (TFA) were obtained from S. D. Fine Chem Ltd., Mumbai, India and used without further purification. *N*-tert-butoxy carbonyl (Boc anhydride), thionyl chloride, *N*-Hydroxybenzotriazole (HOBt) were purchased from Spectrochem Ltd., Mumbai, India. Dichloromethane (DCM), *N,N*-dimethylformamide (DMF), methanol (MeOH), trimethylamine (TEA), pyridine were distilled according to standard procedures prior to use.

5C.2.2. Peptide conjugate synthesis: Conjugate **3** was prepared by standard solution phase peptide synthesis. Scheme **1** shows various synthetic steps:



Scheme 1: Synthetic scheme for peptide 3: (i) 75% TFA–DCM, 4 h, N₂ atmosphere; (ii) N, N'-dicyclohexylcarbodiimide, pyridine, dark.

Boc-L-Tyrosine-L-Phenylalanine methyl ester (1): N-(Boc)-L-Tyrosine (5 g, 17.8 mmol) and HOBt (2.40 g, 17.8 mmol) were dissolved in dry DMF (25 mL) and the reaction mixture was cooled to 0 °C under nitrogen atmosphere. DCC (3.05 g, 14.8 mmol) dissolved in DCM was added to the reaction mixture. L-phenylalanine methyl ester hydrochloride (3.19 g, 14.8 mmol) was added to the reaction mixture followed by TEA (12.40 mL, 88.9 mmol) after 1 h stirring at 0 °C. The reaction mixture was further stirred for 24 h at room temperature. DCU was removed by filtration and filtrate was concentrated under reduced pressure. The residue was dissolved in DCM and the organic layer was washed with 1 N HCl (2×30 mL), 10% NaHCO₃ (2×30 mL) and brine (30 mL). The organic layer was dried over anhydrous sodium sulfate

and concentrated under reduced pressure. The crude compound was purified through silica gel column chromatography by using dichloromethane and methanol to get the pure compound **1** (3.2 g, 64% yield), R_f [7% methanol in dichloromethane] 0.5, HRMS $(M+H)^+$ for $C_{24}H_{30}N_2O_6$: 443.2182 (Calcd.), 443.2187 (Anal.), 1H NMR (500 MHz, $CDCl_3$, TMS, δ ppm): 1.39 (s, 9H), 2.90-3.50 (m, 4H), 3.62 (s, 3H), 4.26 (m, 1H), 4.75 (m, 1H), 5.06 (s, 1H), 6.39-7.25 (m, 9H); ^{13}C NMR (125 MHz; $CDCl_3$, δ ppm): 28.3, 37.4, 38.0, 52.4, 56.0, 65.9, 80.5, 115.7, 127.2, 127.6, 128.6, 129.3, 130.4, 136.1, 155.3, 155.5, 171.2, 171.5.

L-Tyrosine-L-Phenylalanine methyl ester (2): **1** (3g, 6.7 mmol) was dissolved in 75% TFA-DCM (25 mL) and stirred for 1 h under nitrogen atmosphere. After completion of the reaction, the solvent was evaporated *in vacuo* and was subsequently washed with diethyl ether resulting in a white solid. The white solid then dissolved in methanol and passed through activated anion exchange resin and evaporated under reduced pressure to obtain pure **2** (2.46g, 82.2% yield) which was used as it for next step.

L-Tyrosine-L-Phenylalanine methyl ester folic acid conjugate (3): FA (0.250 g, 0.556 mmol), **2** (0.193 g, 0.556 mmol), and DCC (0.701 g, 0.339 mmol) were dissolved in DMSO (5 mL) in presence of dry pyridine (10 μ L). The mixture was stirred overnight, in the

dark, at room temperature under nitrogen atmosphere. Afterwards, the mixture was diluted with deionized water (10 mL) and centrifuged at 1000 rpm for 30 min to separate insoluble DCU. The supernatant was collected and washed with diethyl ether to give a yellow precipitate, which was filtered and dried. The crude compound was further purified by silica gel column chromatography eluting with methanol-dichloromethane, to isolate a pure yellow colored compound (0.167 g, 65% yield). HRMS ($M+H$)⁺ for C₃₈H₄₀N₉O₉: 766.2949 (Calcd.), 766.2940 (Anal.); ¹H NMR (500 MHz, d₆-DMSO, TMS, δ ppm): 1.17-1.47 (m, 4H), 1.56-1.76 (m, 4H), 2.69 (s, 3H), 3.31 (s, 2H), 2.90-3.31 (m, 3H), 3.45-3.52 (m, 2H), 4.44 (m, 1H), 5.53-5.55 (m, 1H) 6.49-7.60 (m, 13H), 7.91-8.16 (m, 3H), 8.34-8.61 (m, 3H), 9.06 (s, 1H), 11.41 (s, 1H); ¹³CNMR (125 MHz; d₆-DMSO, δ ppm): 25.8, 31.3, 33.8, 36.3, 37.1, 46.4, 48.0, 52.2, 54.3, 111.6, 115.3, 121.9, 122.7, 127.0, 128.4, 129.5, 130.6, 137.4, 147.5, 149.2, 151.3, 154.2, 156.2, 157.1, 162.8, 172.0, 174.6, 176.7.

5C.2.3. Microscopy studies

Atomic Force Microscopy (AFM): 10 μL aliquots of samples (1 mM in water) was placed on a silicon wafer at room temperature and allowed to dry by slow evaporation. Subsequently, the samples were dried in vacuo for 30 min prior to imaging. AFM Samples

were imaged with an atomic force microscope (Molecular Imaging, USA) operating under the Acoustic AC mode (AAC), with the aid of a cantilever (NSC 12(c) from MikroMasch). The force constant was 0.6 N/m, while the resonant frequency was 150 kHz. The images were taken at room temperature, with the scan speed of 1.5-2.2 lines/sec. The data acquisition was done using PicoView 1.8® software, while the data analysis was done using PicoView.

Field Emission Scanning Electron Microscopy (FE-SEM): 10 μ L aliquots of peptide samples (1 mM solution) were deposited on a silicon wafer (100) and allowed to dry at room temperature. The samples were dried *in vacuo* for 30 min prior to imaging. Samples were gold-coated and SEM images acquired on FEI Quanta 200 microscope equipped with a tungsten filament gun, operating at a WD 3.5 mm and an operating voltage of 10 kV.

X-Ray Diffraction Analysis (XRD): Samples were studied on PANalytical X-Pert PRO diffractometer with Cu-K α radiation (1.5405 Å).

X-ray photoelectron Spectroscopy (XPS): The samples were studied on XPS; PHI 5000 Versa Prob II, FEI Inc. for X-ray photoelectron spectroscopy.

Raman Spectroscopy: Raman spectra were acquired with a WITec alpha SNOM Raman instrument and the spectra were registered with the laser at 532 nm.

5C.3. Results and Discussion:

5C.3.1. Solution phase self-assembly: We designed and synthesized folic acid conjugate of L-tyrosine-L-phenylalanine dipeptide **3** by standard procedures published in the literature (Scheme 1). Phenylalanine is an essential amino acid, a precursor for tyrosine which is responsible for the synthesis of various neurotransmitters like dopamine, norepinephrine (noradrenaline) and epinephrine (adrenaline). Both phenylalanine¹⁴ and tyrosine¹⁵ amino acids have the ability to self-assemble into fibre-like structures. Based on our prior knowledge, we designed and synthesized folic acid based tyrosyl phenylalanine based peptide (**3**). **3** self-assembled into nanosheets when dissolved in water at a concentration of 1 mM. (Figure 5C.1).

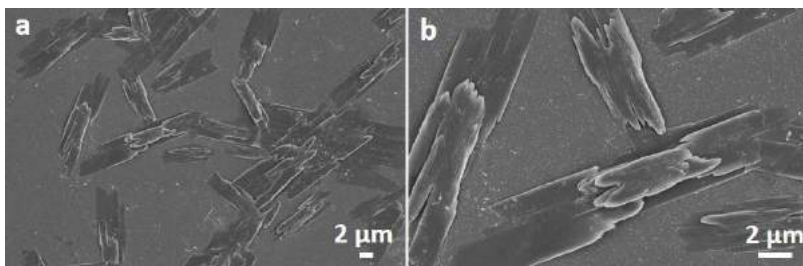


Figure 5C.1: (a,b) SEM images of **3** in the water on Si (100) wafer.

The probable interactions for the formation nanosheets were proposed to be H-bonding and π - π stacking between molecules. Pterin moieties in **3** are capable of forming linear ribbon-like and cyclic disk like H-bondings which could be responsible for nanosheets formation.¹⁶

5C.3.2. Melamine co-incubation: Melamine is a C_3 symmetric molecule with 67% nitrogen by mass and multiple H-bonding sites. It is well known to form spoke-like crystals of melamine cyanurate complex when mixed with cyanuric acid in aqueous solutions (1:1 eq).¹⁷ The complex of cyanuric acid and melamine is held together by H-bonding similar to DNA base-pairing. Along with it, melamine has the ability to assist and modulate self-assembling behavior of systems containing folic acid, riboflavin, and gallic acid, under aqueous conditions.^{16, 18} This intervention is possibly achieved by the formation of multipoint hydrogen bonds between melamine and other interacting partners, which overrides other interactive structures in the absence of melamine.

Working on a similar note, we decided to study the co-self-assembly behavior of **3** with melamine. **3** was mixed with melamine (1:3 eq) in water and the resulting solution was heated

up to 70 °C for 20 min, followed by cooling down to room temperature, for 12 h.

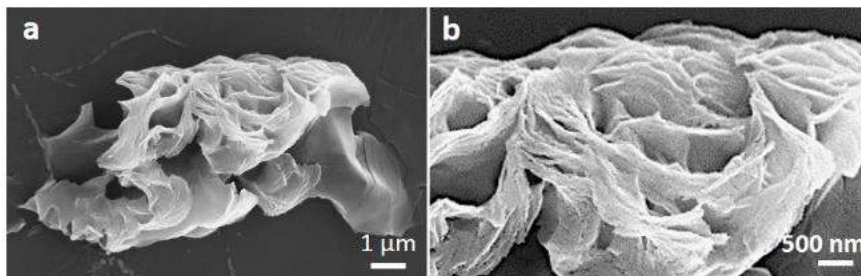


Figure 5C.2: (a,b) SEM images of **3**/melamine (1:3 eq) in water on Si (100) wafer.

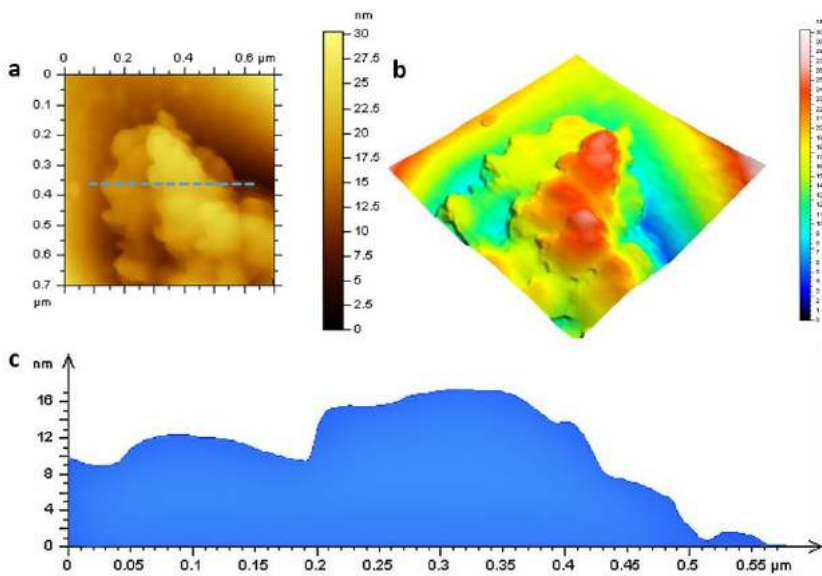


Figure 5C.3: Atomic force microscopy (AFM) image of **3**/Melamine showing 3D profile and height profile of nanosheets.

This heating treatment resulted in formation of clear solution which probably occurred due to enhanced solubility of **3**/melamine complex in water as compared to **3** alone. Microscopic analysis of **3**/melamine complex (1 mM) revealed the formation of nanosheets with a morphological resemblance to graphene sheets (Figure 5C.2). A change in morphology was observed upon co-incubation of melamine with **3** due to the formation of H-bonding interactions among the -NH_2 groups of melamine and pterin ring of folic acid. Possible extension of non-covalent interactions around melamine scaffold, altering the gross morphology of **3**, could be envisaged. The atomic force microscopy analysis revealed the thickness of these nanosheets to be around 3-5 nm (Figure 5C.3).

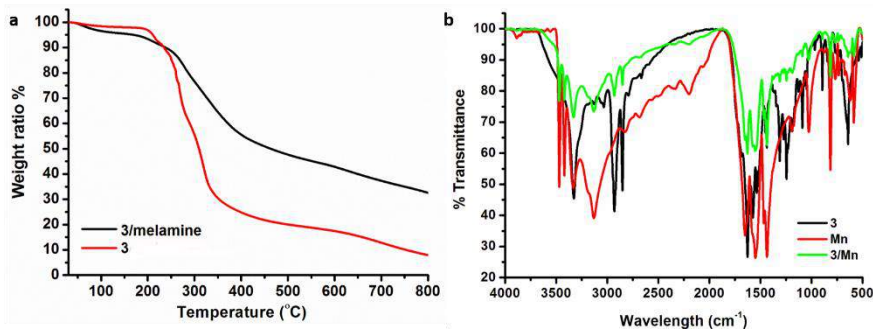


Figure 5C.4: (a) TGA analysis (b)FT-IR of **3**, melamine (Mn) and **3**/Mn.

TGA curves were used to analyze the interactions in **3** and melamine (Figure 5C.4). The weight loss before 100 °C was attributed to the removal of entrapped water due to evaporation. A notable major weight loss around 250-350 °C represented the cleavage of amine ($-\text{NH}_2$), hydroxyl ($-\text{OH}$) and a carboxyl group ($-\text{COOH}$) in **3**/melamine.¹⁹ The interactions between **3** and melamine (Mn) were also confirmed by FT-IR spectroscopy. Melamine showed sharp peaks at 3469 and 3419 cm^{-1} due to $-\text{NH}_2$ vibration stretching band.²⁰

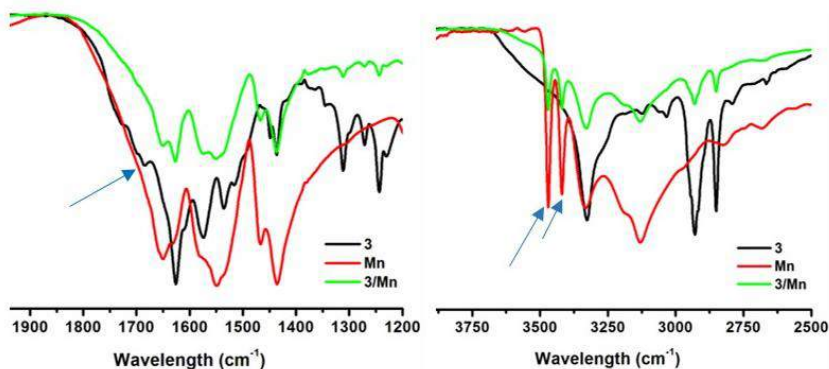


Figure 5C.5: FT-IR of **3**, melamine (Mn) and **3**/Mn (zoomed in).

Due to H-bonding between **3** and melamine, the relative intensity of $-\text{NH}_2$ vibration stretching band decreased (Figure 5C.4). The $-\text{NH}_2$ and $-\text{OH}$ stretching peaks due to pterin ring of **3**

at 3472 and 3328 cm^{-1} were absent after complexation, indicating the formation of H-bonding (Figure 5C.5). The $\text{C}=\text{O}$ stretching vibrations 1685 cm^{-1} of free carboxylic acid disappeared, suggesting H-bond formation between the free carboxylic group and melamine (Figure 5C.5). A possible model of interaction of pterin ring and free carboxylic acid side-chain of **3** with melamine was proposed as shown in Figure 5C.6.

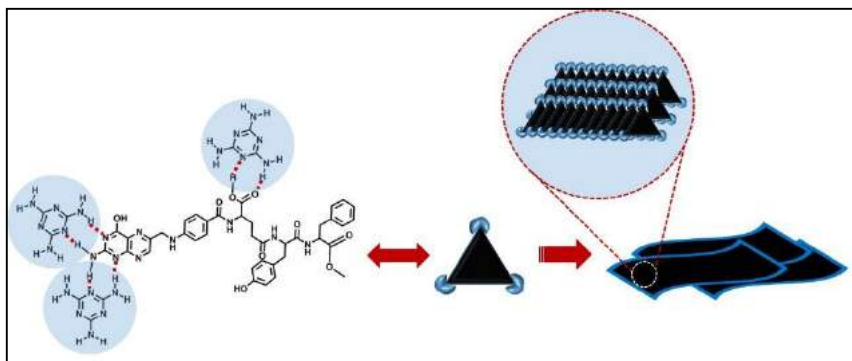


Figure 5C.6: Proposed model showing H-bonding in **3** and melamine which resulted in the formation of nanosheets.

5C.3.3. Carbonization of melamine doped **3**:

Carbonization is a complex process which involves many reactions such as dehydrogenation, isomerization, condensation, hydrogen transfer etc. taking place simultaneously. In general terms, carbonization means conversion of organic matter to a carbon containing residues. High-performance carbon materials

are generally obtained through carbonization which has been employed to study supercapacitor behavior and energy storage.

3/Melamine was heated in air at 250 °C for 2 h followed by carbonization at 900 °C under 150 mL/min argon flow for 4 h, with a 4 °C/min heating rate to obtain a shiny black material (Figure 5C.7). Microscopic analysis of this shiny material revealed the formation of porous material. Energy-dispersive X-ray spectroscopy (EDX) analysis confirmed the presence of carbon, nitrogen and oxygen in carbonized sample (Figure 5C.7). Furthermore, the carbonized material was further characterized by various techniques like XPS, XRD and RAMAN spectroscopy. In XPS spectra, 530, 398 and 284 eV peaks were obtained for O 1s, N 1s and C 1s respectively and were typical peaks present in any nitrogen doped carbonized material indicating carbonized **3**/melamine samples could be nice carbon material.

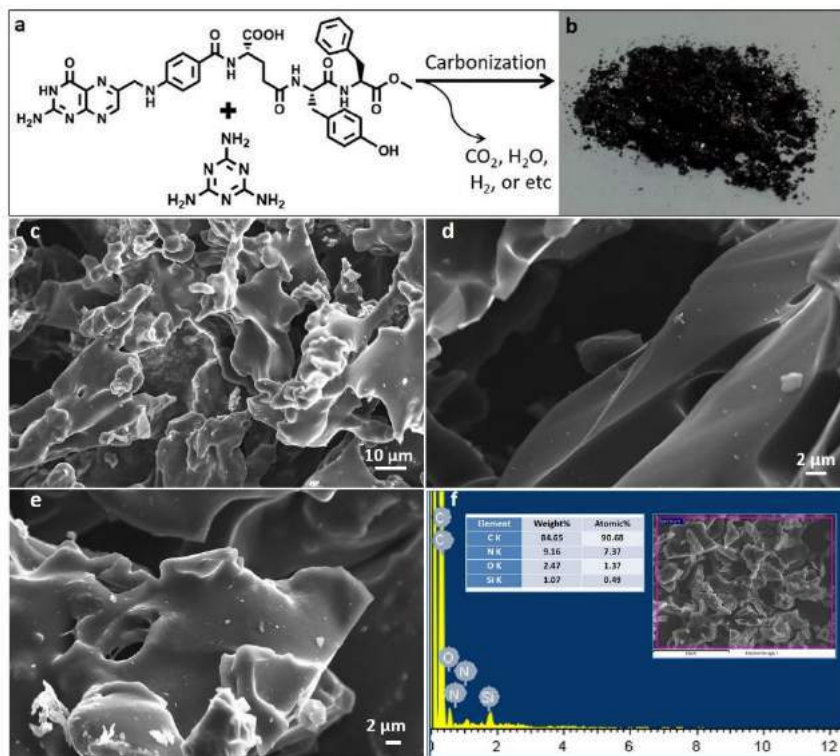


Figure 5C.7: (a) Carbonization of **3**/melamine resulted in (b) shiny black material. (c-e) SEM images (f) EDX of carbonized **3**/melamine sample.

The nitrogen peak represented the presence of pyridinic N (XPS range: 398.0-398.4 eV), pyrrolic N (range 399.8-400.5 eV) and quaternary N (401.0–401.5 eV) in the sample (Figure 5C.8).

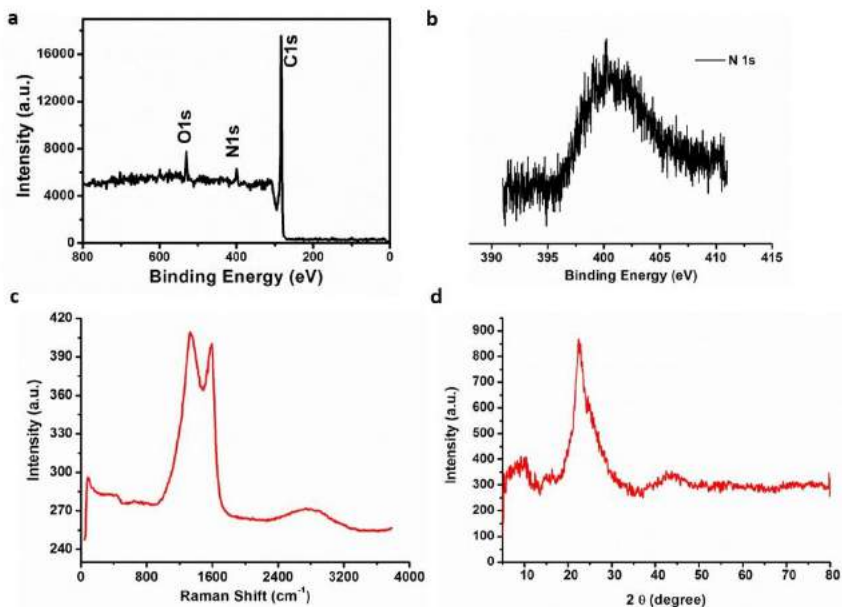


Figure 5C.8: (a,b) X-ray Photoelectron spectroscopy (XPS) (c) Raman Spectrum. (d) XRD spectrum of carbonized **3**/melamine.

Raman spectroscopy was performed on carbonized material to investigate the phase composition and graphitic content. The obtained Raman spectrum displayed three major peaks at 1328, 1588 and 2800 cm⁻¹ corresponding to D, G and 2D bands for sp² bonded carbon (Figure 5C.8).²¹ The D-band is the result of the disordered structure of the graphitic material. These disorders or defects originate due to the edges or restricted crystalline size of graphitic layers. The out-of-plane vibrations of sp² carbon atoms

contribute to D band. The C-C in-plane stretching vibration of sp^2 bonded carbon in graphitic material results in G-band. The G-band represents the presence of crystalline graphene layers. The graphitic material exhibits a strong peak in the range of 2500-2900 cm^{-1} , known as a 2D band, which is a second-order two-phonon process. This band represents surface defects in sp^2 bonded graphitic material. The level of disorder in graphitic materials is estimated by the intensity ratio of D band and G band (I_D/I_G). The I_D/I_G value for carbonized **3**/melamine was 0.836 when calculated from obtained Raman spectrum.

Further, XRD analysis was done to obtain more details about the crystallinity and phase of carbonized **3**/melamine samples. A distant (002) peak at 23.5° in the 2θ range in the XRD pattern was observed (Figure 5C.8), which corresponds to characteristic lattice planes for graphitic materials.

5C.3.4. Electrochemical Capacitive performance:

The electrochemical characterization of the carbonized **3**/melamine samples was further analyzed with a Potentiostat/galvanostat 302N (Autolab, Metroohm) using cyclic voltammetry (CV). The cyclic voltammograms were measured to probe the applications in supercapacitor material.

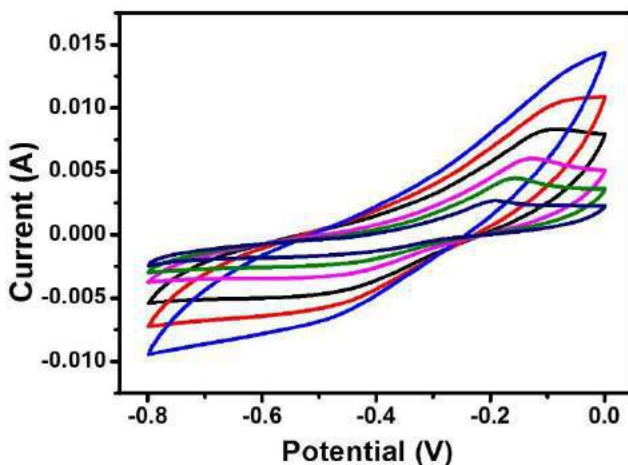


Figure 5C.9: CV plot of carbonized **3**/melamine.

The capacitive behavior of carbonized **3**/melamine sample showed the formation of slightly distorted rectangular shape CV curve. The specific capacitance of carbonized **3**/melamine was determined by CV in the voltage range from -0.8 V to 0 V. CV curve of porous carbon electrodes in 1 M Na₂SO₄ aqueous electrolyte at 25 °C was scanned at 50 mV/s and shown in figure 5C.9. The specific capacitance is proportional to the areas surrounded by CV curves and can be calculated using the equation:

$$C_s = (1/mv\Delta V) \int I(V)V$$

Where m , v , ΔV , $\int I(V)V$ and C_s represent the mass of material, the scan rate, scanned potential window, the integral area under the CV curve and specific capacitance respectively. The specific

capacitance from carbonized 3/melamine material were 38, 19, 14 and 1.5 F/g at current densities 1, 1.5, 2 and 3 A/g respectively (Figure 5C.10).

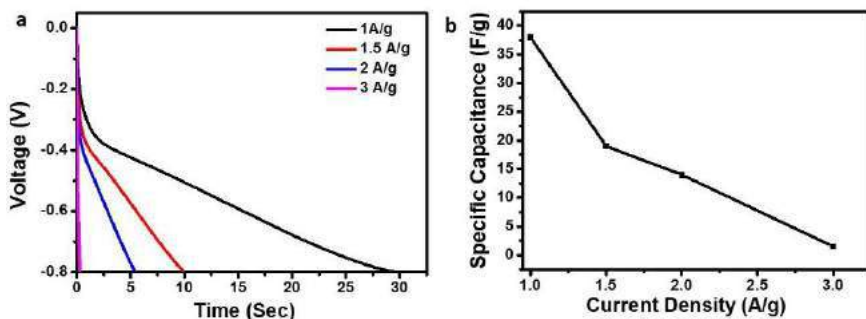


Figure 5C.10: (a) Galvanostatic discharge curve (b) Specific capacitance curve of carbonized 3/melamine.

5C.4. Conclusions:

Folic acid tyrosyl phenylalanine peptide self-assembled into nano-ribbon like structures. The co-self-assembly of these structures with melamine resulted in interesting architectures with morphology similar to graphene sheets. These sheets were characterized through microscopy (SEM and AFM), TGA and FTIR. Pterin ring of folic acid and melamine both were the interesting starting point for the formation of porous nitrogen-doped carbon materials (PNCMs). Folic acid tyrosyl phenylalanine peptide/Melamine sheets were carbonized at 900°C for studying

the electrochemical capacitive behavior. The shiny black carbonaceous material was characterized by SEM, EDX, XPS, XRD and RAMAN spectroscopy. Furthermore, the carbonized samples were tested for electrochemical capacitive performance showed the specific capacitance of 38, 19, 14 and 1.5 F/g at current densities 1, 1.5, 2 and 3 A/g respectively in energy storage application.

5C.5. References:

1. Abbasi, T.; Abbasi, S. A. *Renewable Sustainable Energy Rev.* **2011**, *15*, 1828–1834.
2. (a) Bonaccorso, F.; Colombo, L.; Yu, G.; Stoller, M.; Tozzini, V.; Ferrari, A. C.; Ruoff, R. S.; Pellegrini, V. *Science* **2015**, *347*, 1246501. (b) Du, P.; Hu, X.; Yi, C.; Liu, H. C.; Liu, P.; Zhang, H. L.; Gong, X. *Adv. Funct. Mater.* **2015**, *25*, 2420–2427. (c) Zhao, H.; Wu, Q.; Hu, S.; Xu, H.; Rasmussen, C. N. *Appl. Energy* **2015**, *137*, 545–553. (d) Xu, X.; Li, S.; Zhang, H.; Shen, Y.; Zakeeruddin, S. M.; Graetzel, M.; Cheng, Y. B.; Wang, M. *ACS nano* **2015**, *9*, 1782–1787.
3. (a) Titirici, M. M.; White, R. J.; Brun, N.; Budarin, V. L.; Su, D. S.; del Monte, F.; Clark, J. H.; MacLachlan, M. J. *Chem. Soc. Rev.* **2015**, *44*, 250–290. (b) Linares, N.; Silvestre-Albero, A. M.; Serrano, E.; Silvestre-Albero, J.; García-Martínez, J. *Chem. Soc. Rev.* **2014**, *43*, 7681–7717. (c) Pandolfo, A. G.; Hollenkamp, A. F. *J. Power Sources* **2006**, *157*, 11–27. (d) Lee, J.; Kim, J.; Hyeon, T. *Adv. Mater.* **2006**, *18*, 2073–2094. (e) Davis, M. E. *Nature* **2002**, *417*, 813–821.

-
4. Frackowiak, E.; Beguin, F. *Carbon* **2001**, *39*, 937–950.
 5. (a) Zhang, J.; Cai, Y.; Zhong, Q.; Lai, D.; Yao, J. *Nanoscale* **2015**, *7*, 17791–17797. (b) Kim, M.-H.; Kim, K.-B.; Park, S.-M.; Roh, K. C. *Sci. Rep.* **2016**, *6*, 21182. (c) Gu, W.; Yushin, G. *WIREs Energy Environ.* 2014, *3*, 424–473. (d) Nian, Y. R.; Teng, H. *Electrochem Soc.* **2002**, *149*, 1008–1014. (e) Wang, J.; Kaskel, S. *J. Mater. Chem.* **2012**, *22*, 23710–23725.
 6. Wood, K. N.; O'Hayre, R.; Pylypenko, S. *Energy Environ. Sci.* **2014**, *7*, 1212–1249.
 7. (a) Ou, J.; Yang, L.; Zhang, Y.; Chen, L.; Guo, Y.; Xiao, D. *Chin. J. Chem.* **2015**, *33*, 1293–1302. (b) Zhou, J.; Zhang, Z.; Xing, W.; Yu, J.; Han, G.; Si, W.; Zhuo, S. *Electrochimi. Acta* **2015**, *153*, 68–75. (c) Chen, T.; Pan, L.; Loh, T. A. J.; Chua, D. H. C.; Yao, Y.; Chen, Q.; Li, D.; Qin, W.; Sun, Z. *Dalton Trans.* **2014**, *43*, 14931–14935. (d) Xiang, Z.; Wang, D.; Xue, Y.; Dai, L.; Chen, J.-F.; Cao, D. *Sci. Rep.*, **2015**, *5*, 8307. (e) Hou, J.; Cao, C.; Idrees, F.; Ma, X. *ACS Nano*, **2015**, *9*, 2556–2564. (f) Braghiroli, F. L.; Fierro, V.; Izquierdo, M.T.; Parmentier, J.; Pizzi, A.; Celzard, A. *Carbon*, **2012**, *50*, 5411–5420.
 8. (a) Bhunia, S. K.; Pradhan, N.; Jana, N. R. *ACS Appl. Mater. Interfaces* **2014**, *6*, 7672–7679. (b) Kim, Y. J.; Abe, Y.; Yanagiura, T.; Park, K. C.; Shimizu, M.; Iwazaki, T.; Nakagawa, S.; Endo, M.; Dresselhaus, M. S. *Carbon* **2007**, *45*, 2116–2125. (c) Cho, S. Y.; Yun, Y. S.; Lee, S.; Jang, D.; Park, K.Y.; Kim, J. K.; Kim, B. H.; Kang, K.; Kaplan, D. L.; Jin, H. J. *Nat. commun.* **2015**, *6*, 7145.
 9. (a) Guo, Z.; Zhou, Q.; Wu, Z.; Zhang, Z.; Zhang, W.; Zhang, Y.; Li, L.; Cao, Z.; Wang, H.; Gao, Y. *Electrochimi. Acta* **2013**, *113*, 620–627. (b) Jeong, H.; Kim, H. J.; Lee, Y. J.; Hwang, J. Y.; Park, O.-K.; Wee, J.-H.; Yang, C.-M.; Ku, B.-C.; Lee, J. K. *Mater. Lett.* **2015**, *145*, 273–278.

10. Zhang, Z. J.; Chen, X. Y. *J. Electroanal. Chem.* **2016**, 764, 45–55.
11. Haque, E.; Islam, M. M.; Pourazadi, E.; Hassan, M.; Faisal, S. N.; Roy, A. K.; Konstantinov, K.; Harris, A. T.; Minett, A. I.; Gomes, V. G. *RSC Adv.* **2015**, 5, 30679–30686.
12. Xing, P.; Chu, X.; Ma, M.; Li, S.; Zhang, Y.; Hao, A. *RSC Adv.* **2014**, 4, 36633–36639.
13. Kaur, G.; Shukla, A.; Sivakumar, S.; Verma, S. *J. Pept. Sci.* **2015**, 21, 248–255.
14. Adler-Abramovich, L.; Vaks, L.; Carny, O.; Trudler, D.; Magno, A.; Caflisch, A.; Frenkel, D.; Gazit, E. *Nat. Chem. Biol.* **2012**, 8, 701–706.
15. Ménard-Moyon, C.; Venkatesh, V.; Krishna, K.V.; Bonachera, F.; Verma, S.; Bianco, A. *Chem. Eur. J.* **2015**, 21, 11681–11686.
16. Xing, P.; Chu, X.; Ma, M.; Li, S.; Hao, A. *Phys. Chem. Chem. Phys.* **2014**, 16, 8346–8359.
17. He, L.; Liu, Y.; Lin, M.; Awika, J.; Ledoux, D. R.; Li, H.; Mustapha, A. *Sens. & Instrumen. Food Qual.* **2008**, 2, 66–71.
18. (a) Du, X.; Zhou, J.; Shi, J.; Xu, B. *Chem. Rev.* **2015**, 115, 13165–13307. (b) Chatterjee, S.; Nandi, A. K. *Chem. Commun.* **2011**, 47, 11510–11512. (c) Jun, Y. S.; Lee, E. Z.; Wang, X. Hong, W. H.; Stucky, G. D.; Thomas, A. *Adv. Funct. Mater.* **2013**, 23, 3661–3667. (d) Saha, A.; Roy, B.; Garai, A.; Nandi, A. *Langmuir* **2009**, 25, 8457–8461.
19. (a) Schwab, L. W.; Kloosterman, W. M. J.; Konieczny, J.; Loos, K. *Polymers* **2012**, 4, 710–740. (b) Adler-Abramovich, L.; Reches, M.; Sedman, V. L.; Allen, S.; Tendler, S. J. B.; Gazit, E. *Langmuir* **2006**, 22, 1313–1320.

20. (a) Bairi, P.; Roy, B.; Nandi, A. K. *J. Phys. Chem. B*, 2010, **114**, 11454–11461. (b) Xing, P.; Chu, X.; Ma, M.; Li, S.; Zhang, Y.; Hao, A. *RSC Adv.* **2014**, *4*, 36633–36639.
21. Ferrari, A. C. *Solid state commun.* **2007**, *143*, 47–57. (b) Mondal, K.; Kumar, J.; Sharma, A., *Nanomater. Energy* **2013**, *2*, 121 –133. (c) Sofo, J. O.; Chaudhari, A. S.; Barber, G. D. *Phys. Rev. B* **2007**, *75*, 153401. (d) Verzhbitskiy, I. A.; Corato, M. D.; Ruini, A.; Molinari, E.; Narita, A.; Hu, Y.; Schwab, M. G.; Bruna, M.; Yoon, D.; Milana, S.; Feng, X. *Nano Lett.* **2016**, *16*, 3442–3447.

Appendix

A.1. Crystallographic Data for Chapter 4

Identification code	Cu(II)+4 Complex
Empirical formula	C ₉₀ H ₉₄ Cu ₂ N ₁₀ O ₂₈
<i>Mr</i>	1890.83
crystal system	Triclinic
space group	P1
<i>a</i> /Å	12.0316 (8)
<i>b</i> /Å	13.9710 (10)
<i>c</i> /Å	15.7586 (11)
α /°	73.2190 (10)
β /°	80.012 (4)
γ /°	74.696 (2)
Volume/ Å ³	2432.6 (3)
<i>Z</i>	1
<i>D_x</i> /Mg m ⁻³	1.291
<i>F</i> (000)	986
μ / mm ⁻¹	0.516
θ range for data collection/ °	2.11 to 28.37
Limiting indices	-16≤ <i>h</i> ≤10, -18≤ <i>k</i> ≤14, -21≤ <i>l</i> ≤19
Reflections collected	20414
unique reflections	15130
R(int)	0.0333
Completeness to θ	98.5
<i>T</i> _{max} / <i>T</i> _{min}	0.9038/ 0.8905
Data / restraints / parameters	15130 / 3 / 1179
Goodness-of-fit on <i>F</i> ²	1.043
<i>R</i> 1 and <i>R</i> 2 [<i>I</i> >2σ(<i>I</i>)]	0.0767, 0.1859
<i>R</i> 1 and <i>R</i> 2 (all data)	0.1220, 0.2129
Largest diff. peak and hole/e.Å ⁻³	1.281 and -0.906
CCDC No.	1005702

A.2. Spectral Data for Chapter 3

Figure A.2.1. ^1H NMR of 1

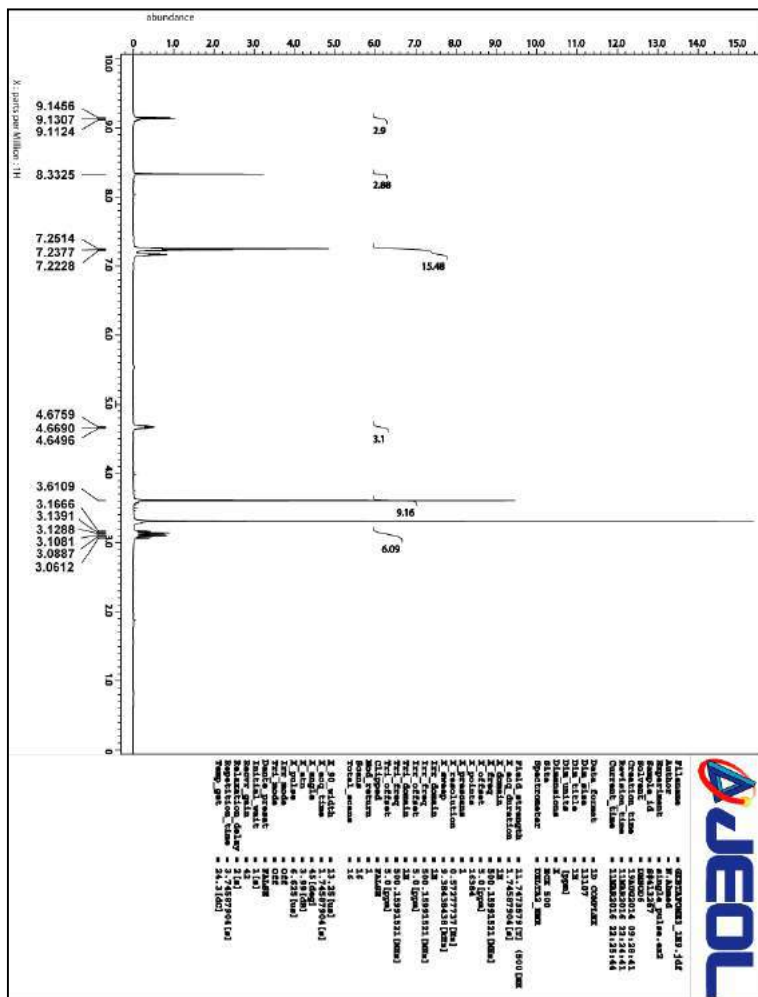


Figure A.2.5. HRMS of 2

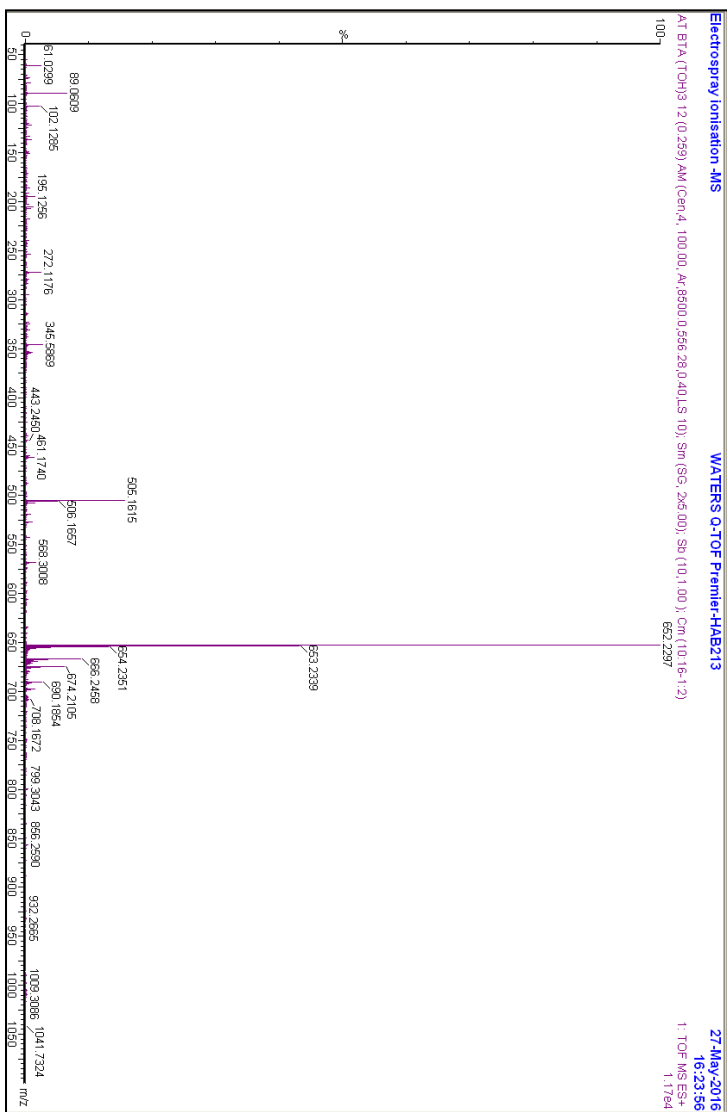


Figure A.3.3. HRMS of 1

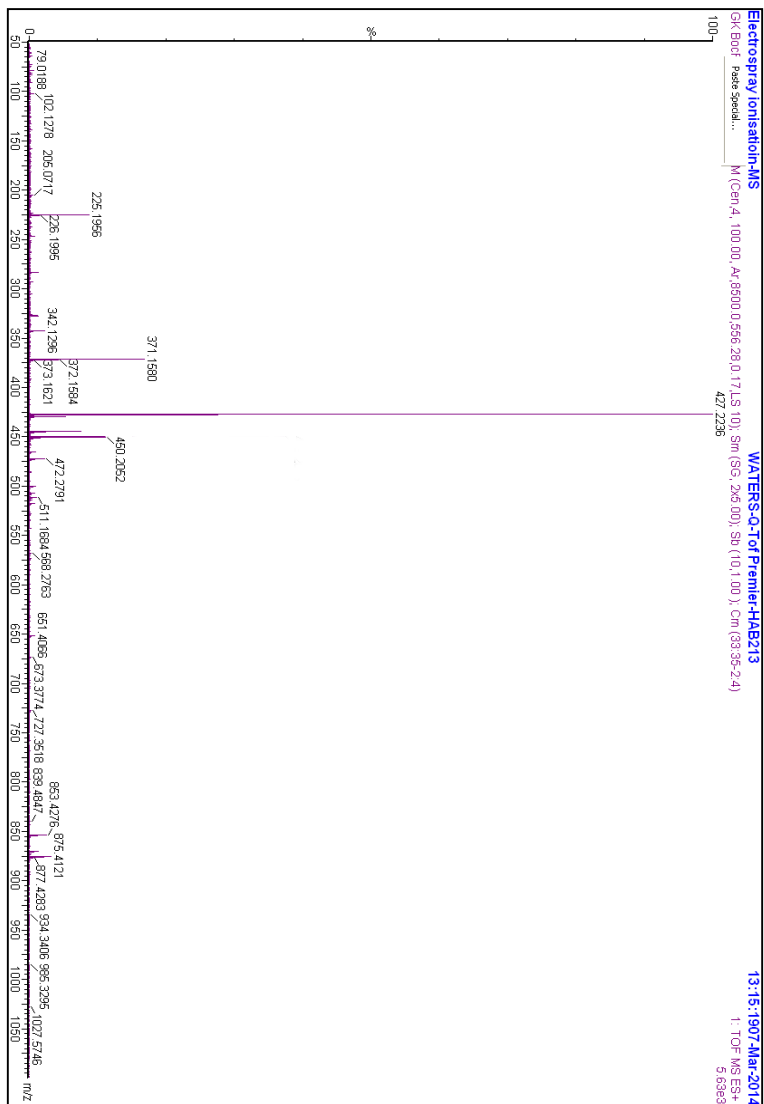


Figure A.3.6. HRMS of 2

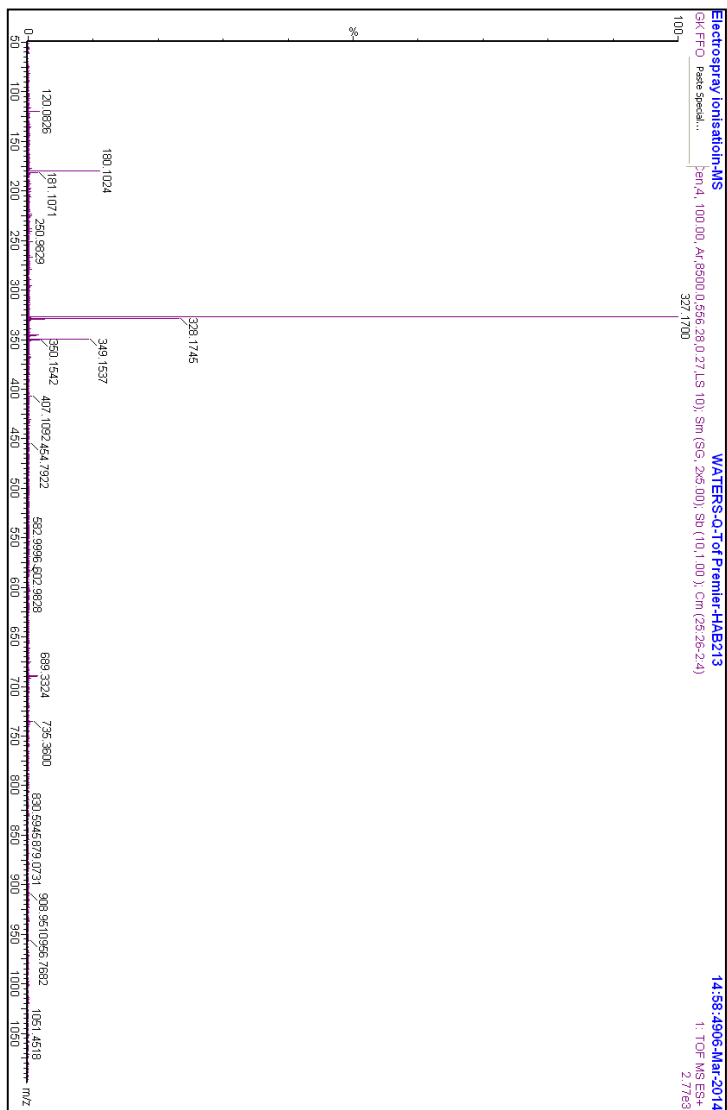


Figure A.3.7. ^1H NMR of **3**

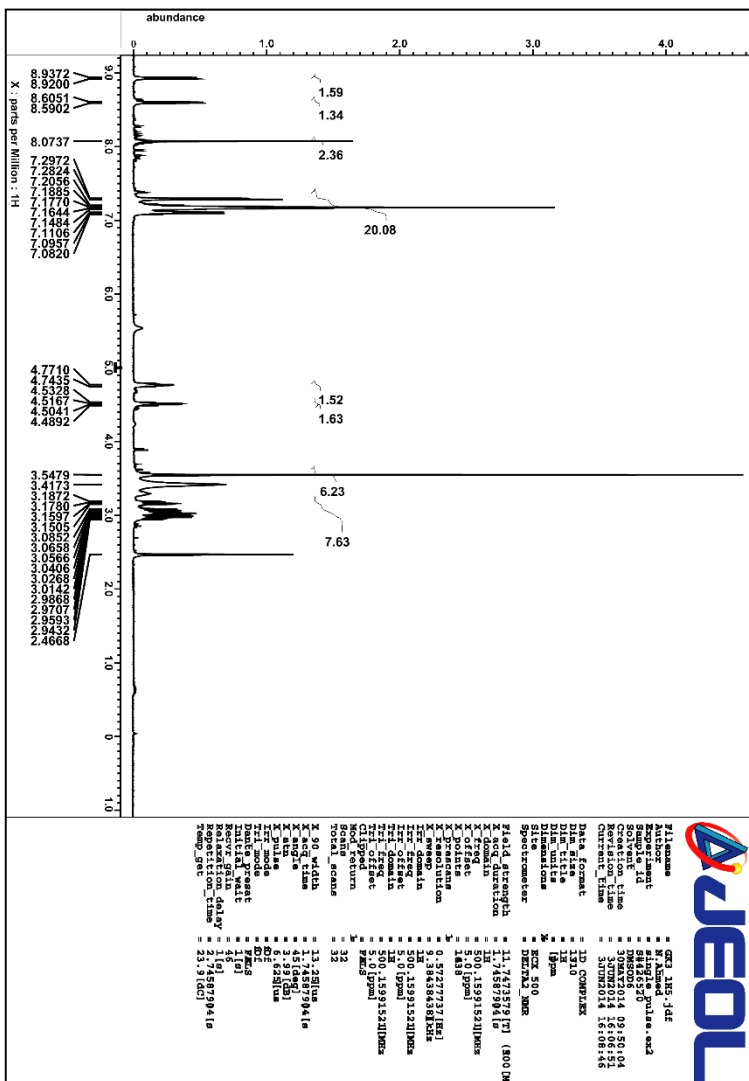


Figure A.3.8. ^{13}C NMR of **3**

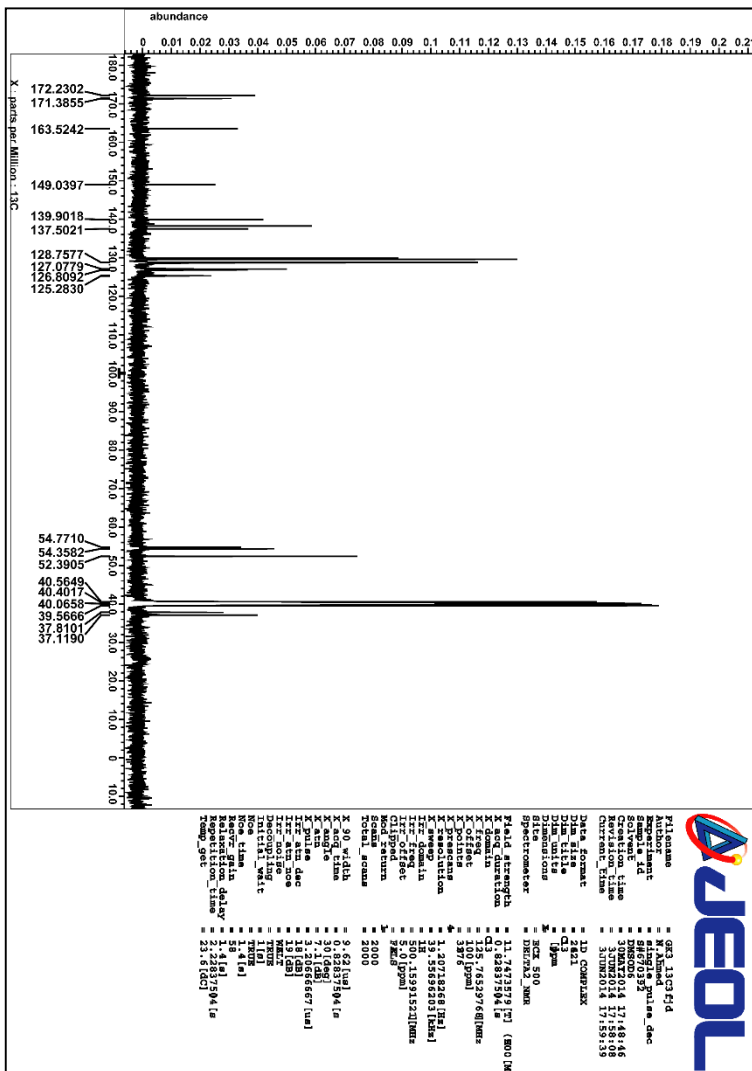


Figure A.3.9. HRMS of 3

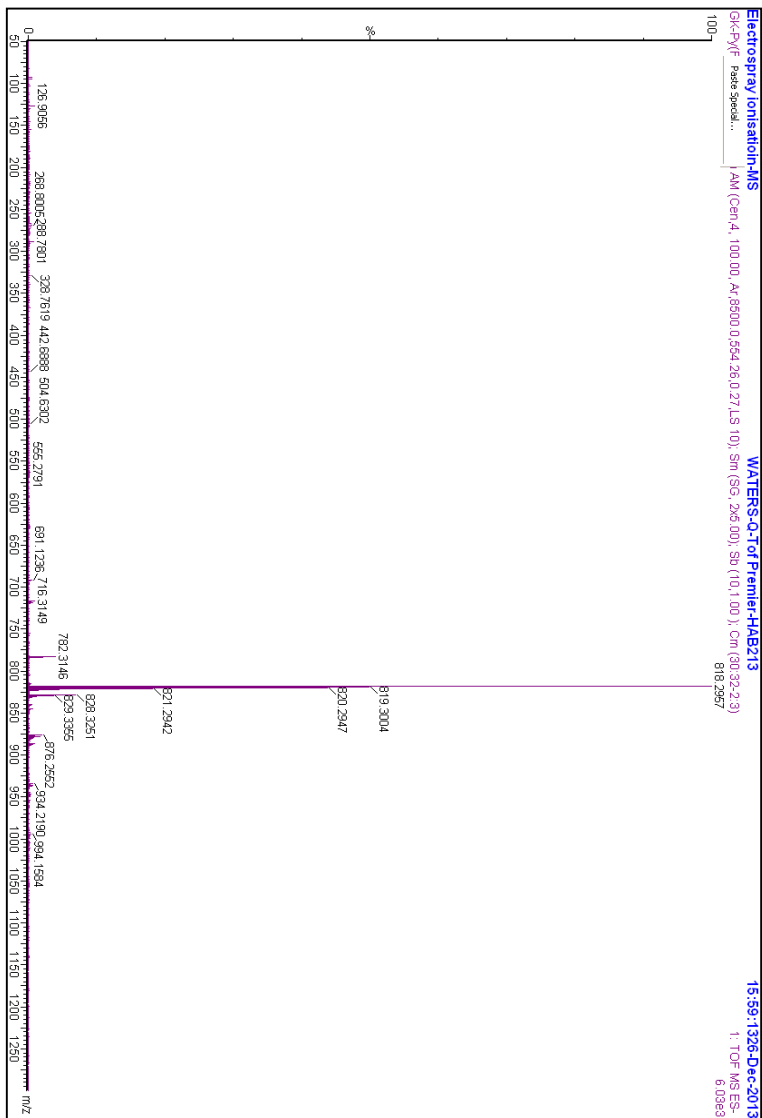


Figure A.3.11. ^{13}C NMR of **4**

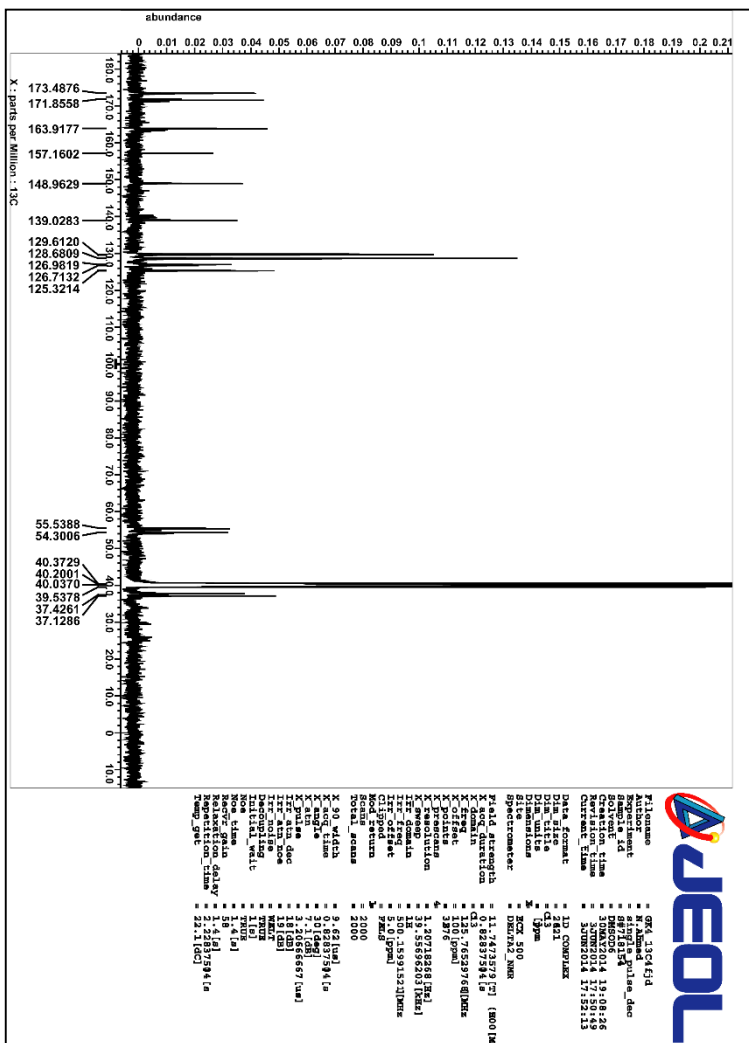


Figure A.3.12. HRMS of 4

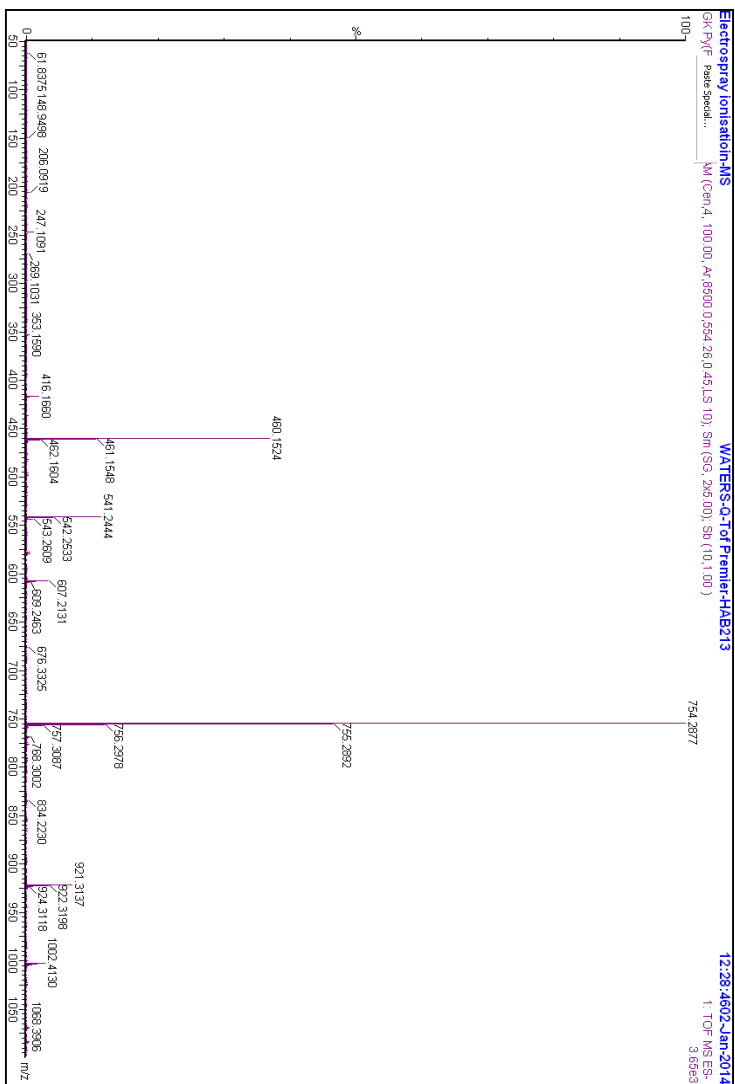




Figure A.4.2. ^{13}C NMR of **3**

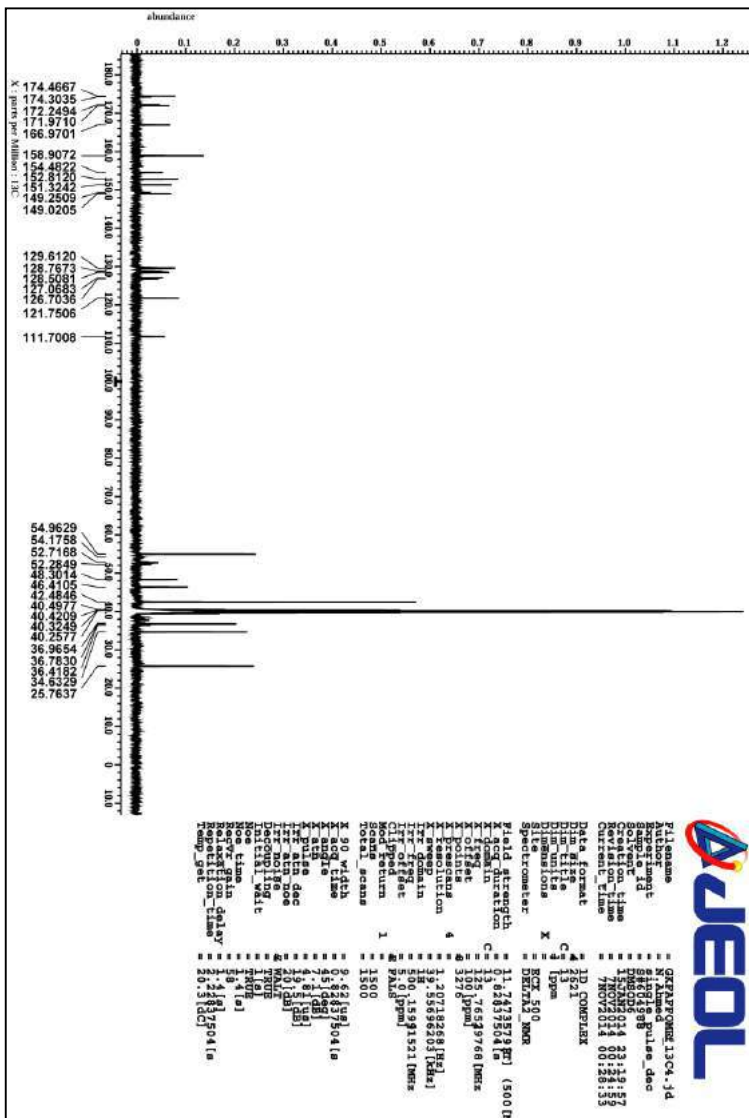


Figure A.4.3. HRMS of 3

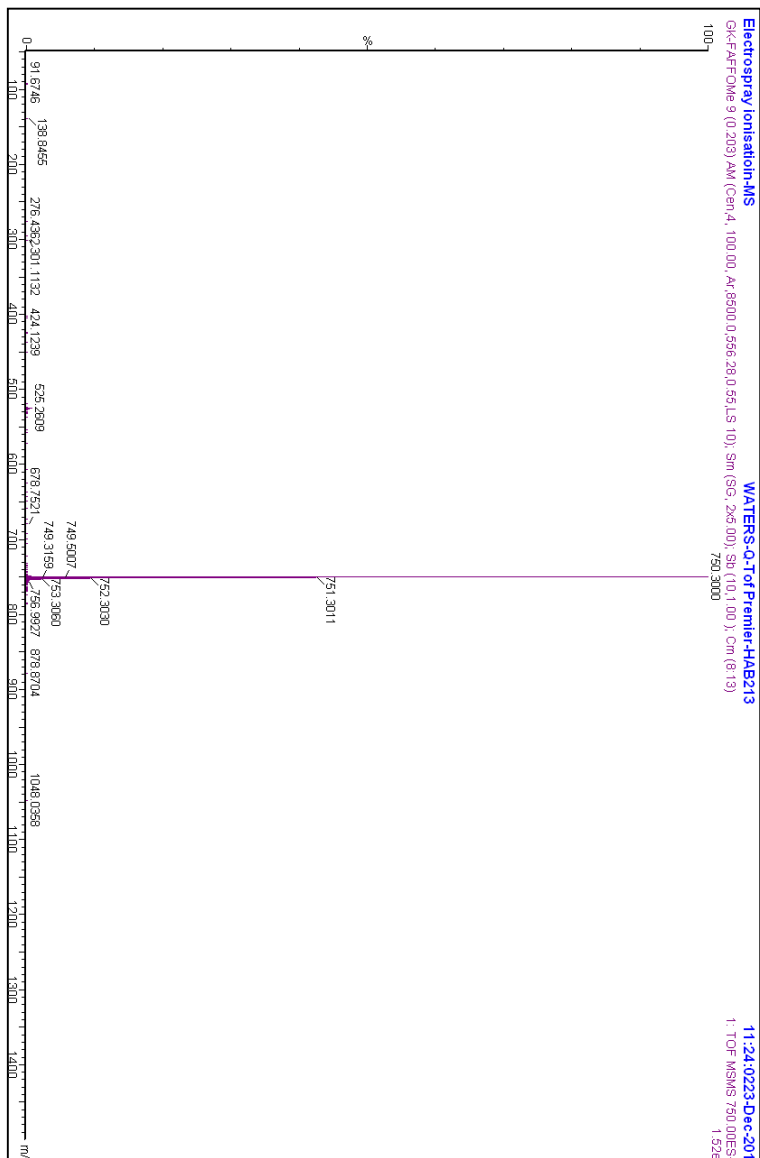


Figure A.4.6. HRMS of 4

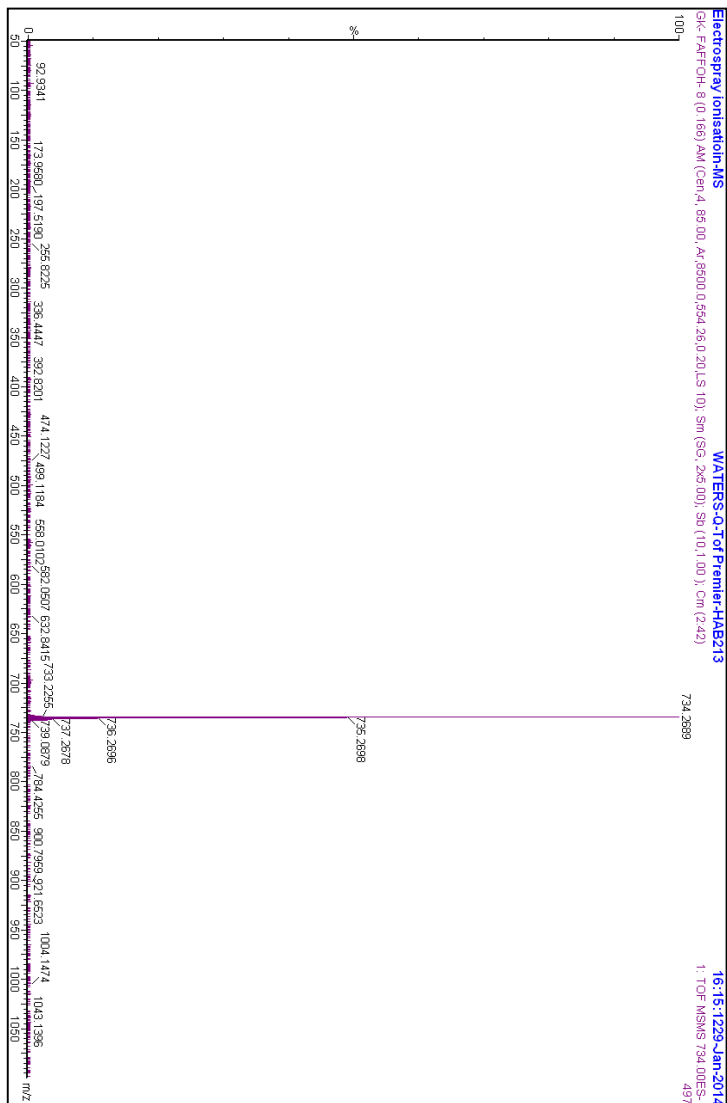


Figure A.5.3. HRMS of 1

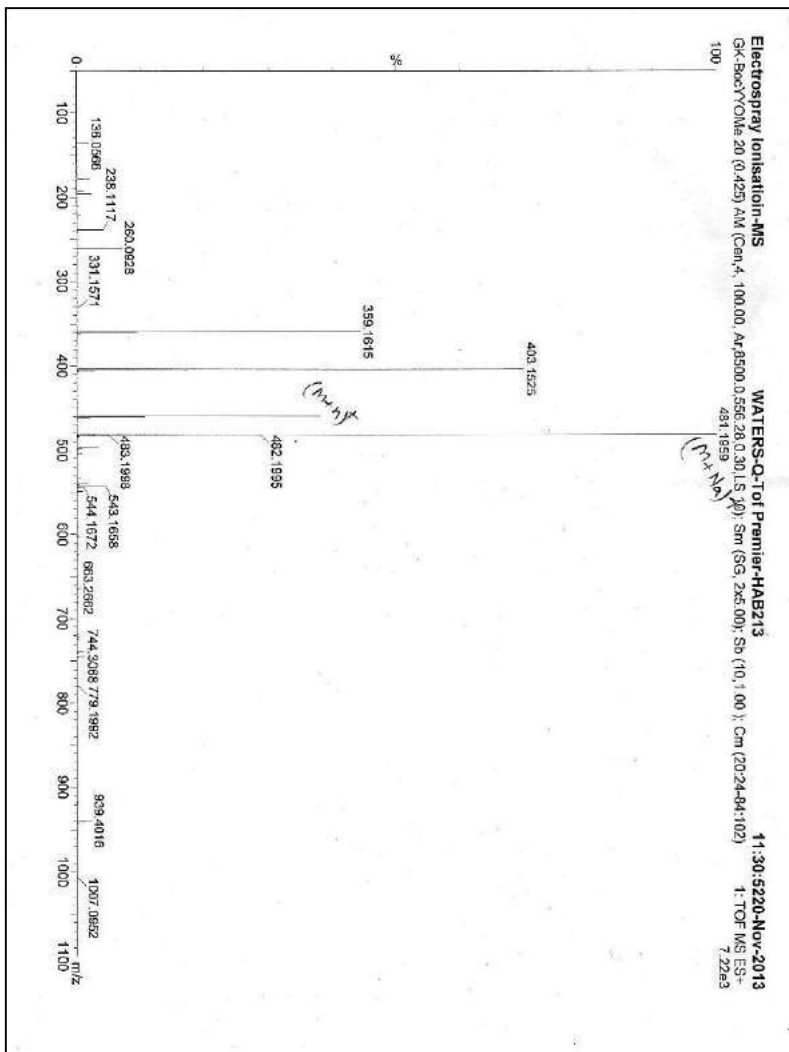
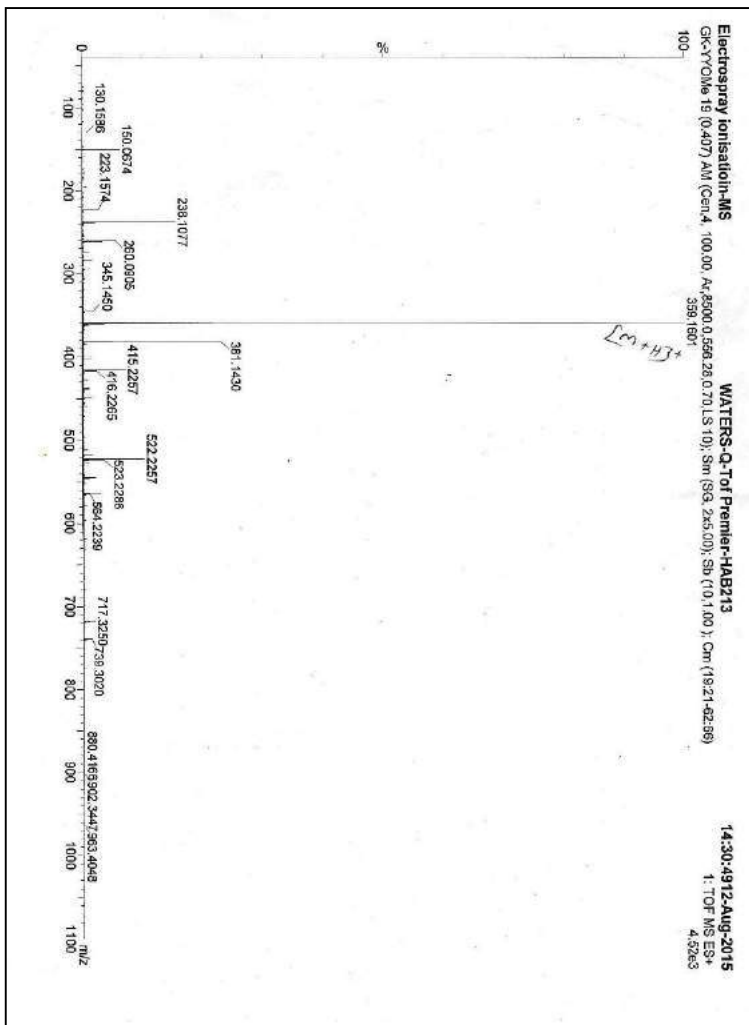


Figure A.5.4. HRMS of 2



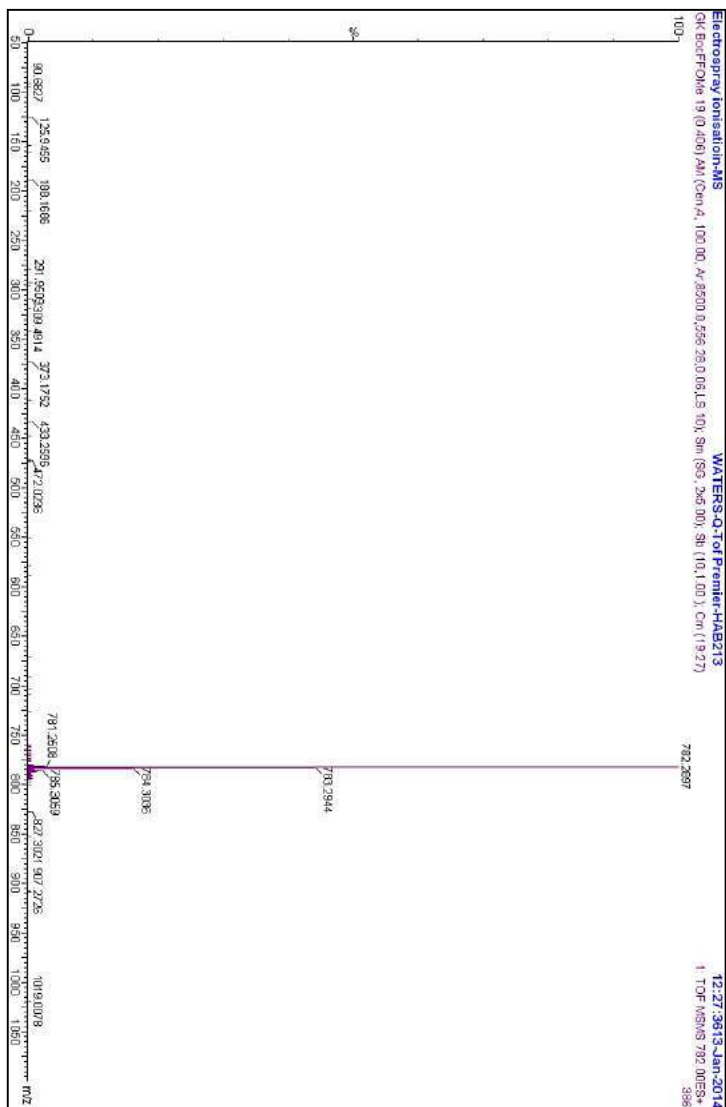


Figure A.6.3. HRMS of 1

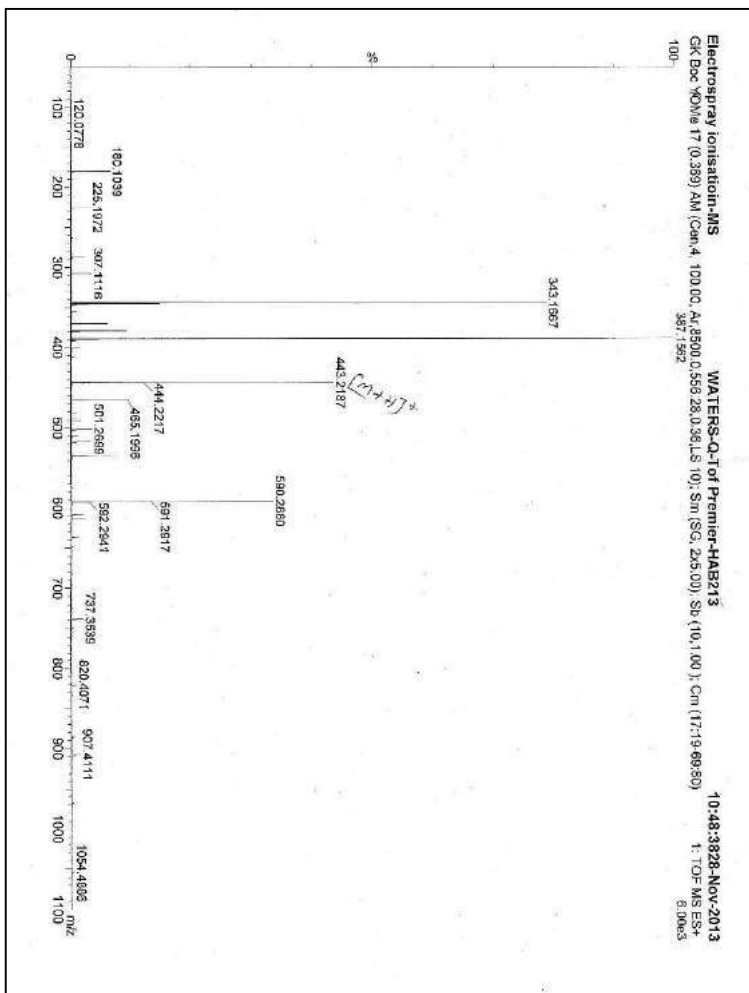


Figure A.6.5. ^1H NMR of 3

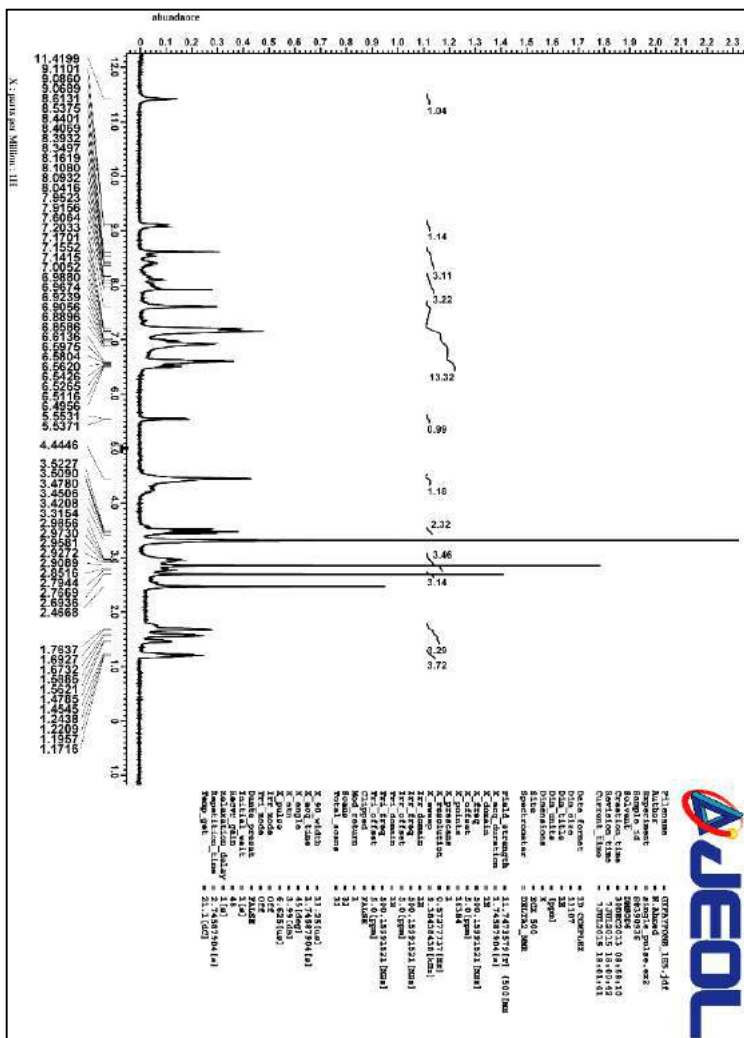
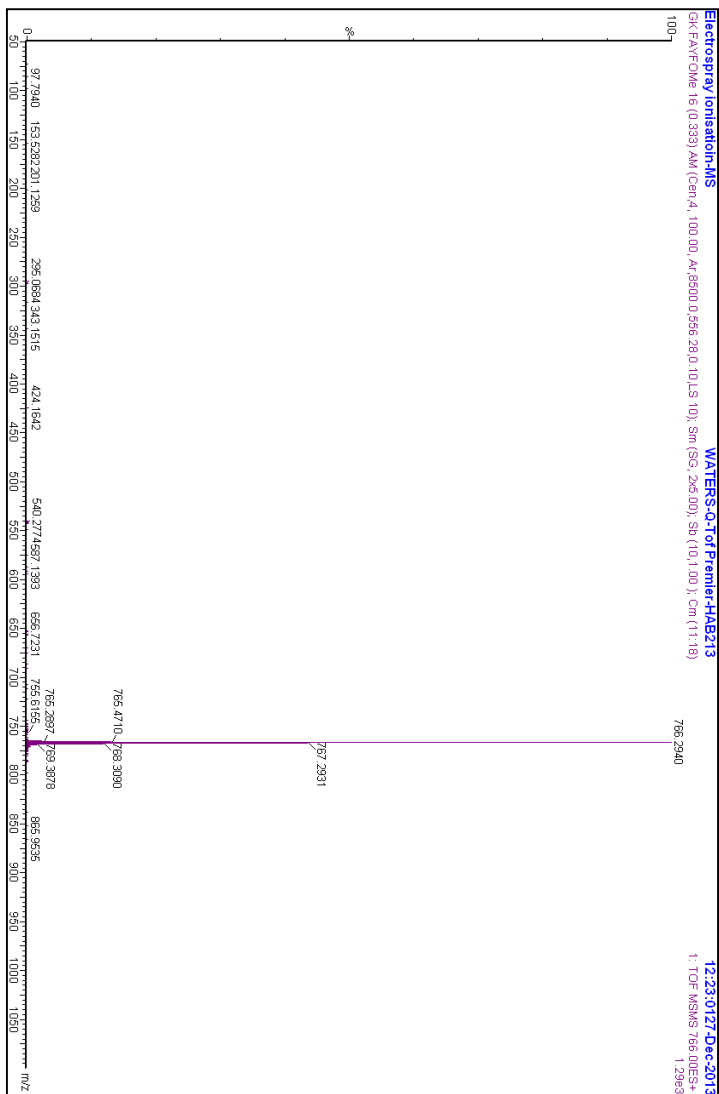


Figure A.6.7. HRMS of 3



Gagandeep Kaur

Research Scholar
Department of Chemistry,
Indian Institute of Technology, Kanpur
Kanpur India
Address: 206E, Core Labs, Department of Chemistry,
Indian Institute of Technology, Kanpur-208016, India
Email: gkaur@iitk.ac.in
Phone: 0512-259-6353

Education

- | | |
|---------------------|--|
| 2011-Present | Doctor of Philosophy (Ph. D.)
Indian Institute of Technology Kanpur, India
(CPI- 8.67) |
| 2007-2009 | Master of Science (M. Sc.)
Panjab University, Chandigarh, India
(1 st Rank in University, 79.7%) |
| 2004-2007 | Bachelor of Science (B. Sc)
Panjab University, Chandigarh, India
(First Class, 78.4%) |

Publications

1. “Self-Exfoliated Guanidinium-Based Ionic Covalent Organic Nanosheets (iCONs)” Shouvik Mitra, Sharath Kandambeth, Bishnu Biswal, Abdul M. Khayum, Chandan Choudhury, Mihir Mehta, **Gagandeep Kaur**, Subhrashis Banerjee, Asmita Prabhune, Sandeep Verma, Sudip Roy, Ulhas Kharul and Rahul Banerjee, *J. Am. Chem. Soc.* **2016**, *138*, 2823.
2. “Decoding the Morphological Diversity in Two Dimensional Crystalline Porous Polymers by Core Planarity Modulation” Arjun

- Halder, Sharath Kandambeth, Bishnu P. Biswal, **Gagandeep Kaur**, Neha Chaki Roy, Matthew Addicoat, Jagadish K. Salunke, Subhrashis Banerjee, Kumar Vanka, Thomas Heine, Sandeep Verma and Rahul Banerjee, *Angew. Chem. Int. Ed.*, **2016**, *55*, 7806.
3. "Soft structure formation and cancer cell transport mechanisms of a folic-acid dipeptide conjugate" **Gagandeep Kaur**, Akansha Shukla, Sri Sivakumar and Sandeep Verma, *J. Pept. Sci.* **2015**, *21*, 248.
 4. "Chemical Sensing in Two Dimensional Porous Covalent Organic Nanosheets" Gobinda Das, Bishnu P. Biswal, Sharath Kandambeth, V. Venkatesh, **Gagandeep Kaur**, Matthew Addicoat, Thomas Heine, Sandeep Verma and Rahul Banerjee, *Chem. Sci.*, **2015**, *6*, 3931.
 5. "Heterocyclic scaffolds and carbohydrate appendages in synthetic peptides" **Gagandeep Kaur**, Anisha Thomas and Sandeep Verma, *Indian J. Heterocycl. Chem.*, **2015**, *24*, 487.
 6. "Ultrastructure of metallopeptide- based soft spherical morphologies" **Gagandeep Kaur**, Lihi A. Abramovich, Ehud Gazit and Sandeep Verma, *RSC Adv.*, **2014**, *4*, 64457.
 7. "Functionalized smart peptides based nanomaterial for disease diagnostics and imaging" **Gagandeep Kaur**, Anisha Thomas and Sandeep Verma, *RSC Book Chapter* (Manuscript submitted)
 8. "Dityrosine folic acid conjugate in electrospun nanofibres for selective cell adhesion" **Gagandeep Kaur**, Piyali Saha, Savita, Sandeep Patil, Subramaniam Ganesh and Sandeep Verma, (Manuscript submitted)
 9. "One- and Two Dimensional Nano-island Growth in C₃ Symmetric Molecule" **Gagandeep Kaur**, Prithwidip saha, T. G. Gopakumar and Sandeep Verma, (Manuscript in preparation)

10. “Folic acid Peptide scaffolds for electrochemical capacitive energy storage” **Gagandeep Kaur**, Rudra Kumar, Ashutosh Sharma and Sandeep Verma, (Manuscript in preparation)

Symposia Proceedings

- Presented a poster titled “Soft structure formation and cancer cell transport mechanisms of a folic-acid dipeptide conjugate” at *Research scholar day* held at IIT Kanpur, India (27thFeb., **2016**)
- Presented a poster titled “Ultrastructure of metallopeptide-based soft spherical morphologies” at *11th Australian Peptide Conference* held at Kingscliff, Australia (25th-30th Oct., **2015**)
- Presented a poster titled “Soft structure formation and cancer cell transport mechanisms of a folic-acid dipeptide conjugate” at *5th Indian Peptide symposium* held at JNCASR Bangalore, India (24th-25th Sep., **2015**)
- Presented a poster titled “Ultrastructure of metallopeptide-based soft spherical morphologies” at *the 10th J-NOST conference* held at Indian Institute of Technology, Madras, India (4-6th Dec., **2014**)
- Presented a talk titled “Metal ion mediation in Self-assembling Peptides” at *Indian Peptide Society Satellite Symposium* held at CSIR-IMT, Chandigarh (21 Feb., **2014**)
- Presented a poster titled “Metal ion mediation in Self-assembling Peptides” at the *5th Annual Retreat Conference*, Konstanz Research School Chemical Biology 2013 held at Gltstein, Germany. (14-16th Aug., **2013**)

Awards

- Won **best poster award** at Research Scholar Day-2016 organized by Department of Chemistry, Indian Institute of Technology, Kanpur
- Won **second prize** in the Artistic Micrography Contest 2015-16, jointly organized by Indian Institute of Metals, Kanpur Chapter and Material Advantage, Kanpur Chapter
- **Travel award** to attend 11th Australian Peptide Conference by Australian Peptide Society
- Qualified National Eligibility Test in Chemical Sciences (UGC-Junior Research Fellowship) in June 2010
- Awarded **Gold medal** in Master of Science (M.Sc.) (**1st** in University) in 2009

Cite this: *RSC Adv.*, 2014, **4**, 64457

Ultrastructure of metallopeptide-based soft spherical morphologies†

Gagandeep Kaur,^a Lihi A. Abramovich,^b Ehud Gazit^{*b} and Sandeep Verma^{*a}

Peptides and proteins offer interesting starting points for triggering self-assembly processes owing to the chemical diversity of side-chains, ease of chemical modifications and the possibility of exploiting several non-covalent and metal-assisted interactions, to stabilize higher order ensembles. Consequently, a variety of nanoscale morphologies such as fibers, vesicles, nanotubes are observed for modified amino acids and short peptides and these biocompatible soft materials have been used for diverse biological, medical and material applications. Herein, we report metal-mediated modification of spherical soft assemblies, by introducing a coordinating linker for the Phe-Phe dipeptide, which results in the coalescence of soft structures. The possibility of copper ion coordination, with the metal-binding peptide conjugate, was confirmed by single crystal analysis. Based on these observations, a model depicting possible interactions leading to soft structure formation and metal-aided coalescence is also presented. The coalescence could be reversed in the case of Au-mediated soft structures with the help of thiol interference. Such an approach, exploiting interfacial metal ion interactions, is expected to provide an entry into novel metallopeptide materials.

Received 16th September 2014

Accepted 18th November 2014

DOI: 10.1039/c4ra05332j

www.rsc.org/advances

Introduction

Self-assembling peptides offer a versatile platform towards formation of ordered nanoscale systems, with various applications in catalysis, delivery, and tissue engineering, to name a few.^{1–8} Control through different physicochemical properties of constituent amino acids, possibility of predictable design based on secondary structural signatures, and high compatibility interaction with other biological systems, are the hallmarks of peptide-based nanoscale materials. Consequently, it is quite advantageous to employ short self-assembling peptides, to obtain diverse hierarchical structures with desired functions. Recent advances along these lines concern interaction of metal ions with self-assembling peptides to afford bio-inspired metallopeptide frameworks (MPE),^{9,10} which may offer combined investigated properties of metal-organic frameworks (MOF) with biocompatibility.

Three different approaches could be envisaged for constructing MPFs: (i) introducing amino acids side chains capable of metal binding¹¹ (ii) use of exogenous ligands supporting MOF architecture¹² (iii) use of covalently linked chiral/achiral connectors. These approaches represent facile route for the design of novel, abiotic oligomers for supramolecular studies. As a specific example, Lehn, Hue and other groups have reported family of oligoamides based on achiral connectivity of 2,6-pyridinedicarboxylic acid, where the resultant oligomers not only self-organized into single helices, but also support formation of double helices under specific conditions.^{13,14} Notably, short oligomers with 2,6-pyridinedicarboxylic acid and related connectors afford planar 'crescent-like' conformation, while longer oligomers exhibit more pronounced propensity to form helical structures.¹⁵ In particular, pyridine diacid oligomers offer hydrogen bonding at the inner rim of helices resulting in ~4.5 monomer per turn of the ensuing helix.

Diphenylalanine (FF) dipeptide motif exhibits spontaneous self-assembly to generate peptide nanotubes in solution.¹⁶ FF nanotubes offer interesting applications as scaffolds for the synthesis of metal nanowires, possess improved mechanical properties, semi-conductivity and serve as potential drug delivery agents.^{17–23} Side chain aromaticity in phenylalanine is implicated for self-assembly properties and key structural features in the solid state.²⁴ In current study, given our continued interest in hierarchical self-assembled peptides systems and our ongoing efforts to prepare covalently linked conjugates of FF dipeptide,^{16,24,26} we decided to synthesize a symmetric FF conjugate using pyridinedicarboxylic acid as an

^aDepartment of Chemistry, DST Thematic Unit of Excellence on Soft Nanofabrication, Center for Environmental Sciences and Engineering, Indian Institute of Technology Kanpur, Kanpur-208016, India

^bDepartment of Molecular Biology and Biotechnology, Department of Materials Science and Engineering, Tel Aviv University, Tel Aviv-69978, Israel. E-mail: sverma@iitk.ac.in; ehudg@post.tau.ac.il

† Electronic supplementary information (ESI) available: Crystallographic data, details structures showing H-bonding and CH $\cdots\pi$ interactions in Cu₄L₄ complex, HRSEM images of 4 + metal ions on copper grid and spectral characterisation. CCDC 1005702. For ESI and crystallographic data in CIF or other electronic format see DOI: 10.1039/c4ra05332j



Soft structure formation and cancer cell transport mechanisms of a folic acid–dipeptide conjugate[‡]

Gagandeep Kaur,^a Akansha Shukla,^d Sri Sivakumar^{b,c,d} and Sandeep Verma^{a,b,c,*}

Folic acid (FA) is a low-molecular-weight micronutrient, which plays a critical role in the prevention of birth defects and cancers. It is also essential for biochemical pathways responsible for DNA synthesis and maintenance and for the generation of new red blood cells. Cellular trafficking of FA and folate is based on its high-affinity binding to cognate folate receptor, a protein commonly expressed in several human cancers. Thus, folate conjugates of drugs, plasmids, biosensors, contrast, and radiodiagnostic imaging agents have been used for assisted delivery in folate receptor-positive cancer cells, via endocytosis pathways. This report describes morphologies of soft structures from a fully characterized FA–dipeptide conjugate and detailed mechanistic studies of its cancer cell uptake, as tracked by the inherent fluorescence of the conjugate. Copyright © 2015 European Peptide Society and John Wiley & Sons, Ltd.

Additional supporting information may be found in the online version of this article at the publisher's web site.

Keywords: folic acid; diphenylalanine; self-assembly; cell delivery

Introduction

Folic acid (FA)-conjugated imaging agents and candidate drugs have evoked considerable interest over the years because of their ability to enter cancer cells, through high-affinity interaction with folate receptor (FR) protein. FRs, particularly FR α , exhibit hyperactivity in several cancer cells such as breast, brain, lungs, cervical, and renal carcinomas [1,2] and offer a key entry point supporting active folate intake in cancer cells [3]. Subsequent to FR binding in cancer cells, folate conjugates are transported inside cells via endocytosis [4,5]. Chemical functionalities in FA play key roles in high-affinity FR binding [6], and subsequent to cellular entry of folate conjugates, enzymatic transformations release bioactive molecules inside cells. Increased involvement of FRs in cancer cells makes this strategy very useful for delivery of drugs and bioactives [7–9]. Over a period of time, many such conjugates have entered different stages of clinical studies to deliver chemotherapeutic drugs to target cells [10,11]. However, main impediments of such conjugates, which limit their widespread use, concern lack of conjugate stability and cytotoxicity.

From the standpoint of supramolecular chemistry, FA consists of a heterocyclic pterin skeleton, which affords self-assembled structures belonging to cholesteric and hexagonal mesophases, under mild alkaline conditions [12,13]. Suitably disposed donor–acceptor sites in pterin skeleton drive hydrogen bond-assisted self-recognition event, in a manner analogous to guanine tetramer formation, and it is shown that the presence of monovalent cations imparts stability to cholesteric phases. A recent study demonstrated that a change in monovalent cations resulted in enhanced FA tetramer rigidity, as a result of favorable stacking interactions and tetrad elongation [14,15].

Given our ongoing interest in peptide soft structures [16–25] and bioananoconjugation based on guanine tetrad formation [26], we

decided to investigate whether bottom-up approach with FA-containing peptide building blocks will reveal interesting structural features and delivery properties. The design of FA conjugates could be achieved via two different routes: first, by making FA-conjugated peptides, followed by their self-assembly, or through postsynthetic modification of *in situ* assembled peptide nanotubes by FA (Scheme 1) [27]. The former approach offers superior control over gross morphology of soft structures and the possibility of additional chemical modifications to create a multivalent, folate-displaying building block. We decided to employ Phe–Phe dipeptide for the synthesis of a FA-conjugated building block (Scheme 2), as both dipeptide and FA demonstrate remarkable ability to self-assemble in solution [12–15,28–32]. Thus, we envisaged that it would be intriguing to study how ensuing covalent conjugation will affect self-assembly and gross morphology. We also decided to perform cytotoxicity assays and study of possible cell uptake mechanism in different cancer cell lines.

* Correspondence to: Sandeep Verma, Center for Environmental Sciences and Engineering, Indian Institute of Technology Kanpur, Kanpur 208016, India. E-mail: sverma@iitk.ac.in

[‡] Invited Article for the Anniversary Issue 2015 of Journal of Peptide Science.

^a Department of Chemistry, Indian Institute of Technology Kanpur, Kanpur 208016, India

^b DST Thematic Unit of Excellence on Soft Nanofabrication, Indian Institute of Technology Kanpur, Kanpur 208016, India

^c Center for Environmental Sciences and Engineering, Indian Institute of Technology Kanpur, Kanpur 208016, India

^d Department of Chemical Engineering, Material Science Programme, Indian Institute of Technology Kanpur, Kanpur 208016, India

Cite this: *Chem. Sci.*, 2015, 6, 3931Chemical sensing in two dimensional porous
covalent organic nanosheets†Gobinda Das,^{†a} Bishnu P. Biswal,^{‡ad} Sharath Kandambeth,^{‡ad} V. Venkatesh,^b
Gagandeep Kaur,^b Matthew Addicoat,^c Thomas Heine,^c Sandeep Verma^d
and Rahul Banerjee^{*ad}

Two new imide-based crystalline, porous, and chemically stable covalent organic frameworks (COFs) (TpBDH and TfpBDH) have been successfully synthesized employing solvothermal crystallization route. Furthermore, thin layered covalent organic nanosheets (CONs) were derived from these bulk COFs by the simple liquid phase exfoliation method. These 2D CONs showcase increased luminescence intensity compared to their bulk counterparts (COFs). Notably, TfpBDH-CONs showcase good selectivity and prominent, direct visual detection towards different nitroaromatic analytes over TpBDH-CONs. Quite interestingly, TfpBDH-CONs exhibit a superior 'turn-on' detection capability for 2,4,6-trinitrophenol (TNP) in the solid state, but conversely, they also show a 'turn-off' detection in the dispersion state. These findings describe a new approach towards developing an efficient, promising fluorescence chemosensor material for both visual and spectroscopic detection of nitroaromatic compounds with very low 10^{-5} (M) analyte concentrations.

Received 10th February 2015
Accepted 29th April 2015

DOI: 10.1039/c5sc00512d

www.rsc.org/chemicalscience

Introduction

Chemical sensing using porous materials, especially Metal-Organic Frameworks (MOFs)¹ and Porous Organic Frameworks (POFs)² has picked up considerable attention recently. An important feature of these frameworks is their flexible and adjustable pores in which guest molecules can freely interact with the pore walls.^{3e,f} However, the sensitivity and selectivity of detection in these materials is generally not sufficient, either due to the poor analyte–host interactions inside the amorphous porous organic frameworks, or due to the chemical instability of the crystalline metal–organic frameworks. Hence, a chemically stable, crystalline and luminescent porous material with electronically adjustable π -conjugation is an attractive choice for acting as an efficient chemical sensor.

Covalent Organic Frameworks (COFs)⁴ are one such class of porous materials that, like MOFs, exhibit a well-defined and predictable crystalline network. A large number of COFs have

been synthesized over the past few years, but these materials have only rarely been explored as chemosensors^{5a} owing to their chemical instability in aqueous and acidic/basic medium. With this in mind, we have synthesized two imide based COFs, each possessing a two dimensional layered structure, that exhibit porosity, crystallinity and chemical stability. Since imide functionalized linkers show good photophysical properties, one might predict that these COFs would act as efficient chemical sensors.⁶ However, the bulk COFs exhibit only moderate chemical sensing ability due to the aggregated π -stacked layers, poor electron mobility and ineffective interaction with analytes. In order to address these shortcomings, we exfoliated the aggregated π -stacked COF layers using the Liquid Phase Exfoliation (LPE) method^{7a,c} to produce Covalent Organic Nanosheets (CONs). Since π - π interactions between the stacked layers are considerably weakened in these two dimensional covalent organic nanosheets (2D CONs), we anticipated that these CONs might show superior chemical sensing capabilities compared to the bulk COF. There have been a few reports on the growth of thin COF layers on 2D surfaces,⁸ but very little effort has been made to isolate such 2D materials in bulk quantities and to investigate their usefulness. In this paper, we show that these exfoliated CONs exhibit highly selective and visual detection of 2,4,6-trinitrophenol (TNP), over other nitroaromatic analytes such as 2,4,6-trinitrotoluene (TNT), 2,6-dinitrophenol (DNP), 2,6-dinitrotoluene (DNT), and 2-nitrophenol (NP), via a "turn-on" mechanism in the solid state and a "turn-off" fluorescence quenching in the dispersed state. Furthermore, the sensitivity of the CONs towards nitroaromatic

^aPhysical and Materials Chemistry Division, CSIR-National Chemical Laboratory, Dr Homi Bhabha Road, Pune-411008, India. E-mail: rbanerjee@ncl.res.in; Fax: +91-20-25902636; Tel: +91-20-25902535

^bDST-Thematic Unit of Excellence on Soft Nanofabrication, Indian Institute of Technology Kanpur, Kanpur-208016, UP, India

^cCentre for Functional Nanomaterials, Engineering and Science, Jacobs University Bremen, Research III, Room 61, Campus Ring 1, 28759 Bremen, Germany

^dAcademy of Scientific and Innovative Research (ASIR), New Delhi, India

† Electronic supplementary information (ESI) available: See DOI: 10.1039/c5sc00512d

‡ G.D., B.P.B. and S.K. contributed equally to this work.

Decoding the Morphological Diversity in Two Dimensional Crystalline Porous Polymers by Core Planarity Modulation

Arjun Halder*, Sharath Kandambeth*, Bishnu P. Biswal*, Gagandeep Kaur, Neha Chaki Roy, Matthew Addicoat, Jagadish K. Salunke, Subhrashis Banerjee, Kumar Vanka, Thomas Heine, Sandeep Verma, and Rahul Banerjee*

Abstract: Two new chemically stable triazine- and phenyl-core-based crystalline porous polymers (CPPs) have been synthesized using a single-step template-free solvothermal route. Unique morphological diversities were observed for these CPPs [2,3-DhaTta (ribbon) and 2,3-DhaTab (hollow sphere)] by simply altering the linker planarity. A detailed time-dependent study established a significant correlation between the molecular level structures of building blocks with the morphology of CPPs. Moreover, a DFT study was done for calculating the interlayer stacking energy, which revealed that the extent of stacking efficiency is responsible for governing the morphological diversity in these CPPs.

Two dimensional crystalline porous polymers (CPPs), including covalent organic frameworks (COFs)^[1] and covalent triazine frameworks (CTFs)^[2] are porous materials constructed by covalently linked light elements, such as C, N, O, H, B, and Si. These materials have triggered substantial research interest because of their extensive applications in molecular storage,^[3] catalysis,^[4] sensing,^[5] and opto-electronics.^[6] However, the overall properties of such porous materials do not rely only on their composition, structure, and porosity,

but also on their nanoscale morphologies.^[7] Therefore, an explicit understanding of the morphology-modulation with respect to their constituents is required.^[8] To achieve such a molecular level understanding, herein we report two CPPs that self-assemble to ribbon and hollow spherical^[9] morphologies upon crystallization in a single step without any templating agents. Hollow spherical structures are considered to be a highly important morphology in polymeric materials owing to several potential applications. However, their existence is extremely rare and often require the usage of templating agents.^[10] The intermediates responsible for producing these above morphologies were prepared at different time intervals to understand the mechanism for the formation of the final morphology (at 72 h).

The CPPs reported here show high crystallinity as revealed from their PXRD patterns (Figure 1). A high intense peak at 2.8° (2 θ) for 2,3-DhaTta and 2,3-DhaTab (Figure 1e and 1f, respectively) appear owing to the strong reflections from the 100 planes. 2,3-DhaTta and 2,3-DhaTab show other minor peaks at 4.9, 5.7, 7.5, and 9.9° (2 θ) owing to the reflections from the 110, 200, 120, and 220 planes, respectively. Peaks at 26° (2,3-DhaTta) and 25.8° (2,3-DhaTab) correspond to their 001 plane reflections. The d-spacing values between the 001 planes were used to calculate the π - π stacking distances between vertically stacked CPP layers [3.3 Å and 3.4 Å in the respected CPPs]. The high crystallinity of these CPPs is attributed to the presence of strong intramolecular O–H...N hydrogen bonding^[11] interactions between the imine nitrogen and the hydroxy functionality of the aldehyde core, which is influential in keeping the phenyl rings in one plane and increases stacking interactions within adjacent CPP layers. To get an overview of the hydrogen bonding effect on the CPP backbone, we crystallized three reference compounds, SaTta, 2,3-Dha-ani,^[12] and SaTab^[9] (Figure 1b–d). X-ray single-crystal structure analysis showed that the three phenyl rings connected to the central triazine core in SaTta are almost in the same plane (torsion angles are 174.7, 176.3, and 179.9°; Supporting Information), whereas for SaTab, the central triphenyl cores are not in the same plane (torsion angles are 145.5, 149.6, and 154.5°) to avoid steric interactions among the ortho hydrogens. On the other hand, in 2,3-Dha-ani, the central benzene ring of the respective aldehyde counterparts are out of plane (torsion angles are 134.5 and 135.9°). Interestingly, the structural features of these reference compounds largely depended upon the intramolecular O–H...N hydrogen bonding [SaTta $D=2.63$ Å, $d=1.98$ Å, $\theta=141.6^\circ$; SaTab 2.61 Å, 1.88 Å, 146.6° ; and 2,3-Dha-ani 2.59 Å, 1.86 Å, 146.6° , respectively].

[*] A. Halder,^[1] S. Kandambeth,^[1] B. P. Biswal,^[1] S. Banerjee, Prof. Dr. K. Vanka, Prof. Dr. R. Banerjee
Academy of Scientific and Innovative Research (AcSIR)
Physical/Materials Chemistry Division
CSIR-National Chemical Laboratory
Dr. Homi Bhabha Road, Pune-411008 (India)
E-mail: r.banerjee@ncl.res.in

J. K. Salunke
Polymer Science and Engineering Division
CSIR-National Chemical Laboratory
Dr. Homi Bhabha Road, Pune 411008 (India)
G. Kaur, Prof. Dr. S. Verma
DST-Thematic Unit of Excellence on Soft Nanofabrication
Indian Institute of Technology Kanpur
Kanpur-208016 (India)

N. C. Roy
Centre for Research in Nanotechnology and Science
Indian Institute of Technology Bombay
Mumbai-400076 (India)

Dr. M. Addicoat, Prof. Dr. T. Heine
Center for Functional Nanomaterials
School of Engineering and Science
Jacobs University Bremen, Research III, Room 61
Campus Ring 1, 28759 Bremen (Germany)

[*] These authors contributed equally to this work.

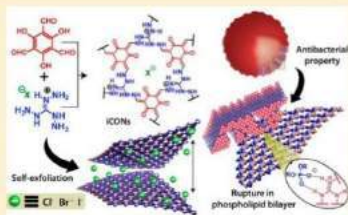
Supporting information for this article can be found under:
<http://dx.doi.org/10.1002/anie.201600087>.

Self-Exfoliated Guanidinium-Based Ionic Covalent Organic Nanosheets (iCONs)

Shouvik Mitra,^{†,∇} Sharath Kandambeth,^{‡,||,∇} Bishnu P. Biswal,^{†,||,∇} Abdul Khayum M.,^{†,||} Chandan K. Choudhury,^{†,||} Mihir Mehta,^{‡,||} Gagandeep Kaur,[‡] Subhrashis Banerjee,^{†,||} Asmita Prabhune,^{‡,||} Sandeep Verma,[‡] Sudip Roy,[‡] Ulhas K. Kharul,^{§,||} and Rahul Banerjee^{*,†,||}[†]Physical/Materials Chemistry Division, [‡]Biochemical Sciences Division, and [§]Polymer Science and Engineering Division, CSIR-National Chemical Laboratory, Pune 411008, India^{||}Academy of Scientific and Innovative Research (AcSIR), New Delhi 110020, India[∇]Department of Chemistry, Indian Institute of Technology, Kanpur 208016, India

Supporting Information

ABSTRACT: Covalent organic nanosheets (CONs) have emerged as functional two-dimensional materials for versatile applications. Although π - π stacking between layers, hydrolytic instability, possible restacking prevents their exfoliation on to few thin layered CONs from crystalline porous polymers. We anticipated rational designing of a structure by intrinsic ionic linker could be the solution to produce self-exfoliated CONs without external stimuli. In an attempt to address this issue, we have synthesized three self-exfoliated guanidinium halide based ionic covalent organic nanosheets (iCONs) with antimicrobial property. Self-exfoliation phenomenon has been supported by molecular dynamics (MD) simulation as well. Intrinsic ionic guanidinium unit plays the pivotal role for both self-exfoliation and antibacterial property against both Gram-positive and Gram-negative bacteria. Using such iCONs, we have devised a mixed matrix membrane which could be useful for antimicrobial coatings with plausible medical benefits.



INTRODUCTION

Covalent organic nanosheets (CONs) are two-dimensional (2D) materials constructed by symmetrically arranged organic linkers, along two dimension, via strong covalent bonds.¹ In recent years, researchers have made considerable efforts to synthesize monolayer or few layered CONs, which could emerge as a porous functional material with a plethora of applications owing to their easy and predesignable functionalization opportunity.^{1,2} On this line, few layered CONs have been synthesized from 2D crystalline porous polymers (CPPs) often known as covalent organic frameworks (COFs)³ and covalent triazine frameworks (CTFs),⁴ using conventional exfoliation techniques such as ultrasonication⁵ and mechanical delamination.^{1(a,b),6} However, the major reasons that prevent the formation of monolayer or few layered CONs by these methods include (i) strong π - π stacking between the layers,¹⁻⁴ (ii) hydrolytic instability for most of the CPPs,⁵ (iii) possible restacking,⁶ and most importantly, (iv) challenging synthetic procedures to obtain the exfoliated nanosheets.^{1(a-c)} However, these shortcomings could be surpassed easily by rational design of chemically stable CONs with inbuilt ionic character to induce self-exfoliation. Moreover, if the ionic building block itself possesses biological significance, the synthesized CONs could be directly used for biomedical applications without further post

synthetic modifications. Nevertheless, the self-exfoliation of 2D CPPs and exploring its biological significance in a single domain is unprecedented and thus remains a daunting task. In the same pursuit, we have introduced the concept of rational design to self-exfoliate guanidinium halide based porous ionic covalent organic nanosheets (iCONs) for antimicrobial applications. Positively charged guanidinium units result in interlayer repulsion to self-exfoliate into few layered iCONs. These iCONs showed permanent porosity, chemical stability and potent antimicrobial property against both Gram-positive (*Staphylococcus aureus*) and Gram-negative (*Escherichia coli*) bacteria. Although substituted guanidinium-based conventional polymeric materials are known to demonstrate antimicrobial property,⁷ but the solubility of guanidinium-based materials limits their usage in heterogeneous water resistant antimicrobial coatings. Hence, the insolubility of iCONs with antimicrobial property could be the key solution in devising antibacterial coatings useful in biomedical sectors. To validate this conception, we have strategically fabricated iCONs@Polysulfone (PSF) mixed matrix membrane for antimicrobial coatings.

Received: December 29, 2015

Published: February 11, 2016

HETEROCYCLIC SCAFFOLDS AND CARBOHYDRATE APPENDAGES IN SYNTHETIC PEPTIDES : REVIEW

Gagandeep Kaur^a, Anisha Thomas^a and Sandeep Verma^{a,*}

^aDepartment of Chemistry and ¹DST Thematic Unit of Excellence on Soft Nanofabrication
Indian Institute of Technology Kanpur, Kanpur – 208016
Email: sverma@iitk.ac.in

Received 21 May 2015; Accepted 25 May 2015

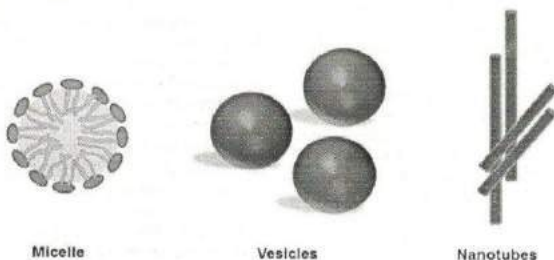
This review presents a brief account of introduction of heterocyclic rings and carbohydrate appendages in peptide conjugates, and their effect on solution-phase self-assembling properties. Such scaffolds bring in geometrical considerations, metal binding sites and water solubility properties, for interesting applications of self-assembled soft matter.

Peptides containing self-assembled soft structures offer immense diversity in terms of the presence of modifiable functional groups and biocompatibility¹. It provides an attractive design platform to construct structures and tune them as per requirements, given the multitude of possibilities due to sidechains variation in constituent amino acids². Heterocyclic scaffolds, when used as linker molecules, add interesting functionalities to peptide constructs³, and these versatile enabling modifications bring out the possibilities of added hydrogen bonding sites and metal interaction sites for possible applications⁴. Aromatic and π - π stacking interactions, enhanced water solubility and recognition by biological motifs⁵, are the other advantages brought in by the attachment of the right heterocyclic motif and carbohydrates. In addition, heterocyclic rings also

provide much needed rigidity and planarity to the flexible peptide units, forcing them to adopt suitable geometries to maximize interactions⁶.

Design Strategies

One strategy to create peptide-based small molecules is using linking scaffolds, either flexible or rigid, to permit intermolecular recognition or pre-patterning of structures to form ordered architectures. Flexible scaffolds such as *tris*(2-aminoethyl)amine (tr^{en}) or diaminoalkane linkers allow for the linking of peptide units giving rise to C_3 or C_2 symmetric structures with potential to form self-assembled structures⁷. Aliphatic chains of appropriate length and heterocyclic rings are used as rigid connectors to engender specific recognition sites. However, it is also possible to use alicyclic rigid scaffolds, such as Kemp's



Schematic representation of micelles, vesicles and nanotubes.

Figure-1

This thesis contains:

- ☐ Synthesis, design and molecular level arrangement of amino acid based C_3 molecule
- ☐ Metal ion coordination in self-assembled nanostructures and formation of Metal peptide frameworks
- ☐ Catalytic studies with Metal peptide framework
- ☐ The cellular uptake studies and uptake mechanism studies of folic acid based peptide in different cancer cell lines
- ☐ Selective adhesion and detection of FR positive cells with peptide/polymer nanomats
- ☐ Carbonized peptide/melamine sheets for electrochemical capacitive energy storage